UNIVERSITE DU QUEBEC

MÉMOIRE PRÉSENTÉ À

L'UNIVERSITÉ DU QUÉBEC À CHICOUTIMI

COMME EXIGENCE PARTIELLE

DE LA MAÎTRISE EN SCIENCES DE LA TERRE

Par

MOÏSE LIONNEL NGUE DJON

CHANGEMENT DE LA MINERALOGIE DES SULFURES, DES MINERAUX DU GROUPE DU PLATINE ET DES TEXTURES AVEC LE DEGREE D'ALTERATION DES ZONES ROBY, TWILIGHT AND HIGH-GRADE DU COMPLEXE DU LAC-DES-ILES (ONTARIO, CANADA).

OCTOBRE 2010

RÉSUMÉ

Les assemblages de sulfures de métaux de base (SMB) en relation avec les assemblages de minéraux silicates ont été analysés dans les roches frais et altérés des zones minéralisées Twilight, Roby et High-grade du Complexe du Lac des îles. Ce travail a été initiée dans le but de déterminer s'il y'avait une relation étroite entre la minéralogie, la texture des minéraux sulfurés et l'altération des minéraux silicatés. En addition, l'analyse in-situ des éléments chalcophiles dans les SMB combiné au calcul de masse balance et l'étude des minéraux du groupe du platine (MGP) ont été effectué dans le but de déterminer les phases qui contrôlent les éléments du groupe du platine (EGP) et de percevoir comment cela varie avec le changement des assemblages sulfures. L'analyse d'images montre qu'il y'a trois assemblages de SMB : l'assemblage pyrrhotite (Po)-pentlandite (Pn)-chalcopyrite (Ccp) ± pyrite (Py) qui est present dans les gabbronorites, l'assemblage pentlandite-chalcopyrite-pyrite et l'assemblage pyrite-chalcopyrite-millerite (Mil) qui sont présents dans les métagabbronorites et dans les chlorite-actinote schists. Ces assemblages de sulfures coexistent avec les Ca-amphiboles et les plagioclases qui s'équilibrent successivement entre 856 et 622°C dans les gabbronorites, 713 et 450 °C dans les métagabbronorites et entre 655 et 417 °C dans les chlorite-actinote schists. Le changement des assemblages de sulfures de haute températures à celles de basses températures semblent être du à la perte du Fe contenu dans les sulfures. Nous avons trouvé que dans l'assemblage Po-Pn-Ccp±Py la majorité de Os, Ir, Ru (IPGE) et Rh sont concentré dans la Po et la Pn. La Po contrôle 20% de Pd et le reste de Pd contrôlé par les MGP comme Pd-Te qui est habituellement associé aux SMB. Le platine a été trouvé principalement comme Pt-As associé aux SMB. Dans l'assemblage Pn-Ccp-Py la majorité des IPGE sont présent dans la Pn et 30% de Pd est présent dans la Pn, avec la balance trouvé dans les MGP associés aux SMB. Dans l'assemblage Ccp-Py-Mil les IPGE et Pt sont principalement présents dans la Py et la Mil. Cependant la majorité de Pd est présent dans la MGP tel que Pd bismuthotelluride, (Pd-Bi-Te) Pd antimonide (Pd-Sb), Pd arsenide (Pd-As), Pd sulfide (Pd-S) et Pd telluride (Pd-Te) qui ne sont pas associés aux SMB. La distribution des assemblages minéraux suggère que la minéralogie des SMB n'évolue pas directement avec l'altération des

minéraux silicatés. Cependant leurs textures sont équilibre dans les roches non altérées contrairement dans les roches altérées mettant en évidence l'altération hydrothermale. Parmi les processus qui sont survenu durant de cette activité on inclus éventuellement la mobilisation du Fe des phases sulfurées. Ce dernier est responsable successivement de la transformation de la pyrrhotite et pentlandite en pyrite et millerite. La présence des IPGE dans la Py xénomorphe implique qu'elle provient de l'altération de la Po et de la Pn magmatique. Par ailleurs, le Pd présent dans les gabbronorites a été concentré par le liquide sulfuré qui a cristallisé la solution solide monosulfuré (MSS). Ce dernier a exsolvé la Pn et la Po et le Pd s'est concentré dans la Pn. Les minéraux de Pd-Te trouvés au sein des sulfures magmatiques ont soit exsolvé des sulfures ou cristallisé directement du liquide sulfuré. Dans les chlorite-actinote schists, le Pd est présent sous forme de plusieurs variétés de MGP qui ne sont pas associés aux sulfures. On suggére que cet enrichissement s'est produit pendant la percolation des fluides à basse température (~ 450°C). Ce fluide déduit comme être riche en Pd, As, Sb et Bi s'est potentiellement introduit dans la zone de cisaillement qui maintenant correspond à la High-grade Zone et a précipité le Pd sous forme de Pd-Bi-Te, Pd-Sb, Pd-As, Pd-S and Pd-Te.

AVANT-PROPOS

Le modèle de ce mémoire de maîtrise en sciences de la Terre est sous forme de publication. Il comporte trois principaux chapitres : une introduction générale en français suivi du manuscrit en anglais qui sera soumit et publié dans le journal *Mineraliun Deposita* et enfin une conclusion générale en français. Je tiens vivement à remercier le professeur Sarah-Jane Barnes pour son encadrement, son soutien, ses conseils et son assistance pendant cette étude. Merci également à mon comité de recherche pour leurs conseils et suggestions utiles. Merci à la Chaire du Canada en métallogénie magmatique pour financement de cette étude. Merci beaucoup au Dr. Paul Bédard, Dany Savard et Julie Fredette à l'UQAC et au Dr. Marc Choquette à l'Université Laval pour leur aide en laboratoire et particulièrement au Dr. Sarah Dare, Dr Philippe Page et Dr. Belinda Godel pour les multiples discussions qui ont grandement améliorées la qualité de ce manuscrit. Enfin je tiens à remercier mes amis et ma famille pour leur soutien moral incessant qui a favorisé l'achèvement de ce projet.

TABLE DES MATIERES

LISTE DES FIGURES

LISTE DES TABLEAUX

CHAPITRE I

INTRODUCTION GÉNÉRALE

La majorité de la production mondiale des éléments du groupe du platine (EGP; Pt, Pd, Rh, Os, Ir et Ru) provient des minéralisations stratiformes de type *reef* enrichies en EGP au sein des larges intrusions mafiques à ultramafiques telle que le Complexe du Bushveld dans la République d'Afrique du Sud (le Merensky *reef* et UG-2 : Naldrett et al. 2002; Von Gruenewaldt et al. 1986) et le Complexe du Stillwater au USA (le *reef* J-M : Zientek et al. 2002). En général, ces gisements sont appauvris en sulfures (< 5% sulfures) et extrêmement enrichies en EGP. Par exemple, le Complexe du Stillwater contient 2% sulfure et 49 à 419 ppm de EGP total (Godel et Barnes 2008). Cependant, contrairement à la majorité des minéralisations stratiformes de type *reef*, le Complexe du Lac-des-Iles (CLDI) est un gisement de type brèchique (Naldrett 2004; Gomwe 2008) caractérisé par un appauvrissement en sulfure (0.1 à 3%) et surtout d'un extrême enrichissement en Pd comparé aux autres EGP (avec les ratios Pd/Pt ~ 10 et Pd/Ir ~ 10000; Gomwe 2008) qui le différentie nettement des autres gisements d'EGP de type *reef* (avec les ratios Pd/Pt entre 0.5 et 3 pour le reef du Merensky et le reef du J-M respectivement; Godel et al. 2007; Barnes et Naldrett 1985).

Localisation et Géologie du Complexe du Lac-des-Iles

Le Complexe du Lac-des-îles (CLDI) est une intrusion mafique à ultramafique située en Ontario, au sud de la sous province de Wabigoon dans la province géologique du Supérieure au Canada. C'est une suite de roches datée à 2689±1 Ma à partir de la

méthode U-Pb (Stone et al. 2003), qui s'est mise en place dans les tonalites (2775-2722 Ma) de Wabigoon le long de la frontière avec la ceinture métasédimentaire de Quetico (Pye 1968 ; Sutcliffe 1986). Le CLDI comprend trois intrusions principales (Fig. 1) : i) La «North Lac des Îles intrusion» située au Centre du Lac et constituée de clinopyroxénites, de webstérites et de gabbronorites (Lavigne et Michaud 2001), ii) la « Mine Block intrusion» située au sud du Lac et constituée de gabbronorites, de gabbros à textures variée et de gabbros à magnétites, iii) la «Camp Lake intrusion» située au sud-est du Lac des Iles est constituée de gabbros à hornblende homogènes (Lavigne et Michaud 2001).

Seule la «Mine Block intrusion» montre des enrichissements importants en palladium (Pd) permettant une exploitation. Elle comporte trois zones minéralisées principales caractérisées par des textures ignées complexes (brèchiques, pegmatitiques) et une distribution lithologique chaotique (Lavigne et Michaud 2001; Fig. 2) : la High-Grade Zone, la Roby Zone et la Twilight Zone.

Les zones minéralisées

La Zone High-Grade se trouve entre la zone brèchique de Roby et le gabbro homogène non minéralisé à l'est. Elle est composée de deux faciès dominant : i) les schistes riches en actinote et en chlorite et ii) les microbrèches de métagabbronorites (Gomwe 2008). Elle possède les teneurs les plus fortes en Pd avec des teneurs de Pd/Pt (20) est plus élevé que dans les zones Roby et Twilight (7). La Zone High-Grade est plus altérée que les zones Roby et Twilight. On observe dans la plupart de roches des minéraux silicatés secondaires (amphibole et chlorite) résultant de l'altération des

minéraux silicatés primaires (orthopyroxène et plagioclase). Les schistes contiennent de faibles proportions de minéraux sulfurés (la plus part < 0,1%). La fraction sulfurée est constituée principalement de chalcopyrite avec de petits grains (> 1mm) de pentlandite et de pyrrhotite (Gomwe 2008). Plusieurs minéraux du groupe du platine (MGP) tel que la vysotskite (PdS), les tellures de Pd, merenskyite (PdTe2), kotulskite (PdTe) ont été decélé dans les interstices des silicates et en inclusion dans les minéraux silicatés secondaires (Sweeny 1989; Watkinson et al. 2002).

La Roby Zone est composée de métagabbronorites et de gabbronorites (Gomwe 2008) auparavant décrite comme étant constitué de gabbronorites, de pyroxénites et d'anorthosites (Lavigne et Michaud, 2001; Hinchey et al. 2005). Quatre vingt sept pourcent (87%) de la Zone de Roby est composée de faciès brèchiques (Lavigne et Michaud, 2001). Ces roches peuvent être sous forme de fragment ou de matrice. Les minéralisations d'EGP sont associées aux gabbros brèchiques hétérolitiques et à textures variées. L'altération observée dans les zones isolées ou dans les zones de mylonitisation est modérée à forte et marquée par l'ouralitisation des pyroxènes (Lavigne et Michaud 2001). Les sulfures de métaux de bases présents en faible quantité (3% environ), sont constitués de pyrrhotite, de pentlandite et de chalcopyrite. Ils sont disséminés dans les roches à grains fins en associations avec les plagioclases et les pyroxènes ou en inclusion minérale dans les phases sulfurées primaire. La pyrite est commune dans la Zone Roby et montre des quantités croissantes avec des degrés élevés d'altérations (Hinchey 2005).

La Zone Twilight est séparée de la Zone Roby à sa limite ouest par un gabbro homogène massif non minéralisé «East Gabbro» et plus au sud par un dyke felsique (Dionne-Foster 2002). Sa composition pétrologique et minéralogique est similaire à la Zone Roby (Gomwe 2008). Cependant la dominance de la composition des faciès est gabbronoritique que métagabbronoritique. Les textures observées sont essentiellement pegmatitique, brèchique ou encore variée. Les minéraux d'altérations tel que épidote, chlorite, séricite, amphibole sont également présent.

Problématique

De part ses caractéristiques géologiques propres, et particulièrement de son contenu inhabituelle en Pd par rapport aux autres éléments du groupe du platine (EGP), le CLDI est considéré comme un gisement unique au monde comparé aux autres gisements d'EGP de type *reef*. Aucun modèle n'explique convenablement l'enrichessement du Pd et la formation de ce dépôt. Certains auteurs suggèrent que les fluides ont joué un rôle majeur dans la formation du dépôt (Watkinson et Dunning 1979) tandis que d'autres suggèrent que les processus magmatiques sont plus importantes (Brugmann et al. 1989). La géochimie sur roche totale indique que, dans la Twilight Zone et Roby Zone il existe une corrélation positive entre le PGE et S indiquant un éventuel contrôle de la PGE par un liquide sulfuré. Toutefois, dans la High-Grade Zone, cette corrélation ne s'applique plus au grand nombre de roches riches en Pd et contenant très peu de S (Hinchey et Hattori 2005; Gomwe 2008). Ces auteurs ont conclu que la minéralisation dans la Twilight Zone et Roby Zone est essentiellement le produit de

l'accumulation de sulfures magmatiques, contrairement à la High-Grade Zone où le Pd a été introduit par les fluides magmatiques tardifs.

Objectifs

Ainsi le but principal de cette étude a été axé sur la détermination des phases minérales qui contrôlent le Pd et les autres EGP dans les roches frais et altérés des zones minéralisées. Il est bien connu que le Pd se concentre dans la pentlandite (Barnes et al. 2008) ou dans les minéraux de Pd (Cabri 2002). Par conséquent notre cible majeure sera basée sur l'étude des minéraux sulfurés et des minéraux du groupe du platine. Les résultats engendrés contribueraient d'avantage à la compréhension des processus de formation du CLDI.

Cependant atteindre notre objectif primaire nécessite au préalable de promouvoir quelques objectifs secondaires parmi lesquels :

- Déterminer les différents assemblages de sulfures de métaux de bases présents et étudier leur distribution en relation avec les minéraux silicatés au sein des zones minéralisées.

- Déterminer les conditions d'équilibres des assemblages de sulfures de métaux de bases.

- Déterminer les concentrations des éléments du groupe du platine et des autres éléments chalcophiles présents dans les sulfures de métaux de bases.

- Déterminer les assemblages de minéraux du groupe du platine et étudier leur distribution et leur association texturale avec les autres phases minérales présentes.

- Effectuer un calcul de bilan de masse pour déterminer les proportions de chaque élément du groupe du platine présentes dans les assemblages de sulfures de métaux de base et de déterminer comment ces proportions varient avec le changement des assemblages de sulfure.

Méthodologie

L'approche méthodologique adéquate pour atteindre nos objectifs primaire et secondaires se présente comme suit :

- La sélection des échantillons

Les études seront axées principalement sur les échantillons prélevés au Lac des Iles par Gomwe (2008). Ces échantillons seront représentatifs des zones minéralisées Roby, Twilight et High-grade Zones. La sélection des échantillons a été axée sur leur contenu en soufre (> 0.5wt%) et en palladium (Pd/Pt > 5)

- Études pétrographiques et pétrologiques

Les études pétrographiques et pétrologiques des sections polies de nos échantillons ont été effectuées à partir d'un microscope électronique assisté à l'analyse d'image. Ceci dans le but de caractériser la minéralogie, la texture et l'altération des échantillons et d'éffectuer l'analyse modale des phases minérales présentes.

- L'analyse in-situ des sulfures de métaux de bases au LA-ICP-MS

Elle nous permettra de déterminer les concentrations des éléments du groupe du platine et en outre, des autres éléments chalcophiles présentes dans les sulfures de métaux de base.

- L'analyse qualitative et quantitative à la microsonde électronique.

Grâce à ses multiples fonctions cet appareil analytique nous permettra de localiser les minéraux du groupe de platine présents et de pouvoir déterminer leur composition chimique de manière qualitative et quantitative. En addition, les analyses quantitatives des minéraux silicatés seront effectuées.

CHAPITRE II

Titre du manuscript (pour la soumission à Mineralium Deposita) :

Changes in the Sulfide and Platinum-Group Mineralogy and in the Texture with Degree of Alteration in the Roby, Twilight and High-Grade Zones of the Lac-des-Iles-Complex (Ontario, Canada).

Auteurs:

Moïse Lionnel Ngue Djon, Sarah-Jane Barnes et Tafadzwa Gomwe.

Contributions des auteurs :

1er auteur : Moïse Lionnel Ngue Djon:

- Analyses en laboratoire et traitement des données
- Rédaction du résumé, de l'introduction, de la géologie, de la méthodologie, des résultats, de la discussion et de la conclusion
- Mise en forme de l'article

2ème auteur: Sarah-Jane Barnes:

- Conseils et suivi du projet
- Conseils à la rédaction de l'ensemble du manuscrit

3ème auteur : Tafadzwa Gomwe

- Collecte des échantillons sur le site d'étude
- Modèle de formation du Complexe.

Abstract

The base metal sulfide (BMS) assemblages and silicate minerals have been analyzed in fresh and altered rocks from the mineralized zones; Twilight, Roby and High-Grade of the Lac-des-Iles-Complex (*LDIC*). The purpose of this work was to investigate whether there is a relationship between the mineralogy and texture of the sulfide minerals and the alteration of the silicate minerals. In addition, in-situ analysis of chalcophile elements in BMS combined with mass balance calculations and study of platinum group minerals (PGM) were carried out to determine which phases control the platinum group elements (PGE) and see how they vary with the change of sulfide assemblages.

Petrographic and image analysis shows that there are three assemblages of BMS: the assemblage pyrrhotite (Po) - pentlandite (Pn) - chalcopyrite (Ccp) ± pyrite (Py) which is associated with gabbronorite, followed by the assemblage pentlandite – chalcopyrite – pyrite and the assemblage pyrite – chalcopyrite - millerite (Mil) which is associated with both metagabbronorite and chlorite-actinolite schist. These sulfide assemblages coexist with Ca-amphibole and plagioclase that equilibrated from 856 to 622 ° C in gabbronorite, from 713 to 450 ° C in metagabbronorites and from 655 to 417 ° C in the chlorite-actinolite schist. The change from magmatic to low-temperature sulfide assemblage appears to be due to loss of Fe from the sulfides.

We found that in the Po-Pn-Ccp assemblage most of the Os, Ir, Ru (IPGE) and Rh are hosted in Po and Pn while ~ 20 % Pd is found in Pn, the remainder of the Pd is hosted in PGM primarily as Pd-telluride which is associated with the BMS. Platinum is

found mainly as mineral of Pt-As associated with the BMS. In the Pn-Ccp-Py assemblage most of the IPGE are present in Pn and ~30 % of the Pd is present in Pn, with the balance found in PGM associated with BMS. In the Ccp-Py-Mil assemblage the IPGE and Pt are found in anhedral Py and Mil. However, most of the Pd is found in Pd-minerals, such as Pd-bismuthotelluride, Pd-antimonide, Pd-arsenide, Pd-sulfide and Pd-telluride bearing phases, which are not associated with BMS. The distribution of the different mineral assemblages suggests that the sulfide mineralogy did not evolve directly with alteration of the primary silicate minerals. The textures of sulphides observed are in equilibrium with the silicate minerals in unaltered rocks in contrast to altered rocks where their textures are in disequilibrium. The major processes which occurred during the alteration were oxidation and mobilization of Fe. These were responsible for the transformation of pyrrhotite and pentlandite to anhedral pyrite and the transformation of pentlandite to millerite. The presence of IPGE in the anhedral pyrite implies that pyrite originated from the magmatic pyrrhotite and pentlandite.

Our results suggest that the Pd in the least altered rocks was concentrated by a sulfide liquid that crystallized monosulfide solid solution (MSS) which exsolved to pentlandite and pyrrhotite and intermediate solid solution (ISS) which exsolved to chalcopyrite. The Pd concentrated in pentlandite. The Pd-Te minerals occur within the magmatic sulfides and either exsolved from the sulfides or crystallized directly from the late sulfide liquid. In the highly altered rocks of the High-Grade Zone, Pd is enriched by a factor of 2 or 3 relative to the Roby Zone and Pd is present as a variety of PGM which are not associated with the sulfides. We suggest that this enrichment occurred during a

fluid percolation event at low temperature (~ 450°C). This fluid is inferred to have been rich in Pd, As, Sb and Bi and was potentially introduced into the shear zone, which now corresponds to the High-Grade Zone, and precipitated Pd in the form Pd-bismuthotelluride, Pd-antimonide, Pd-arsenide, Pd-sulfide and Pd-telluride.

Introduction

The Pd-deposits of the Lac-des-Iles-Complex (LDIC) in northwestern Ontario (Fig. 1) differ from most platinum-group element (PGE) deposits in a number of ways. Most PGE ore deposits occur as stratiform narrow layers within large layered intrusions e.g the Merensky and UG-2 reefs of the Bushveld Complex, (Viljoen 1999; von Gruenewaldt 1986), the JM reef of the Stillwater Complex (Zientek et al. 2002), the Main Sulphide Zone of the Great Dyke (Obethur 2002). In contrast, the Pd deposits of the LDIC, the Twilight, Roby and High-Grade Zones, are all fairly wide and occur within a small concentrically zoned intrusion (Fig. 2; Lavigne and Michaud 2001). The host rocks of most PGE-deposits are fairly primitive; chromite layers, pyroxenites or melanogabbronorites or troctolites. The host rocks to the LDIC Pd-deposits are generally more evolved; gabbronorites and metagabbronorites in the Twilight and Roby Zones and actinolite-chlorite schists in the High-Grade Zone (Lavigne and Michaud 2001; Gomwe 2008). Most of the LDIC host rocks have undergone uralitization (Watkinson et al. 2002). In contrast while some alteration is present in the Bushveld reefs (e.g. Li et al. 2001) and JM reef (Godel and Barnes 2007) it is not very extensive. In the Roby and Twilight Zones the rocks are magmatic breccias with both the matrix and the fragments showing a wide range in textures from pegmatoidal to homogeneous and fine grained.

While many PGE-deposits have pegmatoidal portions most do not contain magmatic breccias. Finally, the LDIC Pd-deposit has unusually high Pd/Ir ratios (Brugmann et al. 1989; Hinchey et al. 2005) as compared to stratiform deposits (Naldrett 2004).

The presence of the uralitization, the pegmatoidal textures and the very high Pd/Ir ratios have led some authors (e.g. Dunning 1979; Lavigne and Michaud 2001; Watkinson et al. 2002) to propose models that the magma at LDIC was infiltrated by fluids and these late magmatic fluids enriched the ore zones in Pd. In contrast, other workers (Brugmann et al. 1989; Naldrett 2004) favoured a model whereby a magmatic sulfide liquid collected the PGE. Recent work (Hinchey and Hattori 2005; Gomwe 2008) suggested that both processes occurred. In the Twilight and Roby Zones, the positive correlation between S, PGE, Au, Cu and Ni suggested that the phases controlling the PGE are base metal sulphides (BMS). In contrast, in the High-Grade Zone Pd and Pt do not correlate with S, while Cu and Ir do (Hinchey et al. 2005; Gomwe 2008) suggesting that some other phase is controlling Pd and Pt in these zones. The rocks of the High-Grade Zone are chlorite-actinolite schist. They are more altered and deformed than those of the other two zones. This has led to the suggestion that Pd, and to a lesser extent Pt, was added to this zone by late magmatic fluids (Hinchey et al. 2005; Gomwe 2008).

If the mineralization in the least altered rocks is magmatic, then the PGE should be controlled by pyrrhotite, pentlandite and chalcopyrite. In particular Pd should be controlled by pentlandite (Barnes et al. 2008; Godel and Barnes 2008). During deuteric alteration and metamorphism the PGE have been shown to exsolve from the BMS and

Pd could be remobilized on the local scale into Pd-Bi-Te bearing minerals (Barnes et al. 2008). Thus in the metagabbronorite we suggested that, the PGE might be present in PGM within the BMS with minor Pd present as Bi-Te phases around the sulfides. If Pd has been added to the High-Grade Zone by late deuteric fluids the Pd could be present in PGM not associated with sulfides.

In order to test whether there is a relationship between the mineralogy and texture of the sulfide minerals, with the alteration of the silicate minerals, and to determine which phases control Pd in LDIC we have carried out a petrographic study combined with an image analysis of the silicate and sulfide mineralogy, the platinum-group element mineralogy and determined the chalcophile and PGE element concentrations of the BMS of samples ranging from the relatively fresh gabbronorite to metagabbronorite to the chlorite-actinolite schist.

Geology

Geological context

The ultramafic to mafic LDIC intrusions (2689±1 Ma; Stone et al. 2003) is exposed in the southern part of the Lac des Iles, located approximately 80 km north of the city of Thunder Bay, Ontario (Fig. 1). The Complex intrudes Archean tonalic gneiss (U–Pb zircon ages ranging from 2722 to 2775 Ma; Stone et al. 2003) of the southern Wabigoon Subprovince (western Superior Province). The tonalitic gneiss outcrops along the boundary with the metasedimentary belt of the Quetico Subprovince (Pye 1968; Sutcliffe 1988; Brugmann 1997). The LDIC is the largest of a series of ultramafic to

mafic bodies, which include the Intrusion at Legris Lake, the Intrusion at Tib Lake, the Intrusion at Wakinoo Lake and the Intrusion at Buck Lake, which together define a circular pattern in the Lac des Iles area that is approximately 30 km in diameter (Lavigne and Michaud 2001; Hinchey and Hattori 2005; Fig. 1).

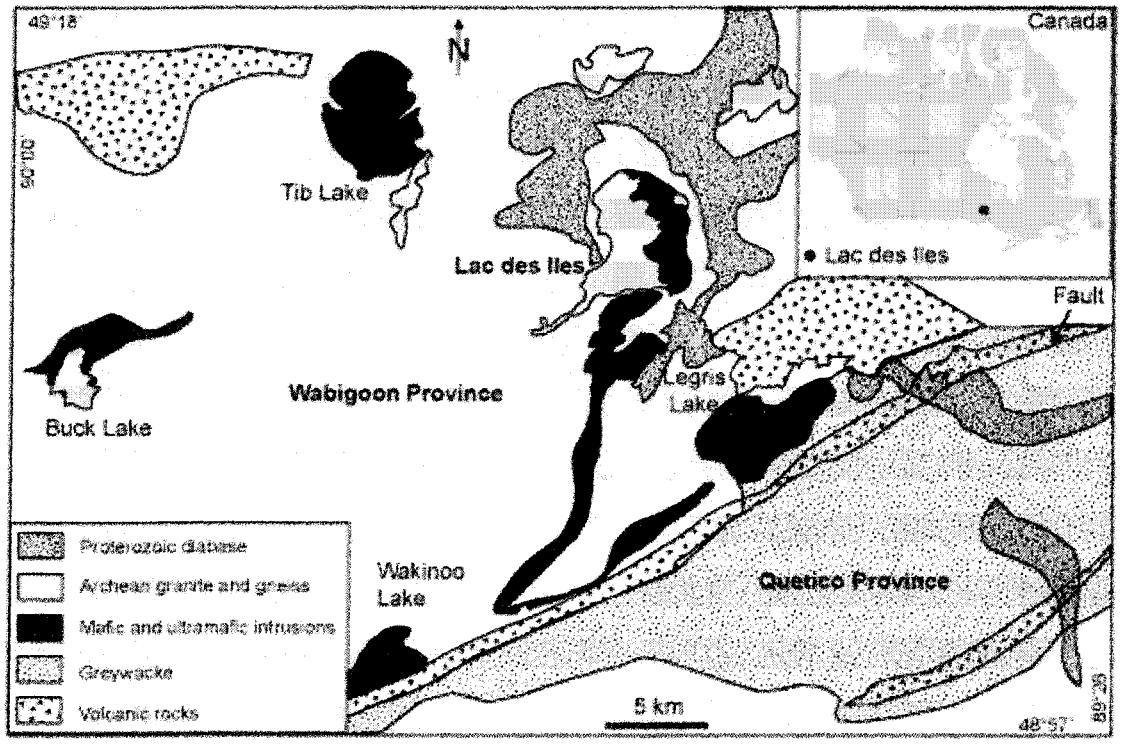

Figure 1. Location map of the Lac-des-Iles-Complex, north of Thunder Bay, Ontario, modified after Hattori and Cameron (2004).

The LDIC is sub-divided into three distinct magma chambers on the basis of its rock types (Brugmann et al. 1989; Lavigne and Michaud 2001; Fig. 2): i) the North Lac

des Iles Intrusion is predominantly ultramafic with a minor mafic component. It is composed of clinopyroxenites, websterites and gabbronorites (Brugmann et al. 1989; Lavigne and Michaud 2001); ii) the Mine Block Intrusion is texturally and compositionally complex with composition ranging from anorthosite, through leuco- to melano-gabbronorites and includes magnetite-rich gabbronorite (Lavigne and Michaud 2001; Watkinson et al. 2002), iii) the Camp Lake Intrusion is homogeneous in composition and consists of hornblende gabbros (Brugmann et al. 1989; Lavigne and Michaud 2001; Michaud and Lavigne 2003).

The Pd-mineralization occurs within magmatic breccias of gabbronorite with various textures and in chlorite actinolite schist. The breccias contain a small quantity of sulfide minerals (typically < 3% modal) and exceptionally high Pd/Pt and Pd/Ir ratios compared to other PGE deposits (Pd/Pt ratio ~ 10, Pd/Ir ratios ~ 10 000; Brugmann et al. 1989; Naldrett 2004; Hinchey et al. 2005). Other major PGE deposits, such as the Merensky Reef and the Stillwater Complex, typically have Pd/Pt ratios (0.5 to 3; Barnes and Naldrett 1985; Barnes and Maier 2002; Godel et al. 2007; Godel and Barnes 2008) much lower than those of the LDIC.

In 2009, the company web site napalladium.com reports 36 million tonnes of measured and indicated resources with a grade of 3.18g/tonne Pd and 0.26 g/tonne Pt.

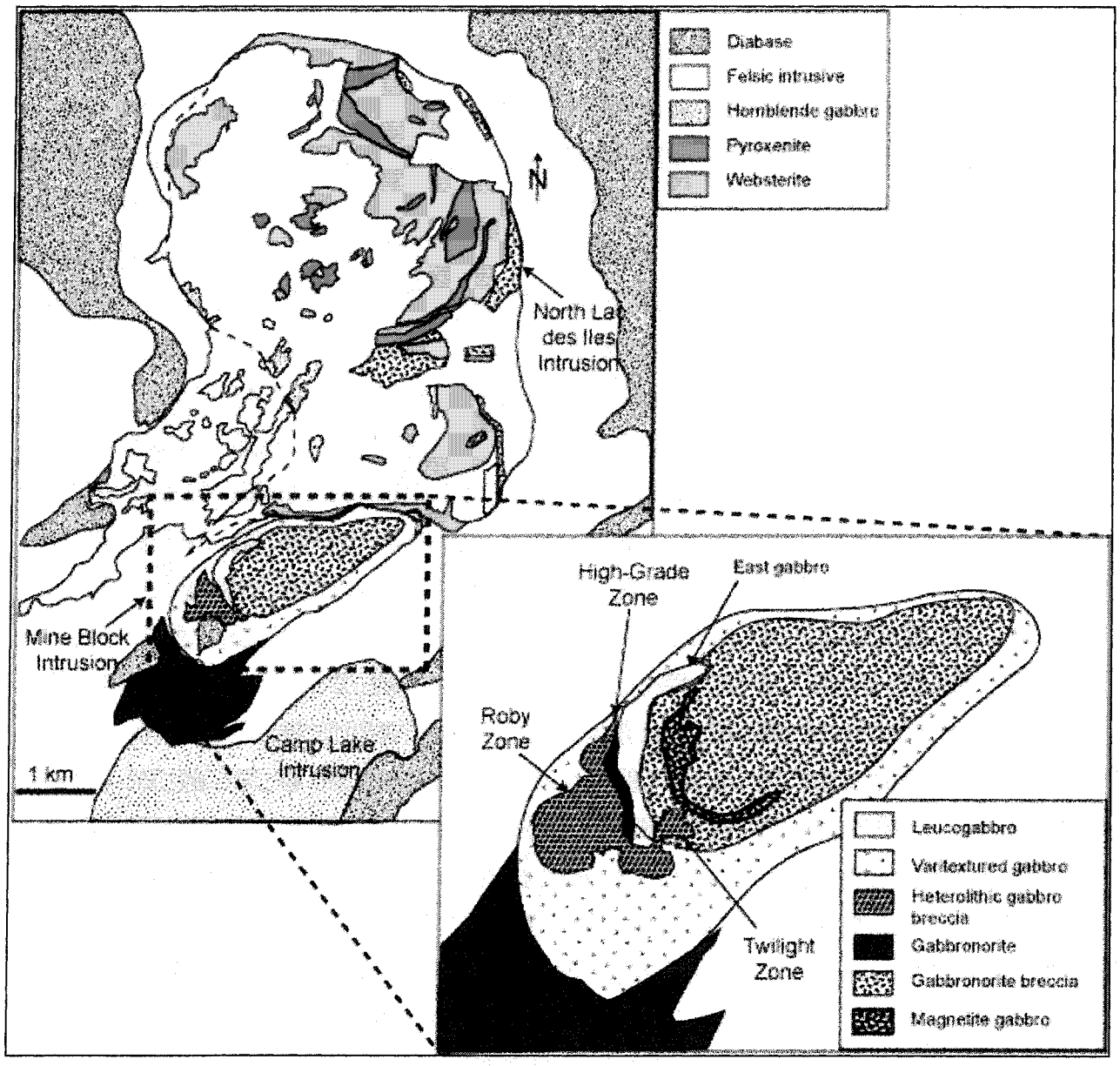

Figure 2. Geology of the Lac-des-Iles-Complex. Simplified geological map of the Mine Block Intrusion which include Roby, Twilight and High-grade zones modified from Lavigne and Michaud (2001) and Watkinson et al. (2002).

The Twilight Zone is weakly to moderately altered and primary magmatic minerals, such as orthopyroxene and plagioclase, are well preserved. In contrast, alteration of the Roby Zone is pervasive, particularly in the mineralized mafic rocks and the primary minerals are replaced to various degrees by amphibole, chlorite, sericite and calcite (Lavigne and Michaud 2001; Hinchey and Hattori 2005; Gomwe 2008). The rock composition of both zones ranges from gabbronorite to metagabbronorite (Gomwe 2008). The breccia is texturally complex and includes vari-textured gabbro and heterolithic gabbro breccia (Michaud 1998; Dionne-Foster 2002; Michaud and Lavigne 2003). Palladium mineralization is present in both brecciated-gabbronorite and brecciated-metagabbronorite (Lavigne and Michaud 2001; Hinchey et al. 2005; Gomwe 2008). Both zones are intruded by felsic dykes which are barren of mineralization.

The High-Grade Zone defined on the basis of Pd grade (> 4ppm Pd) is a Pd-rich shear zone, 15-25m wide and 400 m long, along the contact of the Roby Zone and the East Gabbro (Fig. 2B). Hinchey and Hattori (2005) described the High-Grade Zone as an intensely altered rock that underwent alteration down to fairly low temperatures. More recently Gomwe (2008) showed that this zone varies from micro-brecciated metagabbronorites to actinolite-chlorite schist. At the level currently exposed, most of the High-Grade Zone is dominated by actinolite-chlorite schist ± talc enriched in Pd. The sulfide mineralisation (0.1 - 1% vol.) is not stratabound and is hosted in both micro-brecciated metagabbronorites and actinolite-chlorite schist (Gomwe, 2008).

In the present study, we have investigated 16 samples (Table 1) selected from the 93 originally investigated by Gomwe (2008). The basis for the selection was that: i) they

are mineralized, i.e. Pd content > 100 ppb; ii) the selection cover all 3 zones; iii) There is a range in degree of alteration and deformation

Analytical Techniques and Methodology

Petrographic investigations of silicate and sulfide minerals were carried out on hand specimens, polished thin sections and polished blocks using an Olympus DP71 microscope, digital camera at the Université du Québec à Chicoutimi (UQAC). In order to determine the assemblages of BMS present and to quantify the proportions of the different sulfide minerals we first examined and photographed sulfide blebs (n=478) on 16 polished thin sections. The total area covered by the sulfide blebs ranges from 0.1 to 16 mm^2 for a thin section of 1000 mm^2. The image analysis software (ImagePro Plus) was used to determine area of the various sulfide and oxide minerals using their different colors and reflectivity. The modal percentages (F) of each opaque phase (i) in the samples were calculated using the following equation:

$$\mathbf{Fi = [Ai / (A_{sulf}+A_{ox})]*100}$$

Table 1. Summary of results of image analysis of base metal sulfides from the Lac-des-Iles-Complex

Sample	Zone	Rock Type	Assemblage type	N.b.	N.p	A_{sul} (mm^2)	A_{ox} (mm^2)	A (mm^2)	F_{Po} %	F_{Pn} %	F_{Ccp} %	F_{py} %	F_{mil} %	F_{Mag} %	F_{ilm} %
Tz 1	Twillight	gabbronorite	Po-Ccp-Pn±Py	27	27	6.72	1.76	1000	39.9	12.3	24.7	2.11	0.00	20.8	0.00
Tz 7	Twillight	gabbronorite	Po-Ccp-Pn±Py	44	54	9.72	4.41	1056	50.1	1.43	14.6	2.50	0.00	25.5	5.68
Tz 10	Twillight	gabbronorite	Po-Ccp-Pn±Py	36	39	13.04	0.43	1100	46.9	9.65	40.0	0.09	0.00	2.58	0.66
Tz 15	Twillight	metagabbronorite	Py-Ccp-Pn	30	32	5.31	0.28	1000	1.39	6.45	30.3	56.6	0.00	5.16	0.00
Tz 19	Twillight	gabbronorite	Po-Ccp-Pn±Py	52	36	6.76	0.20	1025	55.02	14.7	26.4	0.81	0.00	2.94	0.00
Tz 21	Twillight	metagabbronorite	Py-Ccp-Pn	27	34	5.89	0.12	1025	1.78	7.59	52.5	35.9	0.00	2.04	0.00
Tz28	Twillight	metagabbronorite	Py-Ccp-Pn	9	11	13.8	0.02	1050	0.00	10.8	44.6	44.4	0.00	0.17	0.00
Rz 3	High-grade	chlorite-actinolite schist	Py-Ccp±Mil	8	5	10.05	0.05	1066	0.001	0.02	20.2	78.5	0.05	0.001	0.00
Rz 8	High-grade	chlorite-actinolite schist	Py-Ccp-Mil	6	14	16.1	0.37	1066	0.06	0.00	2.15	94.5	0.92	2.28	0.00
Rz 13	High-grade	chlorite-actinolite schist	Py-Ccp-Mil	9	12	0.74	2.42	1000	0.003	0.01	1.86	21.70	0.00	37.8	38.6
Rz 17	High-grade	chlorite-actinolite schist	Py-Ccp-Pn	10	25	12.6	0.11	1071	0.19	23.2	63.0	12.6	0.00	0.87	0.00
Rz 26	Roby	metagabbronorite	Py-Ccp-Mil	26	34	7.50	0.09	1066	4.47	0.94	13.4	68.5	10.4	2.05	0.00
Rz 30	Roby	gabbronorite	Po-Ccp-Pn±Py	35	33	6.69	0.09	1092	71.5	11.1	15.4	0.47	0.00	1.42	0.00
Rz 45	Roby	gabbronorite	Po-Ccp-Pn±Py	26	40	7.74	0.28	1092	46.6	23.1	18.9	7.77	0.00	3.57	0.00
Rz 54	Roby	metagabbronorite	Py-Ccp-Mil	24	30	15.7	0.40	1066	0.09	0.00	10.5	64.5	22.2	2.53	0.00
Rz 50	Roby	metagabbronorite	Py-Ccp-Mil	9	23	7.95	0.03	1066	0.02	2.43	8.90	88.1	0.01	0.48	0.00

Abbreviations: N.b. = Number of blebs by sample, N.p = Number of pictures analyzed by sample, A_{sul} = Total area of sulfide phase, A_{ox} = Total area of oxides, A = Total area of the thin section. F_{Po}= percentage of pyrrhotite in opaque phase, F_{Pn} = percentage of pentlandite in opaque phase, F_{Ccp} = percentage of chalcopyrite in the opaque phase, F_{Py} = percentage of pyrite in opaque phase, F_{Mil} = percentage of millerite in opaque phase, F_{Mag} = percentage of magnetite in opaque phase, F_{Ilm} = percentage of ilmenite in opaque phase.

where (Ai) is the total area of the phase i in the image, (A_{sulf}) is the total area of the sulfide phases (mm^2) and (A_{ox}) is the total surface of the oxide phases of the same sample (mm^2). The results of the image analysis are presented in Table 1. The oxide phases were also taken into account to establish their mutual relationship with the sulfide phases. Whole-rock sulfur was determined using an infrared Horiba EMIA 220V sulfur and carbon analyser at UQAC, following the method described by Bedard et al. (2008). The detection limit is ~ 10ppm and the relative standard deviation (RSD) is less than 5% for samples with more 500µg/g of S. The PGE and Au in the whole rock were determined by Ni-sulfide fire assay and Te co-precipitation followed by ICP-MS solution analysis using the technique described in Savard et al. (accepted). An in-house quality control reference material (BB-235) was analyzed with the unknown samples; the PGE and Au results are in good agreement with the working values obtained by both fire assay and isotopic dilution analysis (Savard et al. accepted; Table 2). Whole rock Ni, Cu, Co, Ag, Zn, and As concentrations were determined by Gomwe (2008). The whole rock concentrations are presented in Table 2. Major elements of the minerals were determined by electron microprobe analysis using wavelength dispersive X-ray emission spectrometry using a Cameca SX 100 at Laval University, Québec City. Operating conditions were 15.0 kV accelerating voltage, 20.0 nA beam current, and a beam diameter of 2 to 5 µm, with a counting time of 20 s and 10 s on peaks and backgrounds, respectively. Calibration reference materials used were from the Mineral Standard Mount MINM25-53 of Astimex Scientific Limited.

Table 2. whole rock composition of samples from the Pd-deposits of Lac des Iles Complex.

SAMPLE	Zone	Rock Type	Os ppb	Ir ppb	Ru ppb	Rh ppb	Pt ppb	Pd ppb	Au ppb	S ppm	Ni ppm	Cu ppm	Co ppm	Zn ppm	Ag ppm	As ppm	Sb ppm	LOI wt%	Pd/Pt
Tz 1	Twillight	gabbronorite	1.31	0.6	3.88	8.93	589	5610	405	8986	1530	2800	81	56	1.5	0.4	0.02	0.9	8.6
Tz 7	Twillight	gabbronorite	0.55	0.27	1.93	4.61	240	1779	101	3055	909	1155	81	74	0.5	0.4	0.07	0.81	5.9
Tz 10	Twillight	gabbronorite	0.24	0.13	0.75	2.16	139	1225	113	1934	1160	1815	78	54	1.5	0.9	0.06	0.65	7.7
Tz 15	Twillight	metagabbronorite	0.79	0.40	2.59	6.95	410	3640	271	5648	1355	1835	92	96	1.5	1.2	0.09	3.98	7.2
Tz 19	Twillight	gabbronorite	1.35	0.71	4.08	10.5	527	5096	376	8531	1845	2810	104	76	1.5	0.2	0.02	1.06	8.2
Tz 21	Twillight	metagabbronorite	1.6	0.83	4.95	11.4	773	5472	523	9986	2330	3160	100	60	2.0	0.4	0.48	4.53	6.01
Tz28	Twillight	pegmatite	0.24	0.14	0.70	1.68	148	1059	113	1930	11	n.d.	363	n.d.	0.4	0.11	0.06	2.52	7.8
Rz 3	High-grade	chlorite-actinolite schist	0.29	0.13	0.62	1.153	265	6897	41	123	916	2	80	37	0.5	0.7	1.37	4.99	20.5
Rz 8	High-grade	chlorite-actinolite schist	1.002	0.37	2.17	4.64	730	8928	137	348	718	144	75	4	0.5	1.3	0.62	4.79	9
Rz 13	High-grade	chlorite-actinolite schist	1.8	0.13	5.7	n.d.	237	4133	2491	121	793	60	85	96	0.5	0.6	0.39	4.98	17.4
Rz 17	High-grade	chlorite-actinolite schist	2.06	0.95	4.05	8.63	2213	52490	2003	8011	2684	1998	96	8	2.0	3.1	0.12	3.29	17
Rz 26	Roby	metagabbronorite	0.07	0.04	0.21	0.50	33	262	41	1287	272	361	45	47	0.5	0.5	0.14	2.29	6.7
Rz 30	Roby	gabbronorite	0.37	0.29	0.72	0.49	41	268	41	792	1719	2470	128	68	1.5	0.6	0.07	2.7	6.3
Rz 45	Roby	gabbronorite	2.45	1.09	6.26	13.7	1312	12900	1024	14512	3285	3465	167	n.d.	2.9	1.4	0.16	3.47	9.8
Rz 50	Roby	metagabbronorite	0.41	0.26	1.37	2.65	185	1481	177	5163	983	1757	102	82	0.8	0.8	0.04	3.28	10.8
Rz 54	Roby	metagabbronorite	0.57	0.31	1.51	2.95	406	3174	260	5314	1188	2033	91	13	0.5	1.2	0.27	3.11	6.9
[1]UQAC reference material																			
This study (n=3)			0.17	0.12	1.84	1.57	15.58	15.45	1.18										
Std			0.04	0.01	0.12	0.11	0.97	0.79	0.52										
Working value			0.18	0.12	1.85	1.57	15.50	15.42	1.10										
Std			0.04	0.01	0.12	0.11	0.95	0.76	0.49										

Abbrevation: [1]UQAC = BB-235 for the PGE and AU.

The isotopes (^{59}Co, ^{61}Ni, ^{65}Cu, ^{66}Zn, ^{75}As, ^{77}Se, ^{101}Ru, ^{103}Rh, ^{105}Pd, ^{107}Ag, ^{111}Cd, ^{121}Sb ^{128}Te, ^{185}Re, ^{189}Os, ^{193}Ir, ^{195}Pt, ^{197}Au, ^{209}Bi,) were determined in each BMS using the laser ablation inductively-coupled plasma mass spectrometer (LA-ICP-MS) on polished blocks at UQAC. The laser at UQAC is a New Wave Research UP 213 nm Nd:YAG UV. The laser frequency was 10 Hz and a beam size of 40 μm was used. Each mineral analysis took 90s with 30s of gas blank and 60s for mineral analysis. A helium carrier gas mixed with argon was used. The ablated material was analyzed using a Thermo X7 quadrupole ICP-MS operating in time resolved mode using mass jumping with a dwell time of 10 ms/peak. Sulfur (^{34}S) was used as internal standard.

Sulfide reference materials were used to calibrate and monitor data quality of the LA-ICP-MS analyses. Laflamme (Po727, supplied by Memorial University) is a synthetic FeS phase doped with ~45 ppm PGE and Au and was used to calibrate for PGE and Au (Table 3). Copper, Co, Zn, As, Se, Ag, Sb and Cd were calibrated using a pressed Fe-Zn-Cu-S pellet. MASS-1 supplied by the US Bureau of Standards (Wilson et al. 2002). Nickel was calibrated using the synthetic Ni-blank, for which the Ni has been determined by microprobe. Rhenium, Te and Bi were calculated using the semi-quantitative calibration option of PlasmaLab software. In-house reference materials JB MSS-5 (FeS) doped with 20-100 ppm As, Se, Sb, PGE, Ag, Re, Au, Bi and PO 62 (FeS) were used to monitor the results. The results for the monitors agree within analytical error with UQAC working values given in Table 3. Each reference material was placed with unknowns (BMS in the thin sections) in the

ablation chamber and was analysed at the beginning, after 15 analyses of unknowns and at the end of each analytical session.

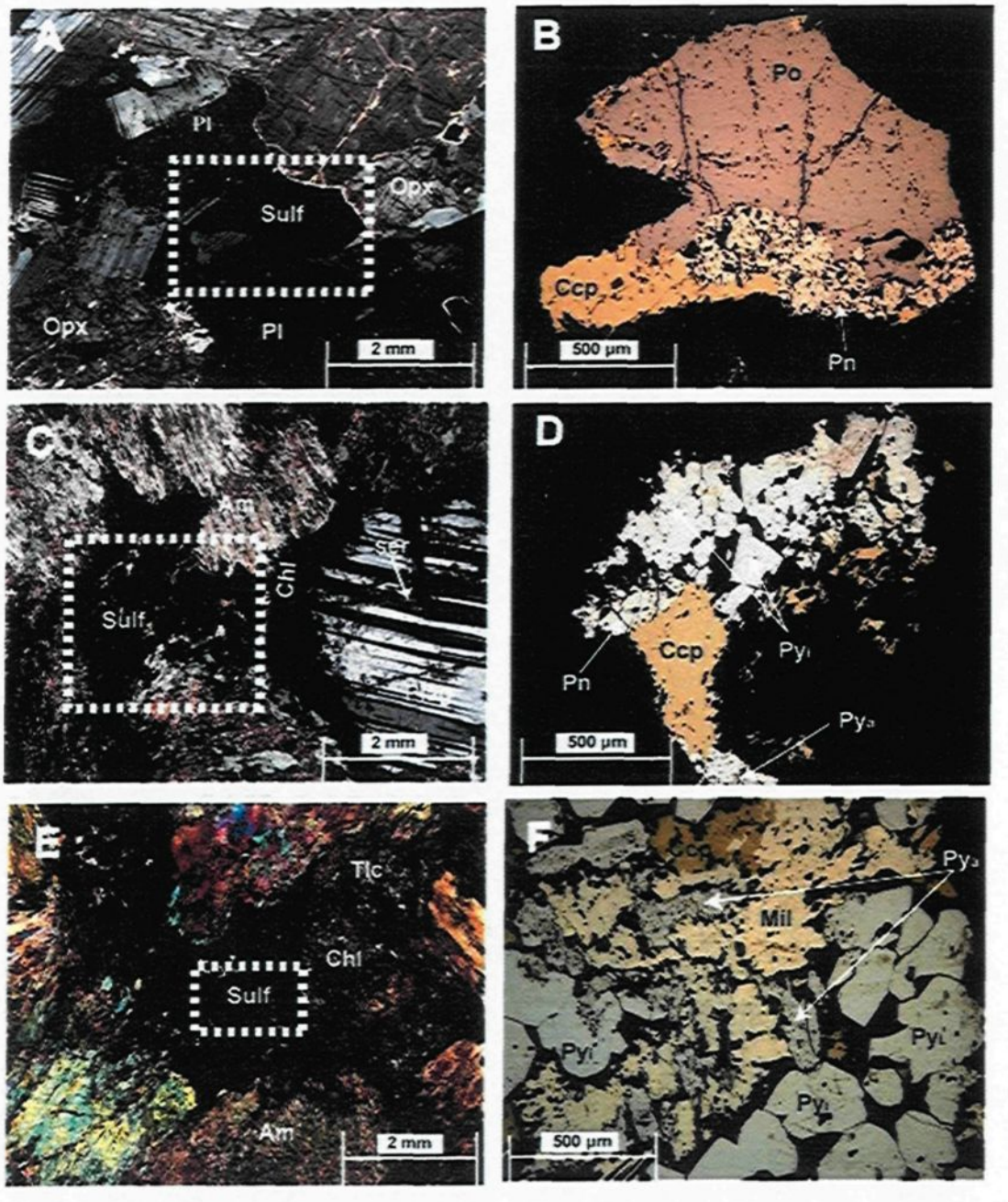

Figure 3. Photomicrographs of silicate and sulfide (Sulf) assemblages in transmitted and reflected light. (**A**) Orthopyroxene (Opx), plagioclase (Pl) and minor amphibole (Am) are associated with pyrrhotite (Po), pentlandite (Pn), chalcopyrite (Ccp) in (**B**). (**C**) Amphibole, plagioclase, sericite (Ser) and chlorite (Chl) are associated with anhedral pyrite (Pya), idiomorphic pyrite (Pyi), Ccp and Pn in (**D**). (**E**) Chlorite, amphibole and talc (Tlc) are associated with Pya, Pyi, Ccp and millerite (Mil) in (**F**).

Table 3. Reference materials used in the calibration of LA-ICP-MS and to monitor data quality.

		JB Mss-5 This study Avg n=16	Std	JB Mss-5 UQAC Working value	Std	Po-62 This study Avg n=20	Std	Po-62 UQAC Working value	Std
57 Fe	%	56.8	1.7	57.4	0.9	60.8	2.02	61.81	0.25
59Co	ppm	0.31	0.08	0.3	0.07				
61Ni	ppm	11452	583	10487	140				
65Cu	ppm	281	59	206	6.2				
66Zn	ppm	18.2	5.3	<10					
75As	ppm	74.9	16.5	79	11				
77Se	ppm	70.3	12.4	47	1.6				
101Ru	ppm	21.0	1.41	21.7	3	1.34	0.12	1.43	0.05
103Rh	ppm	57.8	4.06	61.4	7.2	1.07	0.09	1.25	0.02
105Pd	ppm	57.2	3.79	64.1	5.1	1.07	0.20	1.60	0.13
107Ag	ppm	60.0	3.08	60.7	3.7				
111Cd	ppm	0.22	0.06	0.13	0.06				
121Sb	ppm	63.7	6.29	61.3	7.3				
128Te	ppm	67.3	6.69	69.8	3.0				
185Re	ppm	18.6	1.02	20.7	1.8	1.67	0.16	0.49	0.01
189Os	ppm	62.1	5.33	42.5	0.3	1.24	0.07	1.39	0.27
193Ir	ppm	42.0	2.89	43.1	0.7	0.97	0.03	1.53	0.04
195Pt	ppm	35.5	3.23	39.9	1	1.55	0.13	1.63	0.13
197Au	ppm	35.1	3.01	35.9	4.8				
209Bi	ppm	83.7	4.88	76.1	2.9				

Arsenic, Rh, Sb, Os, Au, Bi, by ICP-MS on aqua regia solution. Ruthenium, Pd, Ir, and Pt by isotope dilution. Nickel by atomic absorption. Cobalt, Zn, Se, Ca, by LA-ICP-MS using NITS-610 and Cu as an internal standard. Fe and Cu by LA-ICP-MS using Po 727 for Fe and the Cu blanck for Cu. Tellurium in semi-quantitative. Abbreviations: Avg. = average, Std = standard deviation, n = number of grains

Nickel and Cu argide interferences on ^{101}Ru (^{61}Ni), ^{103}Rh and ^{105}Pd (^{63}Cu and ^{65}Cu) were monitored and corrected using a synthetic PGE-free $NiFeS_2$ and $CuFeS_2$ blanks. Cadmium (^{111}Cd) was also monitored to correct for interference on ^{108}Pd and ^{106}Pd.

Data reduction was carried out using PlasmaLab software (Thermo Elemental) by subtracting the gas background from each of the analyzed isotopes. The results for the BMS from LDIC are given in Table 4. The detection limits of each element, defined as 3 times the standard deviation of the gas blank, are presented in Table 4. The concentrations of Ni and Cu were monitored to verify that the signal was generated by only one mineral because the analyzed BMS are intergrowths of pyrrhotite, pentlandite, chalcopyrite, pyrite and millerite.

The platinum-group minerals (PGM) were located in 9 polished thin sections and polished blocks using a CAMECA SX100 electron microprobe. The PGM were characterized using energy dispersive spectra. Quantitative analyses were only performed on the largest PGM (>5 μm in size). Backscattered electron (BSE) images were taken for each PGM, and the area measured using Image Pro software using a similar approach to that of Godel et al. (2007).

Results

Petrography

The least altered rocks based on the presence of igneous minerals and textures are the gabbronorites.

The gabbronorites are adcumulates of orthopyroxene and plagioclase (Fig. 3A). Orthopyroxene (1-3 mm) and plagioclase (2-5 mm) grains are generally subhedral or rounded. The anorthite content of plagioclase varies from 0.61 to 0.84 (Table A1). Orthopyroxene compositions are $Wo_3En_{68}Fs_{28}$ or $Wo_3En_{69}Fs_{28}$ (Gomwe 2008). Most grains of plagioclase are slightly altered to sericite, chlorite, and epidote along fractures (Fig. 3A). Alteration of orthopyroxene to amphibole occurs along fractures and at the contact with clinopyroxene exsolution lamellae (3 modal %). Compositions of amphibole range from actinolite to magnesiohornblende (Fig. 4). Magnesiohornblendes have higher TiO_2 concentrations (on average 0.6 wt %) than actinolite (on average 0.17 wt. %; Table A2).

The modal percentage of sulfides varies in from approximately 0.6 to 1.2. The base metal sulfides (BMS) consist of blebs of pyrrhotite (Po; 51 modal %), chalcopyrite (Ccp; 23 modal %), pentlandite (Pn; 12 modal %; Fig. 3B) with minor pyrite (Py; 2 modal %). The rocks that hosted this assemblage will be referred to as A_1. Grains of pyrite are anhedral and occur at the border between pyrrhotite and pentlandite, or are included in pyrrhotite. The boundaries of the sulfide blebs against the primary igneous minerals are gently curved indicating equilibrium conditions (Fig. 3A, 3B). A small quantity of ilmenite and magnetite (up to 6 modal %) are associated with the sulfides.

The metagabbronorites have magmatic textures, but the pyroxene has been completely replaced by amphibole and the plagioclase has been partly replaced. All of the samples still contain some plagioclase (5 – 35 modal %). Alteration of

plagioclase ranges from moderate to pervasive sericitization. The plagioclase compositions cover the range from anorthite 0.67 to 0.79. The amphibole grains are mainly actinolite (Fig. 4).

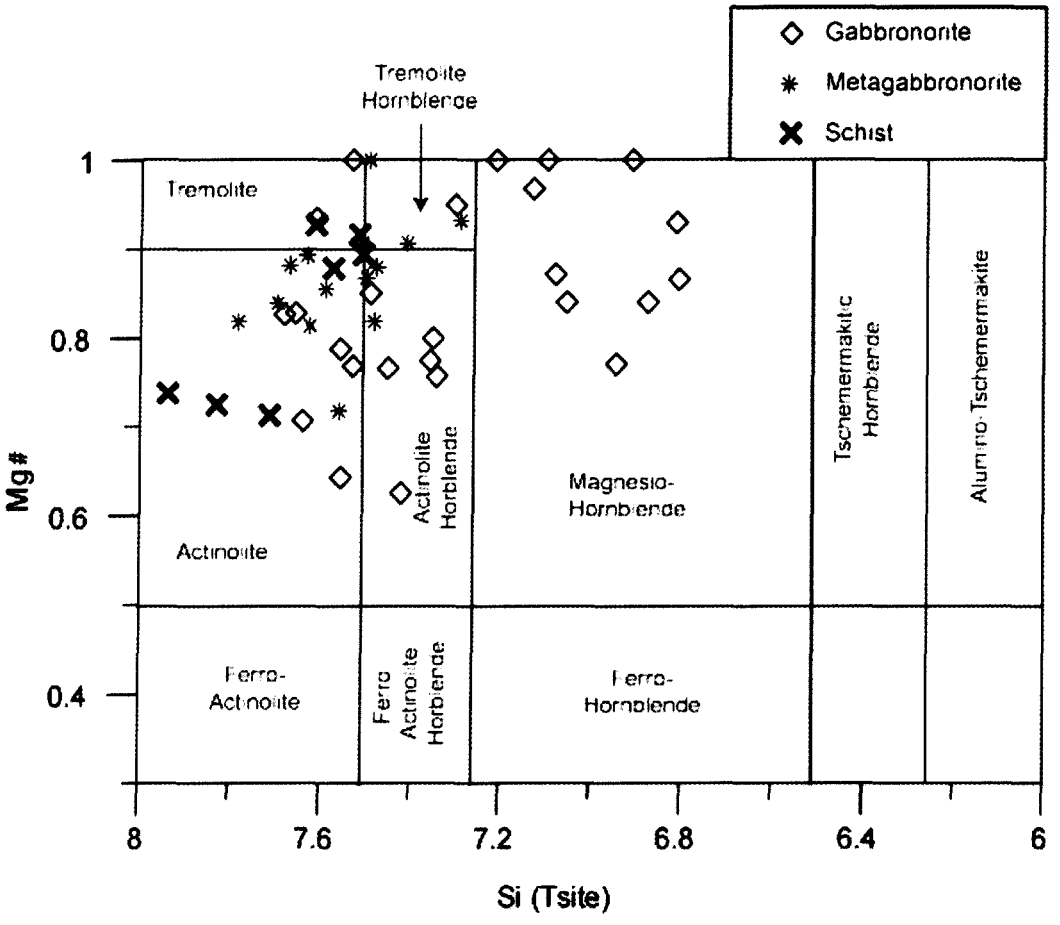

Figure 4. Classification diagram for calcic amphiboles where (Na+K)A < 0.50 and Ti < 0.50 modified from Leake et al. (1997).

Actinolite occurs as 1) aggregates of acicular grains that pseudomorph pyroxene or, 2) as fibrous, intergranular aggregates associated with talc-carbonate, chlorite, and epidote alteration assemblages.

The percentage of sulfides vary approximately from 0.5 to 1.4 modal % (Table 2). Two different sulfide assemblages are present. The first consists of pentlandite (12 %), chalcopyrite (47 %), pyrite (37 %), with minor pyrrhotite (< 1%; Fig. 3D). The rocks with this assemblage will be referred to as A_2. Pyrite displays two types of textures (Fig. 3D). The first is anhedral (Py_a) and similar to pyrite from A_1. The second, and most common pyrite, is idiomorphic (Py_i) and forms a corona texture associated with the remobilized chalcopyrite and the pentlandite (Fig. 3D). The BMS are located predominantly in fractures and along the boundaries between grains of altered orthopyroxene, as well as within fractures in plagioclase. The boundaries of BMS with secondary minerals (e.g., amphibole, chlorite) are interdigitated indicating textural disequilibrium conditions. Trace amounts of magnetite (0.5 modal %) occur in the gangue as very finely disseminated grains or at boundaries between sulfide and silicate grains.

The second sulfide assemblage present in the metagabbronorite consists dominantly of pyrite (67%), chalcopyrite (10%), and millerite (7%) (Fig. 3F). Pentlandite and pyrrhotite concentrations are both below 2%. Chalcopyrite grains are completely remobilized and are generally intergrown with silicate minerals. Both anhedral and idiomorphic pyrite grains are present. Anhedral pyrite, which is less abundant, is associated with millerite and chalcopyrite while euhedral pyrite, which is

more common, forms coronotic textures associated with the remobilized chalcopyrite and millerite (Fig. 3F). The rocks that host this assemblage will be referred to as A_3.

The chlorite-actinolite schists are from the High-Grade Zone, and compositionally they are olivine gabbronorites. The silicates are more intensely altered than in the metagabbronorite (Fig. 3E) and consist mainly of amphibole (30 to 50 modal %), chlorite (20 to 40 modal %) and talc (5 to 15 modal %) with minor plagioclase (1 to 5 modal %). The amphibole is actinolite (Fig. 4), and ranges in size from millimetre to 5cm long; it occurs as aligned fibres. Chlorite occurs as stubby, aggregates of grains interstitial to talc. The same two sulfide assemblages (Pn-Ccp-Py and Py-Ccp-Mil) as occur in the metagabbronorites, are also present in chlorite-actinolite schists.

Progressive change in the assemblages with alteration

Because the pyrrhotite-pentlandite-chalcopyrite ± pyrite assemblage occurs only in the fresh rocks and has equilibrium textures with the silicates, we interpret it to represent a magmatic sulfide assemblage. This sulfide assemblage is associated with the primary silicate assemblage of orthopyroxene-plagioclase ± clinopyroxene and has been preserved in the gabbronorites (Fig. 5). The pyrite-chalcopyrite-pentlandite and pyrite-chalcopyrite-millerite representing the post-magmatic sulfide assemblages and are associated successively with amphibole-plagioclase ± orthopyroxene and tremolite-chlorite-talc ± plagioclase assemblages (Fig. 5).

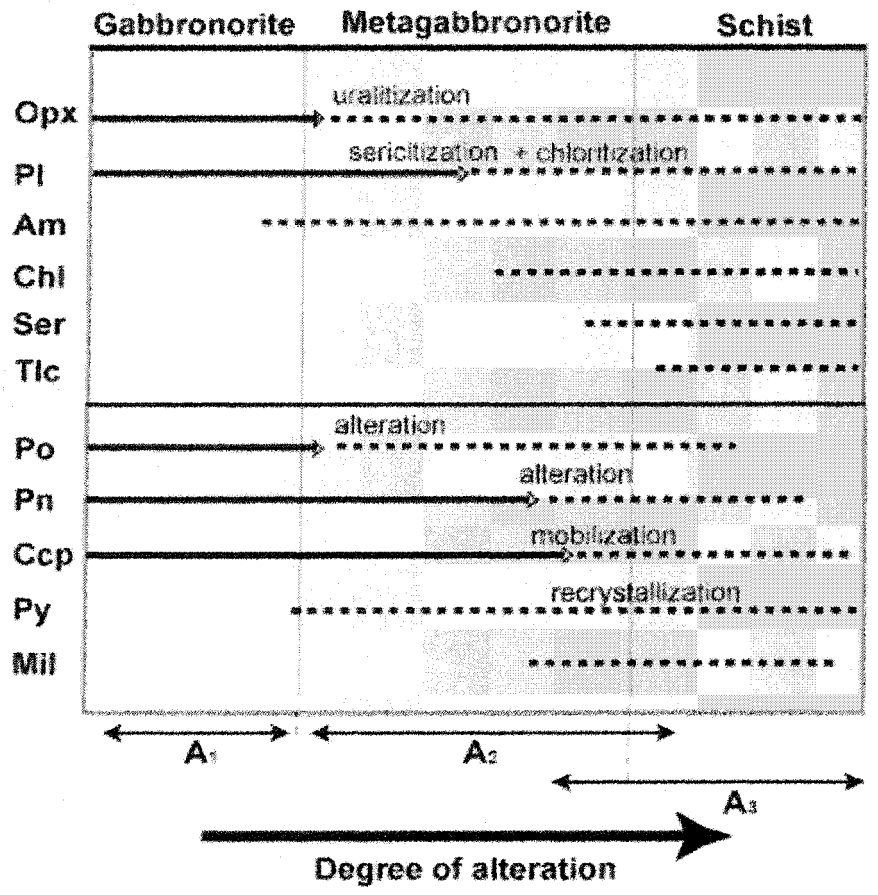

Figure 5. Evolution of mineral assemblages in gabbronorite, metagabbronorite and chlorite-actinolite schist as a function of the increasing degree of alteration. Opx = orthopyroxene, Pl = plagioclase, Am = amphibole, Chl = chlorite, Ser = sericite, Tlc = talc, Po = pyrrhotite, Pn = pentlandite, Ccp = chalcopyrite, Py = pyrite, Mil = millerite. A_1 = rocks with Po-Pn-Ccp±Py assemblage, A_2 = rocks with Pn-Ccp-Py assemblage and A_3 = rocks with Py-Ccp-Mil assemblage. Bold lines = primary minerals, dashed lines = secondary minerals.

Geothermometry

In order to characterize the stability of BMS assemblages relative to the other mineral assemblages present, the equilibrium temperatures for coexisting Ca-amphibole and plagioclase pairs in content were calculated using the geothermometer of Blundy and Holland (1990). The highest temperatures obtained for each rock type show a systematic decrease from the rocks that contain Po-Pn-Ccp±Py assemblage (A_1) (856 °C), through the rocks that contain Pn-Ccp-Py assemblage (A_2) (713 °C) to the rocks that contain Py-Ccp-Mil assemblage (A_3) (655°C). Similarily the lowest temperatures recorded by the amphibole-plagioclase pairs also decrease from 622 °C in A_1 to 417 °C in A_3 (Fig. 6).

In addition to the amphibole-plagioclase geothermometer, the Fe-Ni-S ternary diagram at 350°C was used to determine the process responsible for the sulphide change in mineral assemblage. The weight percent of Fe, Ni and S in the sulfide assemblage has been calculated from the modal analyses of pyrrhotite, pentlandite, pyrite and millerite in each rock from the equation:

$$\mathbf{W(x) = ((FPo/100)*XPo) + ((FPn/100)*XPn) + ((FPy/100)*XPy) + ((FMil/100)*XMil)}$$

where W(x) is the weight percent of element x, FPo is the modal percentage of pyrrhotite, XPo is the weight percent of element x in pyrrhotite, FPn is the modal percentage of pentlandite, XPn is the weight percent of element x in pentlandite, FPy is the modal percentage of pyrite, XPy is the weight percent of element x in pyrite, FMil is the modal percentage of millerite and XMil is the weight percent of element x

in millerite. Afterwards the weight percent of each element is recalculated to 100%. The results are presented on Figure 7.

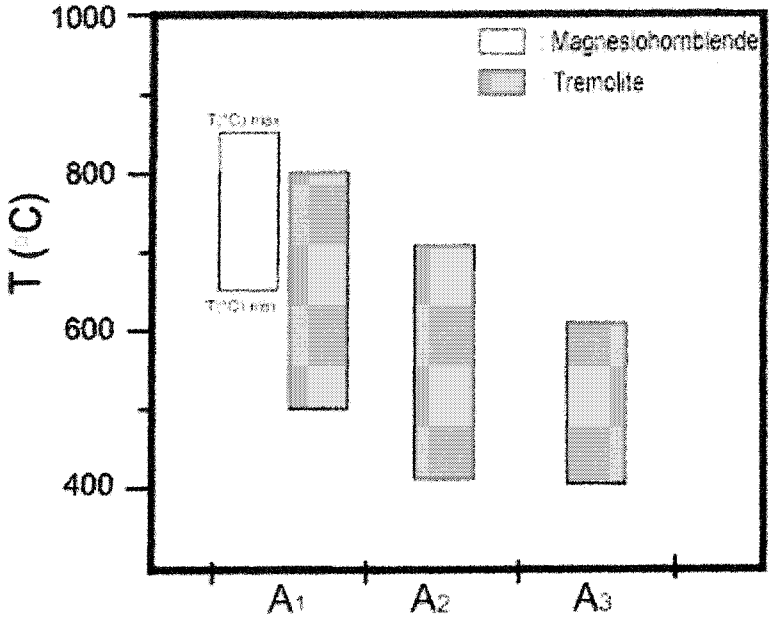

Figure 6. Equilibrium temperatures (T°C) obtained from rocks containing Po-Pn-Ccp±Py assemblage (A_1), rocks with Pn-Ccp-Py assemblage (A_2) and rocks with Py-Ccp-Mil assemblage (A_3) from the Lac-des-Iles-Complex using the Ca-amphibole and plagioclase geothermometer of Holland and Blundy (1990).

The A_1 samples fall in the field of primary ores (Barnes et al. 2009), but the A_2 and A_3 samples lie above this field (Fig. 7). This distribution of rock indicates that most of the A_2 and A_3 samples formed either by loss of Fe or by gain of S relative to initial magmatic ore. If the samples had gained S, then most of these rocks should be richer in S than the A_1 rocks, but it is not the case. Therefore, we consider the loss of Fe to be the most likely cause and probably occurred during alteration as suggested by Barnes et al. (2009) for the Black Swan disseminated nickel sulfide deposit in Australia.

Distribution of chalcophile elements in whole rocks

The concentrations of S, Ni, Cu, PGE, Ag, As, Au, Co, Re, Sb and Zn are listed in Table 2. The average S content for each assemblage is similar and low at ~ 0.6 wt. %, which represents approximately 1.5 modal % BMS. The High-Grade Zone samples have the lowest S content (0.012 wt. %) compared to other zones (0.5 - 1.5 wt. %). In addition Pd, As, and Sb concentrations are 2 to 3 times higher in this zone than the others. However the concentrations of Ni, Cu, Co, and Ir are similar for all samples. Silver concentration varies from 0.5 to 2 ppm in rocks. Osmium, Rh and Ru contents are very low in all samples and are close to the detection limits.

There does not appear to be a direct link between the sulfide assemblages and Pd-enrichment in the High-Grade Zone. The gabbronorites contain a magmatic sulfide assemblage, but have extremely high Pd/Ir and Pd/Pt ratios in the range of

1000 to 10000 and 6 to 10 respectively (Table 1). In the metagabbronorites, post-magmatic

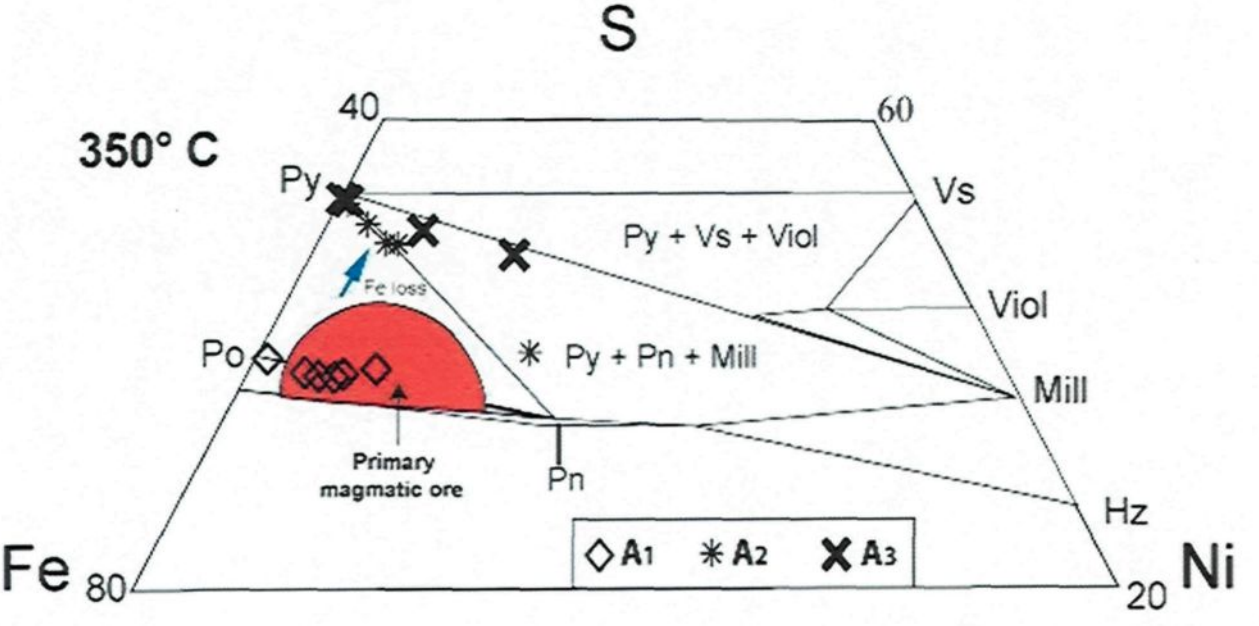

Figure 7. The weight percentage of the S, Ni and Fe from sulfide in whole rock calculated from results of image analysis of BMS for sample from Lac-des-Iles-Complex and plotted on the ternary diagram for 350°C modified from Barnes et al., (2009). Po = pyrrhotite, Py = pyrite, Pn = pentlandite, Mil = millerite, Viol = violarite, Hz = heazlewoodite, Vs = vaesite.

sulfide assemblages are present, but their Pd/Ir and Pd/Pt ratios are similar to those observed in gabbronorites suggesting that the change in sulfide assemblage has not affected these ratios. In the High-Grade Zone, the same sulfide assemblages are present as in the Roby and Twilight Zone metagabbros, but Pd/Ir and Pd/Pt ratios are significantly higher in the 5000 to 8000 range and 7 to 24 ranges (Table 2) respectively.

The whole-rock primitive mantle-normalized graphs for each rock show similar patterns (Fig. 8). There is extreme fractionation of Os, Ir and Ru (IPGE) compared to Pt and Pd (PPGE). In addition the PPGE are more enriched in chlorite-actinolite schist compared to gabbronorite or metagabbronorite. However, Cu is relatively low compared to the PPGE in schist compared to other rock types.

Platinum-group element and chalcophile element concentrations in BMS

Pentlandite is much richer in Pd than the other BMS with a median value of 650 ppm (Fig. 9). All of other BMS except millerite contain negligible amounts of Pd median values < 1ppm (Fig. 9; Table 4). Millerite contains slightly more Pd with a median value of 6.7 ppm, (Fig. 9; Table 4). The observation that pentlandite is the principal host to Pd is in agreement with studies at other ore deposits which have found that pentlandite is the principal host to Pd (Barnes et al. 2008; Dare et al. 2010; Godel et al. 2007; Holwell and McDonald 2007) among the BMS.

The median Pt concentrations in all of the BMS except pyrite are <0.1 ppm (Fig. 9). Pyrite contains some Pt with a median value of 0.2 ppm, but in some cases

Pt values are higher (11ppm). The low concentration of Pt in the BMS in general is in agreement with previous studies (Barnes et al. 2008; Godel et al. 2007). But other authors have reported that Pt is present in pyrite e.g. the Great Dyke of Zimbabwe (Oberthür et al. 1997) and the Aguablanca sulfide deposit of South West Iberia in Spain (Dare et al. 2010; Pina et al. 2010).

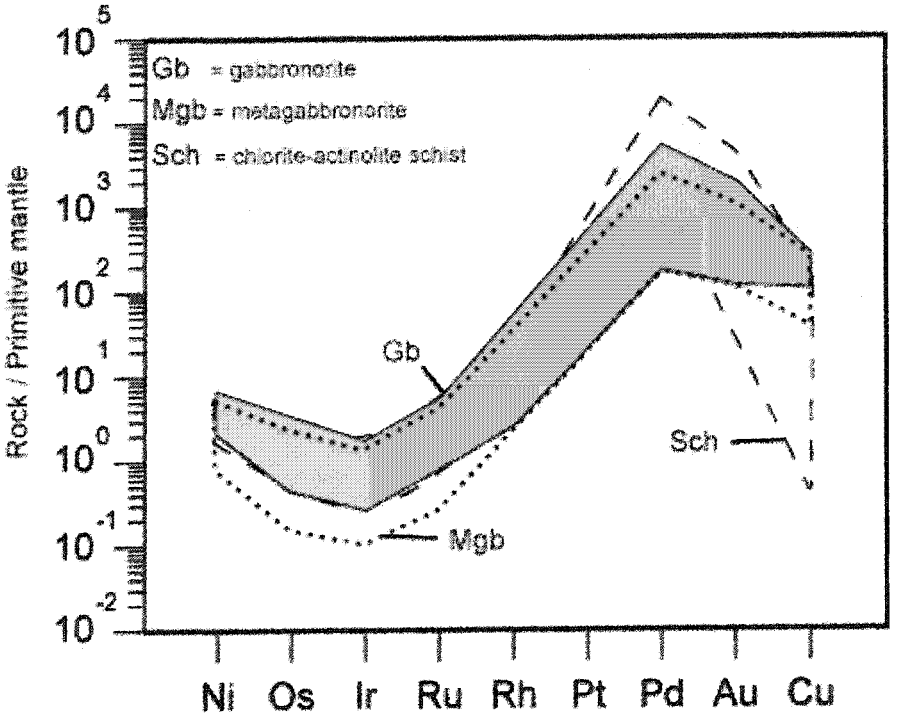

Figure 8. Whole-rock Ni, PGE, Au and Cu normalized to primitive mantle for the rock assemblages of the Lac-des-Iles-Complex. Normalization values are taken from Becker et al. (2006).

Rhodium, Os, Ir and Ru concentrations are highest in pyrrhotite and pentlandite (Fig. 9; Table 4). In general the concentrations are in the 0.01 to 0.2 ppm range. In addition there are positive correlations between Ru and Os (Fig. 10A), Ir and Os (Fig. 10B) and a crude correlation between Ir and Ru (Fig. 10C) for pyrrhotite, pentlandite and pyrite. The concentrations of these elements in the other BMS are close to the detection levels. The very low concentration of these elements in the BMS probably reflects the low concentrations of these elements in the whole rock (Table 2). The preferential concentration of these elements in pyrrhotite and pentlandite is in agreement with previous studies (Barnes et al. 2008; Dare et al. 2010; Godel et al. 2007; Holwell and McDonald 2007). However their presence in pyrite agrees with recent studies (e.g. Dare et al. 2010)

Cobalt is preferentially concentrated in pentlandite and idiomorphic pyrite with median values ~ 1 weight percent (Fig. 9E). There are also significant, but smaller, quantities of Co present in millerite (median values of ~1400 ppm). Cobalt concentrations in chalcopyrite are below detection limit (Table 4).

Zinc and Cd are present principally in chalcopyrite and median concentrations are ~1000 and 1.5 ppm respectively. In the BMS the concentrations are close to detection level (Fig. 9; Table 4,). Silver is also concentrated in chalcopyrite, but millerite is also a significant host (median values are 3.5 and 7 ppm respectively).

Arsenic is mainly concentrated in the idomorphic pyrite than the anhedral pyrite; median values are ~ 43.3 and 0.008 ppm respectively. Arsenic concentrations

in other minerals are close to detection limits. Pyrite preferentially concentrates Bi, but millerite is also an important host (Fig. 9).

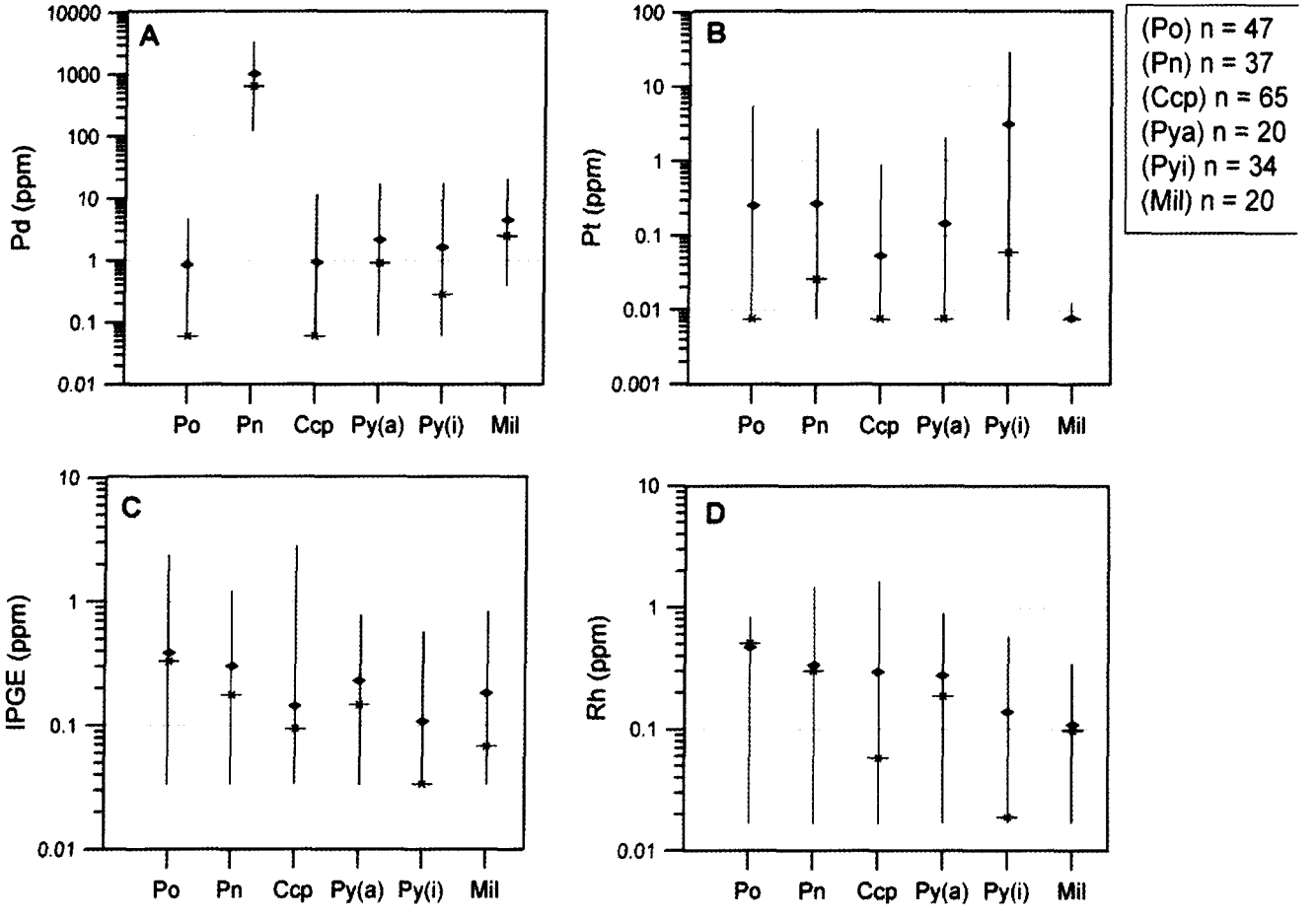

Figure 9a. Range, average concentrations (diamond) and median concentrations (cross-bar) of Pd (A), Pt (B), IPGE (Os, Ir and Ru; C) and Rh (D) present in the base metal sulfide.

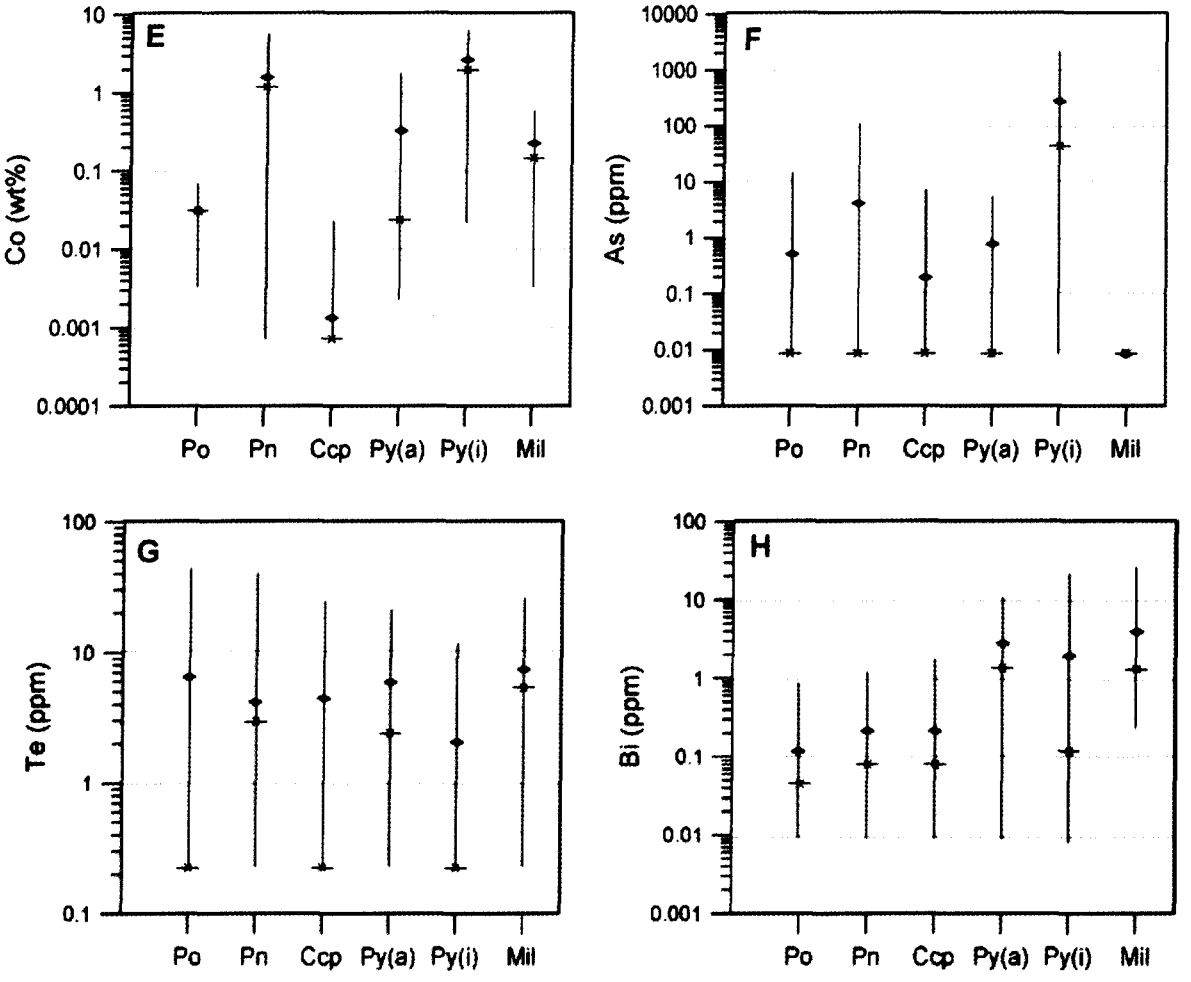

Figure 9b. Range, average concentrations (diamond) and median concentrations (cross-bar) of Co (E), As (F), Te (G) and Bi (H) present in the base metal sulfide.

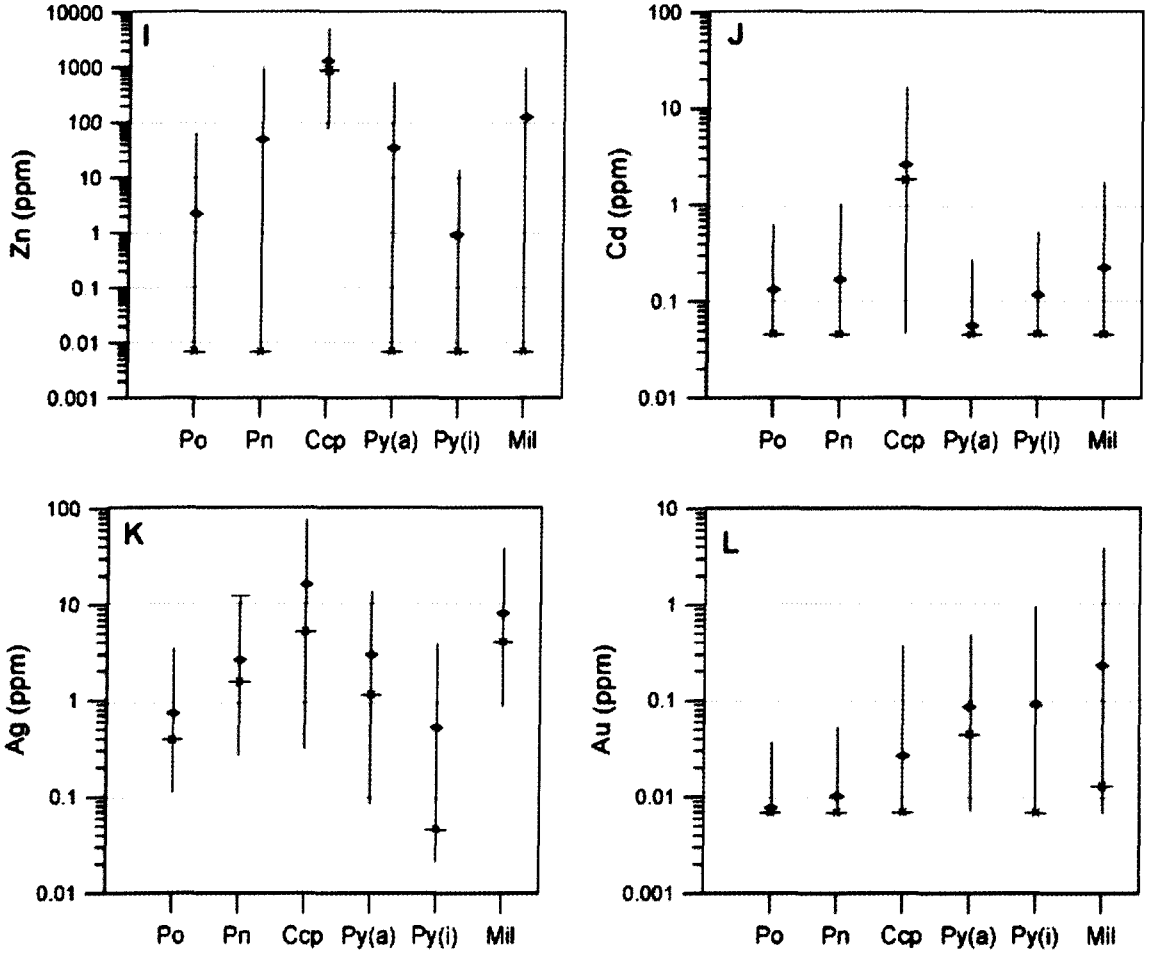

Figure 9c. Range, average concentrations (diamond) and median concentrations (cross-bar) of Zn (I), Cd (J), Ag (K) and Au (L) present in the base metal sulfide.

Table 4. **Results for laser ablation ICP-MS analysis of pyrrhotite, pentlandite, chalcopyrite, pyrite and millerite from the Lac-des-Iles-Complex**

Assemblage	n		59Co ppm	61Ni wt.%	65Cu wt.%	66Zn ppm	75As ppm	77Se ppm	101Ru ppm	103Rh ppm	105Pd ppm	107Ag ppm	111Cd ppm	121Sb ppm	128Te ppm	185Re ppm	189Os ppm	193Ir ppm	195Pt ppm	197Au ppm	209Bi ppm
Po-Pn-Ccp±Py Pyrrhotite																					
Tz 1	13	Avg.	345	0.89	0.28	6.72	1.82	455	0.23	0.42	1.25	1.24	0.28	<0.07	2.6	0.10	0.09	0.03	<0.015	<0.014	0.04
		Std	77	0.14	0.51	18.1	4.19	79	0.16	0.31	1.60	1.08	0.18		5.11	0.07	0.06	0.01			0.03
Tz 7	12	Avg.	431	0.96	0.05	<0.014	<0.017	204	0.20	0.57	0.71	0.47	<0.091	<0.07	0.69	0.09	0.08	0.01	0.01	<0.014	0.11
		Std	83	0.07	0.18			10	0.09	0.19	1.26	0.70			1.09	0.03	0.03	0.01	0.02		0.24
Tz 10	2	Avg.	58	0.98	0.47	7.04	<0.017	401	0.18	0.42	0.19	1.25	0.17	<0.07	1.47	0.13	0.13	0.03	<0.015	<0.014	0.03
		Std	18	0.05	0.60	9.95		70	0.17	0.56	0.19	1.11	0.17		1.77	0.18	0.17	0.03			0.01
Tz 19	13	Avg.	265	0.81	0.02	<0.014	<0.017	273	0.22	0.56	0.26	0.58	<0.091	<0.07	0.83	0.10	0.08	0.02	0.03	<0.014	0.07
		Std	172	0.25	0.05			108	0.10	0.16	0.39	0.29			1.72	0.03	0.03	0.01	0.05		0.06
Rz 30	7	Avg.	399	0.79	<0.004	<0.014	<0.017	344	0.14	0.30	0.94	0.34	0.15	<0.07	20.9	0.16	0.05	0.03	1.34	<0.014	0.23
		Std	166	0.33				94	0.05	0.07	1.18	0.17	0.19		12.6	0.01	0.01	0.01	1.92		0.20
Rz 45	6	Avg.	67	0.45	<0.004	<0.014	<0.017	295	0.35	0.38	1.32	0.41	0.04	<0.07	17.8	0.14	0.17	0.06	0.29	<0.014	0.22
		Std	33	0.07				25	0.55	0.13	1.60	0.30	<0.091		15.7	0.01	0.28	0.08	0.60		0.21
Pentlandite																					
Tz 1	5	Avg.	22692	35.7	0.04	11.1	4.38	419	0.37	0.74	650	0.93	0.25	<0.07	2.33	0.12	0.14	0.04	<0.015	<0.014	0.04
		Std	3741	4.10	0.08	24.9	4.14	27.6	0.11	0.17	166	0.28	0.25		1.93	0.05	0.07	0.03			0.02
Tz 7	7	Avg.	23285	28.3	0.05	15.2	15.6	169	0.11	0.18	648	1.88	0.10	0.10	1.76	0.06	0.05	0.02	0.09	0.015	0.29
		Std	10447	11.5	0.11	20.3	41.2	15	0.13	0.16	402	2.14	0.10	0.17	1.96	0.07	0.03	0.01	0.06	0.01	0.24
Tz 10	1	Avg.	5414	33.9	0.80	65.4	0.008	388	0.10	0.19	257	1.80	0.05	<0.07	3.13	0.20	0.12	0.02	0.02	<0.014	0.39
		Std																			
Tz 19	4	Avg.	12915	36.3	0.07	6.37	<0.017	253	0.10	0.34	570	1.24	0.15	<0.07	0.98	0.06	0.07	0.04	0.16	<0.014	0.15
		Std	752	2.51	0.14	12.7		31.9	0.06	0.31	55.4	1.04	0.13		1.51	0.03	0.04	0.03	0.02		0.23
Rz 30	4	Avg.	38337	46.6	0.08	295	1.36	258	<0.036	0.07	326	1.72	0.42	<0.07	3.50	0.03	<0.017	0.01	1.19	<0.014	0.44
		Std	16315	2.12	0.15	428	2.70	115		0.06	28.3	0.57	0.47		4.03	0.04		0.02	1.29		0.26
Rz 45	5	Avg.	6826	24.6	0.12	48.2	<0.017	271	0.07	0.23	679	1.77	0.10	<0.07	13.38	0.09	0.09	0.03	0.07	<0.014	0.27
		Std	1711	6.74	0.25	107		31.4	0.06	0.13	291	1.08	0.13		16.05	0.05	0.15	0.05	0.12		0.50
Chalcopyrite																					
Tz-1	6	Avg.	<14	<0.01	52.5	2301	<0.017	332	0.10	<0.034	0.94	2.95	7.97	<0.07	13.46	<0.012	<0.017	<0.007	0.06	<0.014	0.09
		Std			3.71	1760		26.1	0.04		0.57	3.10	5.09		4.26				0.10		0.05
Tz 7	4	Avg.	<14	0.01	29.8	786	<0.017	171	0.08	<0.034	2.94	1.36	0.96	<0.07	13.73	<0.012	<0.017	<0.007	0.22	<0.014	0.69
		Std		0.01	2.29	214		6.19	0.07		2.50	0.38	0.15		8.52				0.41		0.48
Tz 10	4	Avg.	<14	<0.01	32.7	2607	<0.017	258	0.06	0.15	2.28	3.46	8.37	<0.07	18.60	<0.012	<0.017	<0.007	0.09	<0.014	0.24
		Std			2.38	831		16.4	0.03	0.12	0.98	2.96	2.12		9.61				0.06		0.15
Tz 19	4	Avg.	<14	0.04	31.2	984	<0.017	239	0.10	<0.034	<0.12	3.57	3.56	0.09	<0.44	<0.012	<0.017	<0.007	0.06	<0.014	0.10
		Std		0.04	1.41	512		9.07	0.04			1.03	1.25	0.02					0.06		0.03

Assemblage		n		59Co ppm	61Ni wt.%	65Cu wt.%	66Zn ppm	75As ppm	77Se ppm	101Ru ppm	103Rh ppm	105Pd ppm	107Ag ppm	111Cd ppm	121Sb ppm	128Te ppm	185Re ppm	189Os ppm	193Ir ppm	195Pt ppm	197Au ppm	209Bi ppm
	Rz 30	4	Avg.	19.2	0.07	50.9	710	<0.017	221	0.05	<0.034	2.7	2.11	1.01	<0.07	5.61	<0.012	<0.017	<0.007	0.02	<0.014	0.11
			Std	24.2	0.14	13.5	227		41.0	0.03		5.3	2.13	0.27		1.03				0.01		0.08
	Rz 45	4	Avg.	<14	<0.01	31.3	1359	<0.017	220	0.06	0.12	<0.12	2.75	2.67	<0.07	0.85	<0.012	<0.017	<0.007	0.08	<0.014	0.03
			Std			0.98	169		9.08	0.03	0.12		1.24	0.43		1.26				0.06		0.02
	Pyrite (anhedral)																					
	Tz 10	1	Avg.	13080	0.59	0.03	<0.014	<0.017	592	0.34	0.89	1.19	1.27	<0.091	<0.07	4.57	0.22	0.30	0.05	0.03	0.04	1.65
			Std																			
	Tz 19	3	Avg.	3479	0.28	0.02	10.7	<0.017	426	<0.036	0.73	0.21	5.96	0.12	<0.07	<0.44	0.17	0.13	0.04	0.26	0.07	4.62
			Std	3255	0.09	0.03	18.4		54.3		0.11	0.14	6.12	0.13			0.01	0.03	0.01	0.16	0.04	4.54
	Rz 45	2	Avg.	6833	1.30	<0.004	0.007	0.009	430	0.11	0.27	0.76	2.51	<0.091	<0.07	2.86	0.17	0.04	0.03	0.01	0.05	0.85
			Std	1894	0.17				28	0.02	0.07	0.23	1.09			3.73	0.02	0.00	0.01	0.00	0.03	0.31
	Pyrite (idiomorphic)																					
	Rz 45	2	Avg.	18765	0.61	<0.004	21.1	33.5	453	0.07	0.28	2.96	3.95	<0.091	<0.07	5.98	0.15	0.01	0.01	1.40	0.08	2.06
			Std	1562	0.83	0.00	29.8	47.3	37.5	0.03	0.11	3.62	5.53			8.15	0.03	0.01	0.00	1.97	0.10	2.57
Pn-Ccp-Py	Pentlandite																					
	Tz 15	7	Avg.	81	39.27	0.15	35.4	2.44	196	0.26	0.60	795	6.20	0.16	<0.07	5.02	0.14	0.11	0.02	<0.015	<0.014	0.21
			Std	149	1.90	0.36	93.7	6.45	25.3	0.25	0.44	97	3.71	0.15		6.53	0.13	0.11	0.01			0.29
	Rz 17	4	Avg.	10147	57.24	<0.004	<0.014	<0.017	572	0.25	0.08	3262	3.40	<0.091	<0.07	1.80	0.12	0.19	0.10	0.80	<0.014	<0.017
			Std	405	0.91				46.5	0.18	0.02	78	0.92			1.88	0.22	0.15	0.06	0.91		
	Chalcopyrite																					
	Tz 15	6	Avg.	44.9	0.09	27.88	1671	1.20	157	0.07	0.24	1.30	32.5	1.52	0.08	3.07	0.01	0.02	<0.007	0.02	<0.014	0.16
			Std	92.4	0.19	3.24	979	2.92	12.3	0.04	0.32	1.72	7.67	0.95	0.08	3.33	0.01	0.02		0.02		0.29
	Tz 21	3	Avg.	<14	0.06	31.01	1002	<0.017	266	0.07	<0.034	3.91	8.12	1.35	<0.07	1.48	<0.012	<0.017	<0.007	<0.015	0.018	0.05
			Std		0.10	3.71	686		46.7	0.015		6.68	6.39	0.53		2.18					0.01	0.05
	Tz 28	7	Avg.	<14	0.02	34.33	370	0.71	250	0.05	0.06	0.17	22.5	0.84	<0.07	3.29	<0.012	<0.017	<0.007	<0.015	<0.014	0.03
			Std		0.03	1.87	342	1.87	9.16	0.04	0.12	0.18	10.7	0.78		3.40						0.01
	Rz 17	4	Avg.	<14	<0.01	33.15	313	<0.017	250	0.13	1.17	<0.12	8.08	1.93	<0.07	<0.44	<0.012	0.016	<0.007	<0.015	<0.014	<0.017
			Std			1.33	38		19.0	0.15	0.42		0.79	0.43				0.015				
	Pyrite (anhedral)																					
	Tz-15	1	Avg.	74.9	0.77	0.01	<0.014	4.97	302	0.19	0.50	1.40	5.37	<0.091	<0.07	0.22	0.10	0.05	0.04	<0.015	0.14	0.51
			Std																			0.00
	Tz 21	1	Avg.	25.5	0.29		<0.014	0.008	359	<0.036	0.05	0.06	0.08	<0.091	<0.07	<0.44	<0.012	<0.017	<0.007	<0.015	0.008	0.03
			Std																			0.00
	Rz 17	3	Avg.	139	0.03	0.00	<0.014	<0.017	436	0.04	<0.034	0.06	0.65	<0.091	<0.07	<0.44	<0.012	<0.017	<0.007	<0.015	<0.014	0.02
			Std	55.6	0.03	0.00			31.3	0.03		8.50	0.28									0.01

Assemblage	n		59Co ppm	61Ni wt.%	65Cu wt.%	66Zn ppm	75As ppm	77Se ppm	101Ru ppm	103Rh ppm	105Pd ppm	107Ag ppm	111Cd ppm	121Sb ppm	128Te ppm	185Re ppm	189Os ppm	193Ir ppm	195Pt ppm	197Au ppm	209Bi ppm
Pyrite (idiomorphic)																					
Tz-15	4	Avg.	22177	0.67	0.02	<0.014	20.7	349,00	0.30	0.50	1.37	2.40	<0.091	<0.07	5.44	0.11	0.07	0.014	<0.015	0.07	1.47
		Std	5979	0.15	0.02		23.8	24.8	0.09	0.10	1.87	1.43			2.44	0.02	0.02	0.006		0.07	0.82
Tz 21	2	Avg.	41570	0.11	0.01	<0.014	8.51	488,00	<0.036	0.02	1.30	0.14	<0.091	<0.07	<0.44	<0.012	<0.017	<0.007	1.25	0.02	1.10
		Std	17734	0.08	0.01		1.85	32.1		0.01	1.74	0.09							0.75	0.01	0.94
Rz 17	1	Avg.	18110	1.79	0.07	<0.014	<0.017	631	0.17	0.30	18.7	3.64	<0.091	<0.07	<0.44	0.016	0.114	0.05	<0.015	0.28	0.02
Mil-Ccp-Py Millerite																					
Rz 26	8	Avg.	4764	68.01	0.56	154	<0.017	296	0.04	0.11	6.33	13.34	0.45	<0.07	14.0	0.06	0.03	0.012	<0.015	0.02	3.22
		Std	1000	5.79	0.96	320		69.9	0.04	0.027	6.15	13.21	0.56		6.43	0.02	0.02	0.008		0.03	1.68
Rz 50	3	Avg.	1495	43.72	<0.004	19.9	<0.017	191	0.12	<0.034	9.05	7.95	<0.091	<0.07	4.90	<0.012	0.07	<0.007	<0.015	1.33	16.24
		Std	79.2	1.02	0.00	34.5		18.3	0.17		7.80	3.45			8.11		0.07			2.29	10.21
Rz 54	9	Avg.	188	69.46	0.18	130	<0.017	236	0.20	0.14	1.06	3.28	<0.091	<0.07	2.27	0.05	0.05	0.016	<0.015	0.03	0.51
		Std	6319	0.02			59.8	3.87			0.55					0.02			0.19		0.00
Chalcopyrite																					0.00
Rz 50	4	Avg.	<14	<0.01	33.95	286	<0.017	159	0.33	0.39	<0.12	75.53	0.12	<0.07	<0.44	<0.012	0.41	0.05	0.23	0.03	0.58
		Std		0.00	0.54	207		7.64	0.51	0.32		5.13	0.173				0.77	0.1	0.44	0.03	0.82
Rz 54	7	Avg.	22.8	0.05	38.34	142	<0.017	191	0.08	0.40	<0.12	1.94	0.12	<0.07	<0.44	<0.012	<0.017	<0.007	<0.015	0.04	0.13
		Std	41.4	0.09	1.62	103		13.3	0.05	0.24		1.77	0.21							0.03	0.11
Rz 3	5	Avg.	<14	<0.01	32.38	2498	<0.017	298	0.07	1.21	<0.12	10.47	3.15	<0.07	<0.44	<0.012	<0.017	<0.007	<0.015	0.09	0.77
		Std			2.91	627		16.7	0.05	0.31		0.61	0.92							0.16	0.29
Rz 8	3	Avg.	<14	<0.01	33.44	1012	<0.017	272	0.10	0.28	<0.12	70.89	2.70	<0.07	<0.44	<0.012	<0.017	<0.007	<0.015	0.15	<0.017
		Std			1.20	82		27.6	0.05	0.19		2.43	0.52							0.10	
Pyrite (anhedral)																					
Rz 26	2	Avg.	294	0.35	0.00	<0.014	2.76	392	0.04	0.15	0.31	0.38	0.04	<0.07	11.6	0.05	0.04	0.007	0.008	0.01	1.31
		Std	336	0.04	0.00		3.89	25.6	0.04	0.03	0.35	0.38			2.22	0.005	0.003	0.001		0.00	0.85
Rz 54	6	Avg.	463	0.87	0.15	88	0.78	284	0.13	0.24	2.06	1.24	<0.091	<0.07	11.8	0.08	0.14	0.04	<0.015	0.12	2.86
		Std	910	0.52	0.27	216	1.91	77.1	0.06	0.13	1.10	1.04			8.61	0.06	0.14	0.03		0.18	2.87
Pyrite (idiomorphic)																					0.00
Rz 26	9	Avg.	49363	0.08	0.02	<0.014	726	408	0.06	0.20	1.22	0.07	0.29	<0.07	4.13	0.05	0.03	0.013	3.64	0.22	2.53
		Std	7879	0.02	0.03		852	84	0.05	0.19	1.79	0.09	0.17		5.03	0.02	0.03	0.012	4.87	0.42	4.02
Rz 50	6	Avg.	17270	0.09	0.08	18.7	200	144	<0.036	<0.034	2.22	0.48	<0.091	<0.07	<0.44	0.02	<0.017	<0.007	11.1	0.04	7.08
		Std	5535	0.05	0.08	32.5	303	53.4			3.91	0.44				0.01			12.3	0.04	8.37
Rz 3	4	Avg.	15407	0.07	<0.004	<0.014	130	167	<0.036	0.03	<0.12	<0.043	<0.091	<0.07	<0.44	<0.012	<0.017	<0.007	0.20	<0.014	0.02
		Std	729	0.02			112	46											0.23		0.03
Rz 8	6	Avg.	9075	0.07	<0.004	<0.014	76.1	66	<0.036	<0.034	0.36	<0.043	<0.091	<0.07	<0.44	0.02	<0.017	<0.007	0.09	<0.014	<0.017
Detection Limit		Avg.	14	0.01	0.004	0.013	0.017	0.03	0.036	0.034	0.12	0.04	0.091	0.07	0.45	0.012	0.017	0.007	0.015	0.014	0.017
		Std.	2.9	0.0004	0.0008	0.001	0.0008	0.002	0.003	0.003	0.008	0.005	0.01	0.003	0.03	0.0007	0.001	0.002	0.002	0.003	0.009

Abbreviations: Po = pyrrhotite, Pn = pentlandite, Ccp = chalcopyrite, Py = pyrite, Mil = millerite, Avg. = average, Sd = standard deviation, n = number of grains analyzed.

Selenium and Te are present at approximately equal concentrations in all the BMS with median Se values in the range 230-360 ppm (Table 4) and Te in the 1.5 to 5 ppm range (Fig. 9).

Gold and Sb are below detection, (< 0.017 and 0.07 ppm respectively) in all of the BMS.

Mineralogy of platinum-group minerals

Two hundred and twenty-one PGM grains were identified in polished thin sections (Table 5) in addition 22 PGM inclusions were observed in the laser spectra (Table A3). There are 9 types of PGM phases, in decreasing order of the abundance, they comprise (Fig. 11a) : (i) Pd tellurides (Pd-Te), (ii) Pd arsenides (Pd-As), (iii) Pt arsenide (Pt-As), (iv) Pd sulfides (Pd-S), (v) Pt sulfides (Pt-S), (vi) Pt tellurides (Pt-Te), (vii) Pd antimonides (Pd-Sb); (viii) Pd bismuthotellurides (Pd-Bi-Te), (ix) Pt bismuthides (Pt-Bi). Our observations contrast with those of Cabri and Laflamme (1979), who found that braggite [(Pd, Pt)S] was the dominant PGM phase in their samples from LDIC. The proportion of PGM present varies with the sulfide assemblage. In Po-Pn-Ccp±Py and Pn-Ccp-Py assemblages Pd-Te is the dominant PGM with minor Pd-As and Pt-As. In the Py-Ccp-Mil assemblage the proportion of Pd-As, Pt-As, Pd-S, Pd-Sb and Pd-Bi-Te are much higher than in the previous assemblage (Fig. 11b). In addition, the size and location of the PGM changes with the sulfide assemblage and the degree of alteration of the rocks (Fig. 12)

In A_1 the PGM grains are subhedral or rounded and their size varies between 0.3 to 110 μm^2. Most of these grains are either in contact between silicates and BMS

(54 %; Fig. 13A), included in BMS (27%; Fig. 13B) or included in silicate minerals (18%).

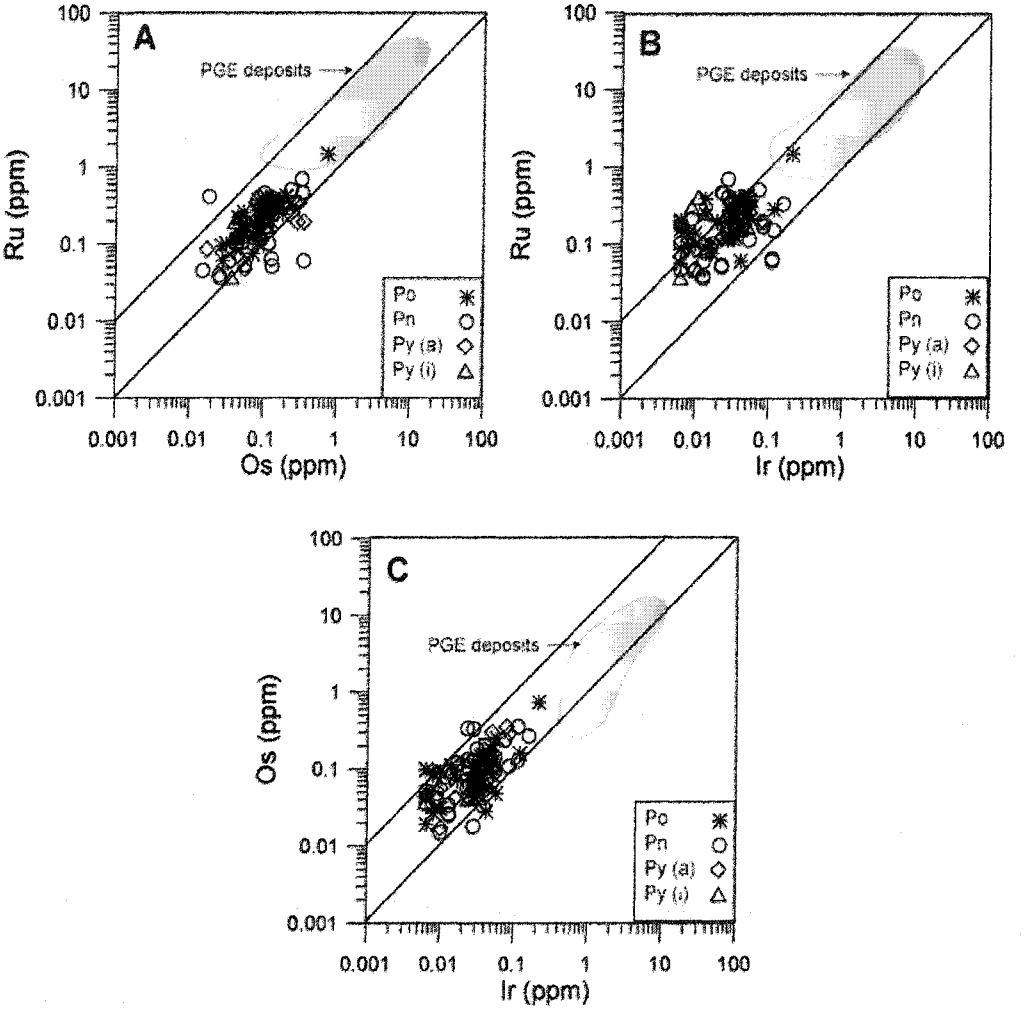

Figure 10. Binary diagrams. Concentrations of Os versus Ru (**A**), Ir versus Ru (**B**) and Os (**C**) in base metal sulfides from the studied samples of the Lac-des-Iles-Complex. There is similar tendancy for correlation between Os and Ru, Ir and to a lesser extent correlation between Ir and Ru than PGE deposits. With Po = pyrrhotite, Pn = pentlandite, Py (a) = anhedral pyrite and Py (i) = idiomorphic pyrite. Data of PGE deposits from Barnes et al., 2008; Godel et al., 2008; Godel et al., 2007.

The shape and size of the PGM in A_2 are similar to those from A_1. The majority of these PGM are found at the contact between silicates and BMS (50%; Fig. 13C) or included in silicates (40%; Fig. 13D). A few (< 10%) are included in BMS (Fig. 13D).

Finally in A_3, the shape of PGM is similar to those found in A_1 and A_2 but the grains are larger between 3.6 to 650 μm^2. Most are included in silicates (76%; Fig 13E and F). Only 12 % are included in BMS or in contact between BMS and silicates.

During laser ablation, signals from 22 micro-inclusions enriched in PGE were observed within the BMS or at the contact between the BMS and the silicates. The most common inclusions are Pd-rich (70%) and can be summarized as follow; (i) Pd-Te, (ii) Pd-Sb, (iii) Pd-As, (iv) Pd-Bi-Te and (v) Pd-Te-As (Table 6). A few Pt-rich inclusions were observed with Pt being associated with Te (Pt-Te), As (Pt-As) and Bi (Pt-Bi). Thirty six percent of Pd inclusions are found included in BMS while 25% are in contact between BMS and silicates. Ninety percent of Pt-rich inclusions are found at the contact between BMS and silicates. The size of the inclusions observed in the time-resolved analysis was estimated using the methods detailed by Godel et al. (2007) by making the assumption that the shape of the inclusion is cubic. The average ablation rate was calculated to be ~ 2 μm/s and is similar to that reported in Godel et al. (2007). Most (~ 90%) of the PGM inclusions observed are ~1 to ~4 μm in length.

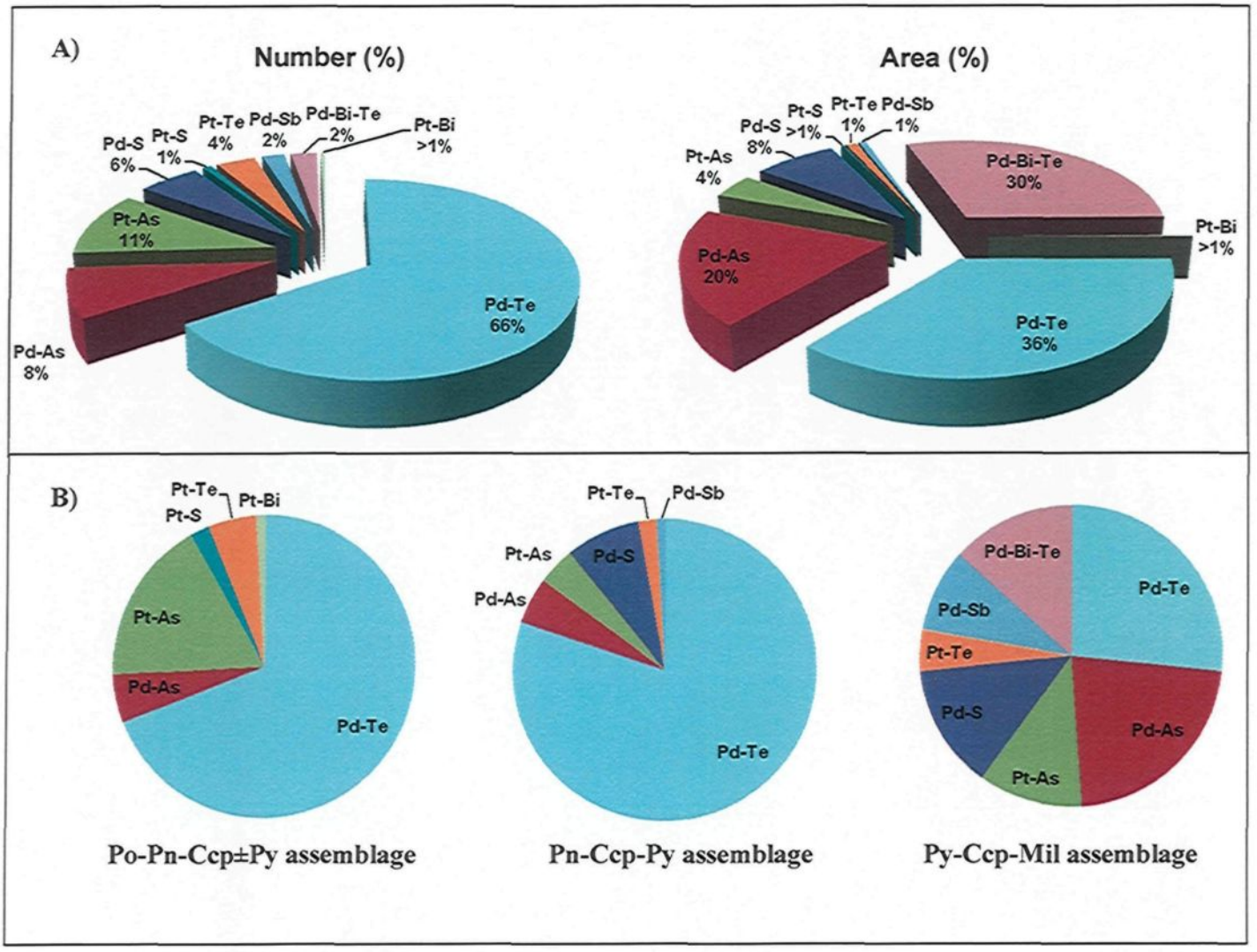

Figure 11. Type and proportion in number and area percent of PGM phases found in rocks from Lac-des-Iles-Complex (A). Distribution of the PGM following the sulfide assemblages based on their area (B).

These results are similar to the size of the PGM inferred from the BSE image analysis as described above. The results are given in the Table 5.

No inclusions or PGM hosting Ir, Os, Ru as major components have been found. Quantitative microprobe analyses of a few grains (n=17) indicate that the Pd-Te phases are similar to kotulskite (PdTe) according to the classification of Cabri (2002). A few of the PdTe grains in A_3 are enriched in Bi (up 30 to 32 wt. % of Bi Table A3) and represent Bi-rich kotulskite (Fig. 14) and not michenerite (PdBiTe) or sobolevskite (PdBi). Probably this implies an extensive substitution of Bi for Te at temperatures of formation below 500°C (Ortega et al. 2004). Image analysis show that the sizes of Pd-Te-Bi grains are large (~ 1 to 600 μm^2) compared to those of Pd-Te (~ 0.5 to 110 μm^2).

Discussion

Mass balance

A mass balance calculation was carried out to determine how much of the PGE and Au are present in the BMS and how these proportions changes as the BMS assemblage changes. The proportion (P) of each element (i) present in each BMS was calculated using the following equation:

$$\mathbf{Pi = F*(Ci/Cwi)* (\rho sul/\rho sil)}$$

where (F) is the modal fraction of BMS present as determined by image analysis, (Ci) is the concentration of the element (i) in the relevant BMS, (Cwi) is the concentration of the element (i) in the whole-rock, ρsul is the density of the BMS and ρsil is the density of the

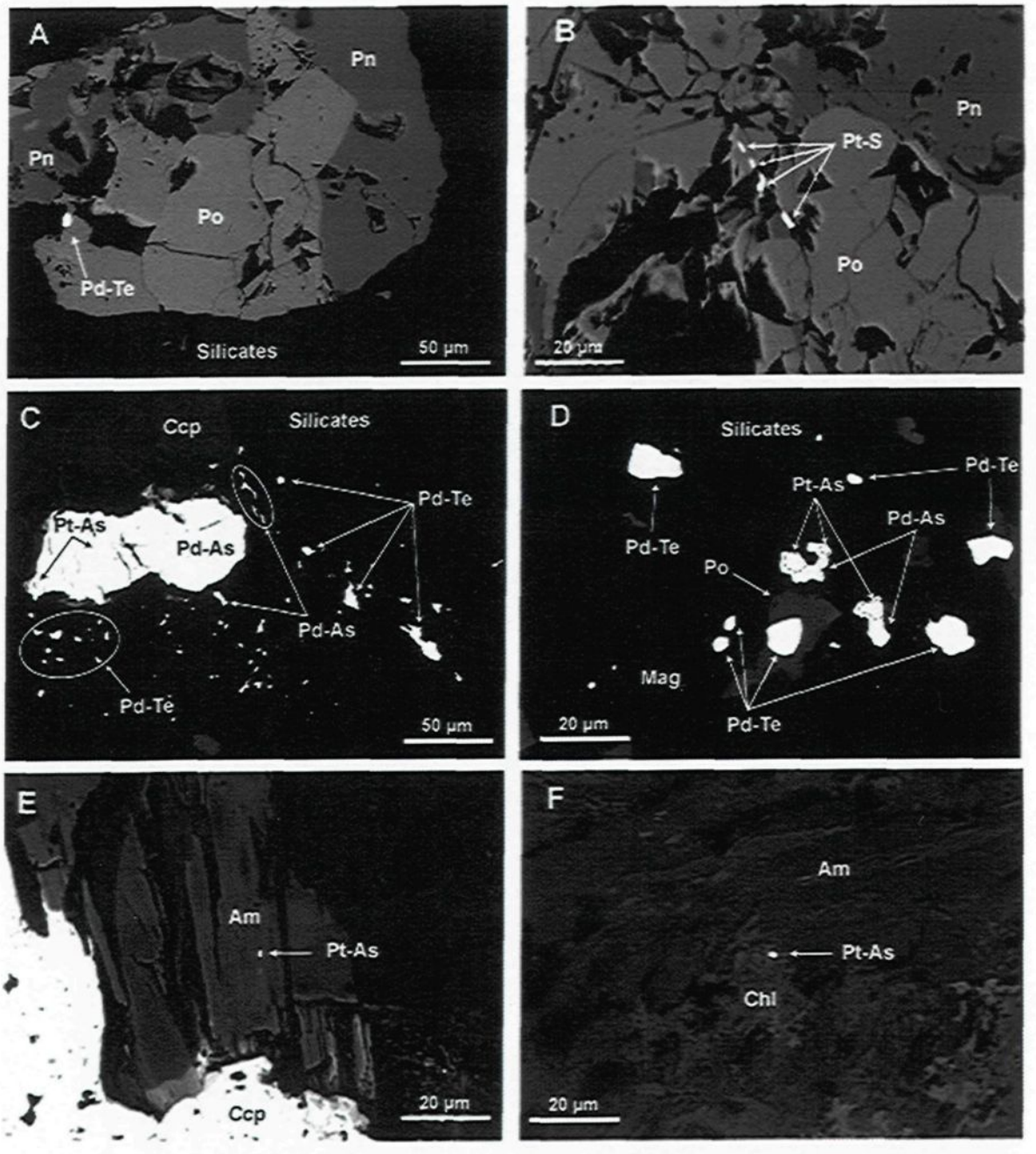

Figure 12. Photomicrographs of phases of platinum group minerals (PGM) observed in the Lac-des-Iles-Complex samples. Subhedral grains of Pd-Te (**A**) and Pt-S (**B**) located at the contact between base metal sulfides and silicates in the rocks containing Po-Pn-Ccp±Py assemblage (A_1). Pd-Te, Pd-As and Pt-As included in silicates or at the contact between sulfide (**C**) and silicate or and oxide (**D**) in the rocks containing Pn-Ccp-Py assemblage (A_2). Pt-As associated with secondary silicates; amphibole (Am) (**E**) and chlorite (Chl) (**F**) in the rocks containing the Py-Ccp-Mil assemblage (A_3). Po= pyrrhotite, Pn = pentlandite, Ccp = chalcopyrite, Mag = magnetite.

Table 5. Platinum-group minerals found in analyzed samples from the Lac-des-Iles-Complex

Assemblage	Sample	**Pd-Te**	**Pd-As**	**Pt-As**	**Pd-S**	**Pt-S**	**Pt-Te**	**Pd-Bi-Te**	**Pd-Sb**	**Pt-Bi**
Po-Pn-Ccp±Py	Tz1	34	4	12						
Po-Pn-Ccp±Py	Tz7	1		1						
Po-Pn-Ccp±Py	Tz19	6	1	1			2			
Po-Pn-Ccp±Py	Rz30	12		3		2	2			1
Po-Pn-Ccp±Py	Rz45	14					1			
	Area min (μm^2)	0.9	2.7	0.3		8.0	2.8			
	Area max (μm^2)	115	88	82		8.3	13			16.5
Pn-Ccp-Py	Tz15	2		1					1	
Pn-Ccp-Py	Tz21	11								
Pn-Ccp-Py	Tz28	7								
Pn-Ccp-Py	Rz17	61	5	3	8		2			
	Area min (μm^2)	0.3	5.1	0.4	6.6		13			
	Area max (μm^2)	62.2	134	68	111		21			
Mil-Ccp-Py	Rz26	4	2	1				1		
Mil-Ccp-Py	Rz50	2								
Mil-Ccp-Py	Rz54	5	5	4	6		1		4	
Mil-Ccp-Py	Rz8		4				1	5		
	Area min (μm^2)	3.2	0.8	0.7	1.4		1.9	1.2	2.5	
	Area max (μm^2)	25.1	221	21	148		4.3	677	15.6	

silicate portion of the rock (2.9 g/m^3). The median for each mineral in each assemblage is shown in Figure 15.

The main BMS that hosts Pd is pentlandite in both the Po-Pn-Ccp±Py and Pn-Ccp-Py assemblages (Fig. 15), which is consistent with what have been found in other deposits (Barnes et al. 2008; Godel et al. 2007; Holwell and McDonald 2007). In the Py-Ccp-Mil assemblage which lacks pentlandite, some Pd is present in millerite and pyrite (1%), but most be of Pd must present in phases other than BMS. These observations are in agreement with studies of PGM which found that the Py-Ccp-Mil assemblage contained larger grains and a wider varity of Pd phases in A_3.

Neither Au nor Pt is present in BMS from Po-Pn-Ccp±Py or Pn-Ccp-Py assemblages. The absence of Pt in the BMS is consistent with the presence of numerous Pt-minerals. This is in agreement with previous studies of PGE-reef sulfides (Barnes et al. 2008; Dare et al. 2010; Godel et al. 2007; Holwell and McDonald 2007). However in the A_3 rocks, the pyrite contains a significant amount of the Pt (~15 %) and a small amount of the Au (~0.5 %).

In all of the assemblages most of the Os, Ir, Ru and Rh is present in BMS (Fig. 14). In the Po-Pn-Ccp±Py assemblage Os, Ir, Ru and Rh are mainly controlled by pyrrhotite with minor amounts in pentlandite. In Pn-Ccp-Py assemblage these elements are controlled by pentlandite and pyrite with minor amounts in chalcopyrite. In Py-Ccp-Mil assemblage pyrite is the main phase that hosts these elements (Fig. 15).

Evolution of the sulfide assemblages

The Po-Pn-Ccp±Py assemblage represents a magmatic sulfide assemblage and occurs in fresh gabbronorite. As has also been found at other PGE- dominated deposits (Barnes et al. 2008) most of the PGE, except Pt, are within the BMS, with Os, Ir, Ru, Rh concentrations

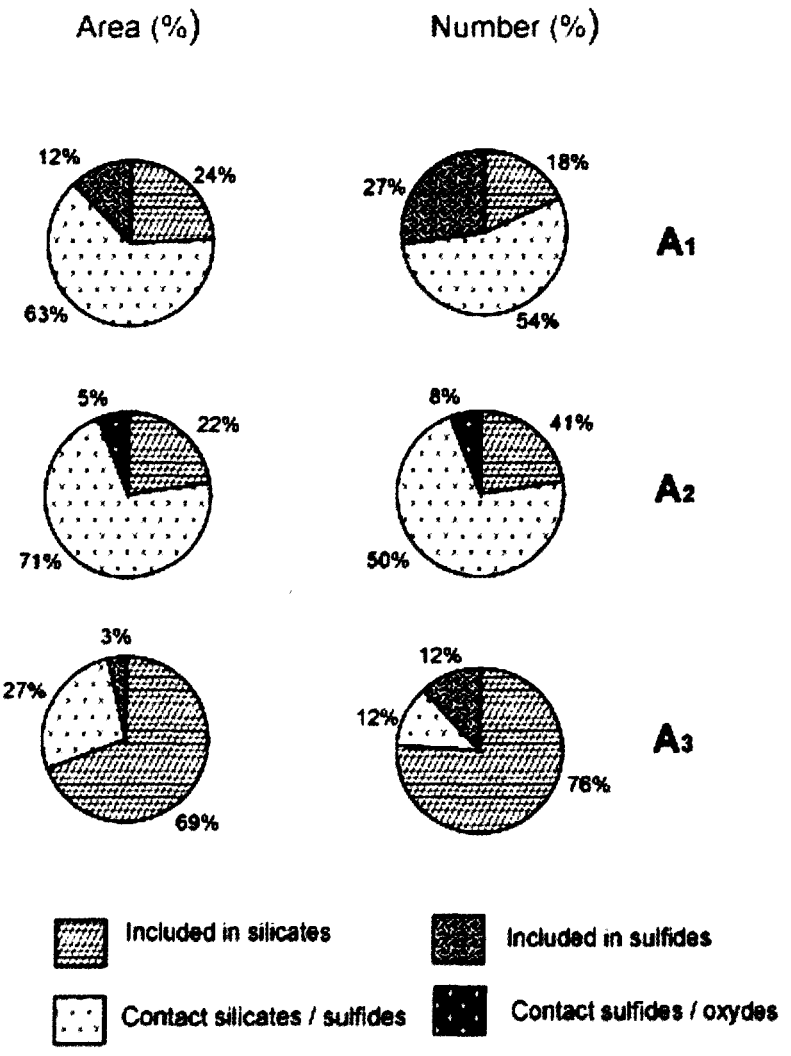

Figure 13. Details of the textural association for PGM found in the rocks containing Po-Pn-Ccp±Py assemblage (A_1), in the rocks containing Pn-Ccp-Py assemblage (A_2) and in the rocks containing Py-Ccp-Mil assemblage (A_3) at the Lac-des-Iles-Complex.

in pyrrhotite; Pd and some IPGE and Rh are in pentlandite. Chalcopyrite does not appear to host significant amounts of PGE. Palladium is also present in PGM and almost all the Pt is present in PGM. The PGM are largely located within, or at the margins of, BMS. The overall model for this type of assemblage has been outlined by a number of workers (Holwell and McDonald 2007; Godel et al. 2007; Barnes et al. 2008) and consists of the collection of the PGE from a silicate magma by a sulfide liquid followed by crystallization of that liquid as monosulfide solid solution (MSS) and intermediate solid solution (ISS). Osmium, Ir, Ru and Rh partition strongly into the MSS. Ni and Co also enter MSS, but not as strongly. Both Pd and Pt concentrate in the sulfide liquid. As the temperature falls, MSS exsolves into pyrrhotite and pentlandite which both inherit the IPGE and Rh that were originally in the MSS. The partition coefficient of Pd into MSS is ~ 0.2 (Li et al. 2001), thus there would have been a little Pd in the MSS. Palladium and Co appear to be more readily accommodated in pentlandite than in pyrrhotite and these elements diffuse into pentlandite. The remaining Pd and most of the Pt crystallized as tellurides and arsenides possibly from the fractionated sulfide liquid that remained.

Both the Pn-Ccp-Py and Py-Ccp-Mil assemblages, which appear to represent the post-magmatic sulfide assemblages, do not occur in fresh rocks. The plagioclase-amphibole equilibration temperatures determined in rocks that contain these sulfide assemblages show that these latter assemblages were stable at relatively low temperature (below 500°C; Fig. 6). However the presence late of these post-magmatic sulfide assemblages in the metagabbronorite and chlorite-actinolite schist suggests

that the increasing degree of alteration of the silicate assemblage is not directly linked to the degree of alteration of the sulfide minerals. Therefore, the relative chronology of the respective stages and developments of sulfide assemblages would be difficult to determine. The focus will thus be on the identification of the different processes responsible for the change in sulfide assemblages.

The gradual disappearance of pyrrhotite and pentlandite in association with the gradual appearance of pyrite and millerite (Table 2) are evidence that hydrothermal activity occurred within rocks that host sulfides. This process is the main reason why the magmatic sulfide assemblage changes and they elements contain are remobilized.

In general, pyrite and millerite are unusual minerals in sulfide or PGE magmatic deposits, therefore, the trace element concentrations in the magmatic context are still poorly known. Previously workers (e.g. Kelley and al. 2004; Large et al. 2007) show that pyrite from hydrothermal deposits can concentrate Co, Ni, Cu, As, Ag, Bi and Te. In this study, anhedral and idiomorphic pyrite contains Co, Ni, As, Pt, IPGE and Rh (Fig. 9). However in idiomorphic pyrite, Co and As concentrations are high compared to Ni whereas in anhedral pyrite is richer in Ni compared to Co and As (Fig. 9, 16). No correlation between these elements has been observed in either form of pyrite suggesting that complicated process occurred. The distribution of both Co and Ni appears to be caused by the extensive substitution of these elements for Fe in pyrite, reflecting the fact that Co^{2+} and Ni^{2+} have similar ionic radii to Fe^{2+}, and the fact that both CoS_2 and NiS_2 adopt the pyrite structure (Vaughan and

Craig 1978; Tossell et al. 1981). The presence of As-rich idiomorphic pyrite could be suggest that they have formed at relatively low temperatures (below 400°C, according to the equilibrium temperatures of these rocks) during hydrothermal activity by the recrystallization of anhedral pyrite as indicated from the textures (Fig. 3D, F).

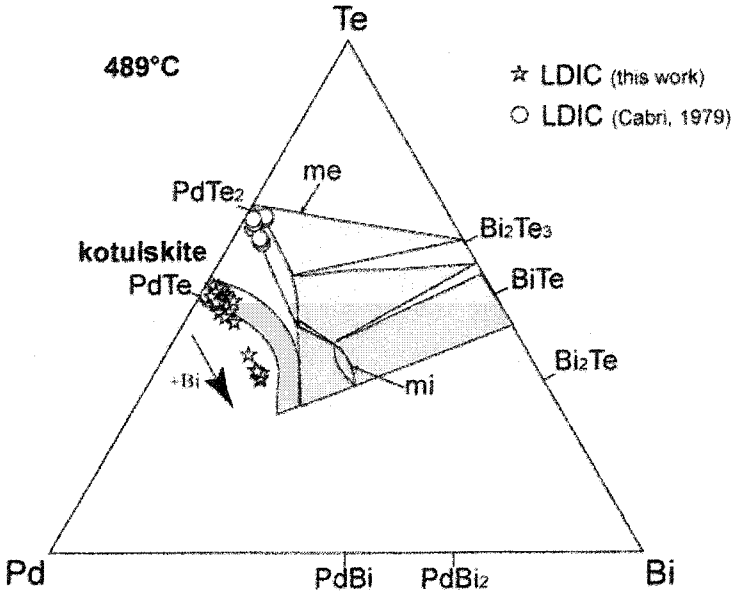

Figure 14. Phase diagram for the Pd-Bi-Te system at 489°C showing the field for Pd-Te phases from samples of the Lac-des-Iles-Complex (modified from Cabri and Laflamme 1981). The composition of the Pd-Te phase is mainly kotulskite (PdTe) and shows an enrichment of Bi. me = merenskyite, and mi = michenerite.

The IPGE and Rh contents are higher in anhedral pyrite than the idiomorphic pyrite. This suggests that either anhedral pyrite was derived from alteration of both pyrrhotite and, or pentlandite (Fig. 16), or that anhedral pyrite has directly exsolved from MSS. The results of the mass balance, and the positive correlations observed between Os, Ru and Ir or Ru and Os in pyrite, pyrrhotite and pentlandite (Fig. 10), support both hypotheses. However, if anhedral pyrite exsolves directly from MSS, then pyrrhotite and pyrite were the first sulfides which exsolved from MSS at high temperature (~ 700°C) and pentlandite exsolved at low-temperature (~300°C; Kullerud, 1963). Therefore, pyrrhotite and pyrite should be accommodating more IPGE than pentlandite. But this is not the case, the amount of IPGE contained in pyrite is the same as in pyrrhotite and pentlandite (0.08 to 1 ppm; Fig. 9). We propose that pyrite replaced the pyrrhotite and probably pentlandite also during the loss of Fe from the BMS assemblage. This is in agreement with the increase in the modal proportion of oxide minerals (magnetite and ilmenite) following the increasing degree of alteration of the sulfide minerals (Table 1). The predominance of pyrrhotite in fresh gabbronorite compared to metagabbronorite and chlorite-actinolite schist shows that the oxidization from the fluids increased along with the degree of alteration of the sulfide. This could explain why pyrite represents < 5 % (modal %) in A_1 assemblage.

We found that Co, Pd, Ag, Te and Bi are concentred in millerite. This nickel sulfide (NiS) has been described by many authors (Keele and Nickel 1974, Barnes et al. 2009) as a common metamorphic mineral which replaces pentlandite within mafic

to ultramafic rocks. In our samples, millerite is associated with secondary chalcopyrite and pyrite in the samples which are depleted in pentlandite (Table 1).

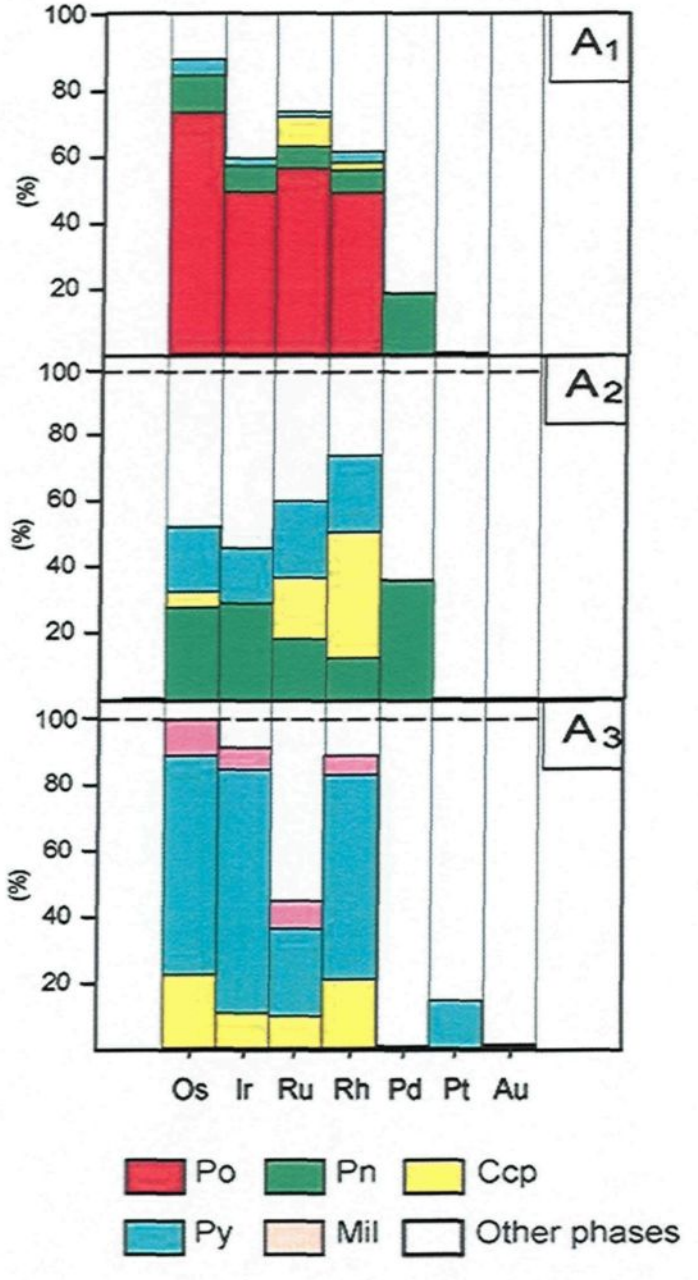

Figure 15. Mass balance of PGE and Au present in pyrrhotite (Po), pentlandite (Pn), chalcopyrite (Ccp), pyrite (Py) and millerite (Mil) in rocks containing Po-Pn-Ccp±Py assemblage (A_1), in rocks containing Pn-Ccp-Py assemblage (A_2) and in rocks containing Py-Ccp-Mil assemblage (A_3) of the Lac-des-Iles-Complex.

We suggest that millerite at LDIC replaced pentlandite mainly by the mobilization of Fe from pentlandite to the silicate minerals during the hydrothermal activity. Sulfur, Ni and the remaining Fe reach equilibrium and form millerite and pyrite following the equation:

pentlandite = millerite + pyrite + Fe

During the alteration of pentlandite Co partitioned into pyrite to form Co-rich pyrite (Fig. 16). Hinchey et al. (2005) noted the occurrence of siegenite (cobalt nickel sulfide) in the High-Grade Zone which could also accommodate Co.

We found trace amounts of Pd and Ag in millerite. It is possible that these elements were remobilized from pentlandite (Pd) and chalcopyrite (Ag) to millerite by fluid during hydrothermal alteration of these minerals.

Conditions of PGM formation and interaction of fluids

The study of PGM shows that their textural association with the other minerals changed with the degree of alteration of the rocks. In A_1 and A_2 the PGM occur either as inclusions within BMS or at the margins of BMS grains, silicate and oxides. However in A_3 most of PGM are associated with secondary silicate grains. In addition, the distribution of PGM varies in number, size and composition as the sulfide assemblage changes. Following the textural association and the distribution of PGM, we propose some process that responsible of the PGM formation in rock.

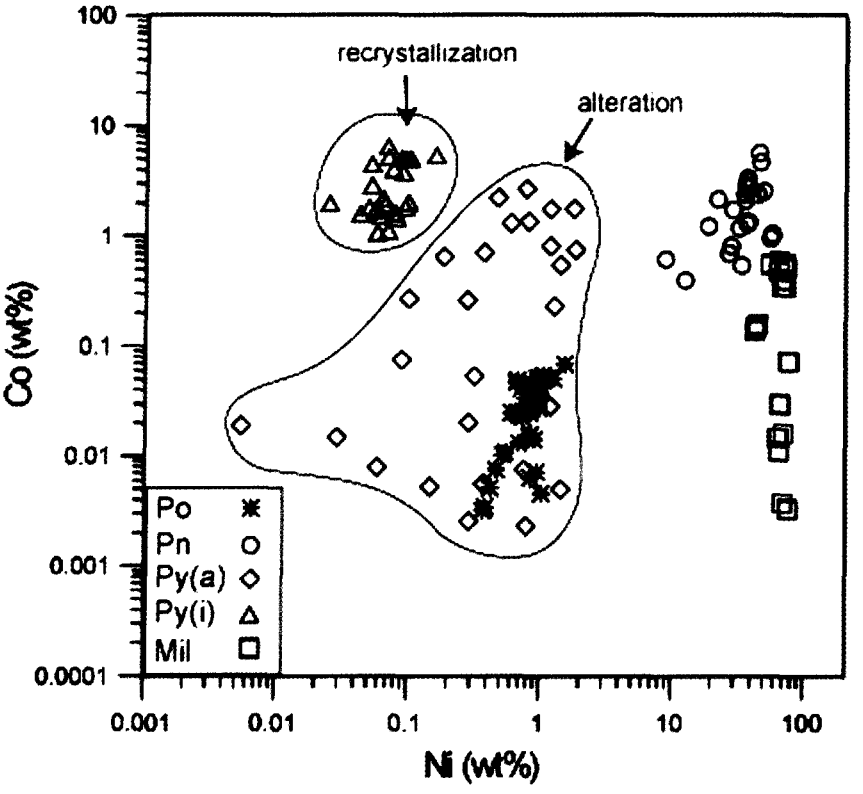

Figure 16. Binary plot of Co versus Ni. Anhedral pyrite (Pya) and millerite come from the alteration of pyrrhotite (Po) and pentlandite (Pn). Idiomorphic pyrite (Pyi) comes from the recrystallization of Py(a) enriched in Co.

The PGM observed at the margins or as inclusions in BMS could have exsolved from the base metal sulfides during cooling (Hoffman and MacLean 1976; Ortega et al. 2004; Helmy et al. 2007; Barnes et al., 2008). This may be the case for Pd-Te , Pd-As or Pd-S found mainly in A_1 corresponding to igneous gabbronorite and A_2 (Fig. 13A). However grains of PGM arsenides found in association with BMS could have formed by another process. Some authors (Cabri and Laflamme 1976, Li and Naldrett, 1993a) in their study of the Sudbury Complex have shown that certain elements such as As, Te, Sb and Bi are partitioned in to immiscible sulfide magma. During the crystallization of the sulfide liquid, As, Te, Bi and Sb could have preferentially concentrated them in the Cu-rich liquid. PGM might form by crystallisation from this liquid (Dare et al. 2010).

The presence of the isolated PGM found in silicate minerals may be interpreted in a number of ways. One suggestion is that they may result from dissolution of the BMS hosting Pd leaving isolated insoluble Pd-PGM (Barnes et al. 2008; Godel and Barnes, 2008). Alternatively, the Pd may become remobilized from the base metal sulfides and move into the surrounding silicates (Barnes et al. 2008). An alternative suggestion is that PGM crystallized directly from a silicate melt. However, this process requires local redox conditions favourable for the PGM to crystallize (Kaukonen 2008), but these minerals are not observed. The PGM which form are IPGE PGM, such as laurite (RuS_2), or an IPGE alloy and coexist with primary magmatic minerals such as olivine or chromite (Wagner 1925). The experimental work of Andrews and Brenan (2002) showed that if both IPGE-PGM

and Ru-Ir-Os alloy crystallize from a sulfur-undersaturated magma at high fS_2, a relatively oxidized, low-FeO magma is required. In our case PGM of IPGE and IPGE alloys were not observed in the samples. In addition, no olivine or chromite minerals were observed in our samples. Therefore, we suggested that similar conditions for PGM formation did not exist in LDIC. Finally, another possibility is that PGM precipitated directly from an aqueous fluid (Boudreau and Meurer 1999). This hypothesis is possible because isolated PGM are mainly hosted by secondary silicate minerals (amphibole and chlorite) particularly in chlorite-actinolite schist. The presence of a variety of PGM such as Pd-Te-Bi, Pd-Sb and Pd-As phases suggests that this fluid was enriched in Pd, Bi, As and Sb. Whole rock concentrations show that chlorite-actinolite schist is enriched in As and Sb in relation to gabbronorite and metagabbronorite. In addition Gomwe (2008) noted that there is correlation of Pd with As and Sb in the High-Grade Zone indicating that the hydrothermal process may have been enriched in these elements. Therefore, it is possible that As and Sb have been added by the same fluid that precipitated Sb and As-PGM observed in High-Grade Zone. These hypotheses are in agreement with Talkington and Watkinson (1984a) who noted the occurrence of Te, As, Bi containing PGM together with hydrous minerals and suggested that the PGE precipitated as PGM from the fluid that caused the amphibolitization. Watkinson and Lavigne (2002) conclude that the fluid was deuteric. It mobilized and favored the concentration of Pd at LDIC.

The mechanism by which Pd is transported is still poorly known. Mountain and Wood (1988b) and Wood et al. (1992) found that chloride complexes are

important agents for transporting Pt and Pd in solutions under acidic and relatively oxidizing conditions in experiments where temperature is below 300°C. However, there is no evidence that chloride complex are present in LDIC and the bulk compositions are not enriched in Cl. However, if the fluid was deuteric and in equilibrium with the host rocks, the process of transportation is less important than the process of deposition. Gomwe (2008) proposed that the accumulation of Pd at the High-Grade Zone is due to the presence of a fixant that would draw out the Pd from the circulating fluid. This fixant would be present throughout the complex, but in lower concentrations in the Roby and Twilight Zones than the High-Grade Zone which would explain the correlation between S and Pd in the samples from Roby and Twilight Zones (Gomwe 2008). We suggest that the fixant could be As, Bi or Sb. These elements coexist with Pd at high temperature (above 500 °C) in deuteric fluids, however when the temperature decreased fluid precipitated this element as PGM. This is in agreement with the amphibole-plagioclase geothermometry determined from chlorite-actinolite schist which suggests that this deuteric fluid existed below 500°C, similar to the temperature of stability of Bi-rich PGM such as michenerite (Hoffman and MacLean 1976; Makovicky 2002).

The hornblende-plagioclase geothermometry in combination with the composition of the amphibole in each rock group indicates that the amphibole equilibrated progressively with the fluid in place. Thus, it is possible that the deuteric fluid was present from fairly high temperatures and contributed to the various processes which occured during the alteration of the sulfide minerals. However, its

contribution increased systematically as the system cooled, and its chemical composition changed as temperature decreased. The presence of a late shear zone in the High-Grade Zone through which fluid was introduced probably explains the more significant degree of the alteration in this area.

Proposed model for the formation of the Lac-des-Iles-Complex

Our model builds on the model proposed by Gomwe (2008). We suggest that there was a minimum of two magma chambers (Fig. 17A). The upper chamber consisted of partially consolidated leucogabbronorite emplaced on either side of the East Gabbro of the proto MBI. This leucogabbronorite originated from a second, deeper, feeder chamber. This lower chamber contained disseminated sulfides which had a normal magmatic composition. In the first step a new S-undersaturated magma was introduced into the lower chamber and this partially dissolved the disseminated sulfide to form IPGE-rich mss, a Fe-Pt alloy and to enrich the magma in Cu, Pd and Te (Fig. 17B), by analogy with experimental work by Peregoedova et al. (2004). In the second step the Fe-Pt alloys and MSS remained in the feeder chamber and the Cu- and Pd-enriched magma was then injected into the overlying chamber. This injection of magma resulted in the formation of magmatic breccias in the Roby and Twilight Zones (Fig. 17C). The liquid sulfide segregated from the silicate magma and S, Fe, Ni, Cu Pd and Te, crystallized amongst the cumulate silicate grains, mainly as sulfides (pyrrhotite, pentlandite, chalcopyrite: Fig. 17C). The magma in the lower chamber becomes saturated in flied and infiltrated the upper chamber. Between 650 and 450 °C, deuteric alteration progressively intensified and as shown by the

mobilization of Fe and Co from BMS and the simultaneous hydrous alteration of primary silicate minerals (pyroxene and plagioclase) to secondary silicate minerals (amphibole, chlorite and talc). The formation of the High-Grade Zone occurred as the temperature decreased (< 450°C). The deuteric fluid could no longer penetrate the rocks pervasively, but became channelled within the shear zone next to the East Gabbro (Gomwe, 2008) (Fig. 17D). The Pd, Pt and Au-rich fluid precipitated PGM minerals, accompanied by Bi, Sb and As, and this lead to the creation of the Pd-rich High-Grade Zone. The focusing of the lower temperature aqueous fluid along the fractures in the shear zone accentuated the level of alteration in this zone and provided a large surface area of host rock for the fluid to interact. The presence of various PGM and the low S content in the High-Grade Zone rocks, suggests that a process of deposition occurred which involvd Bi, Te, Sb, and As. The presence of these elements resulted in the precipitation of Pd as bismuthotellurides, antimonides and arsenides that are not spatially related to the sulfide mineralization.

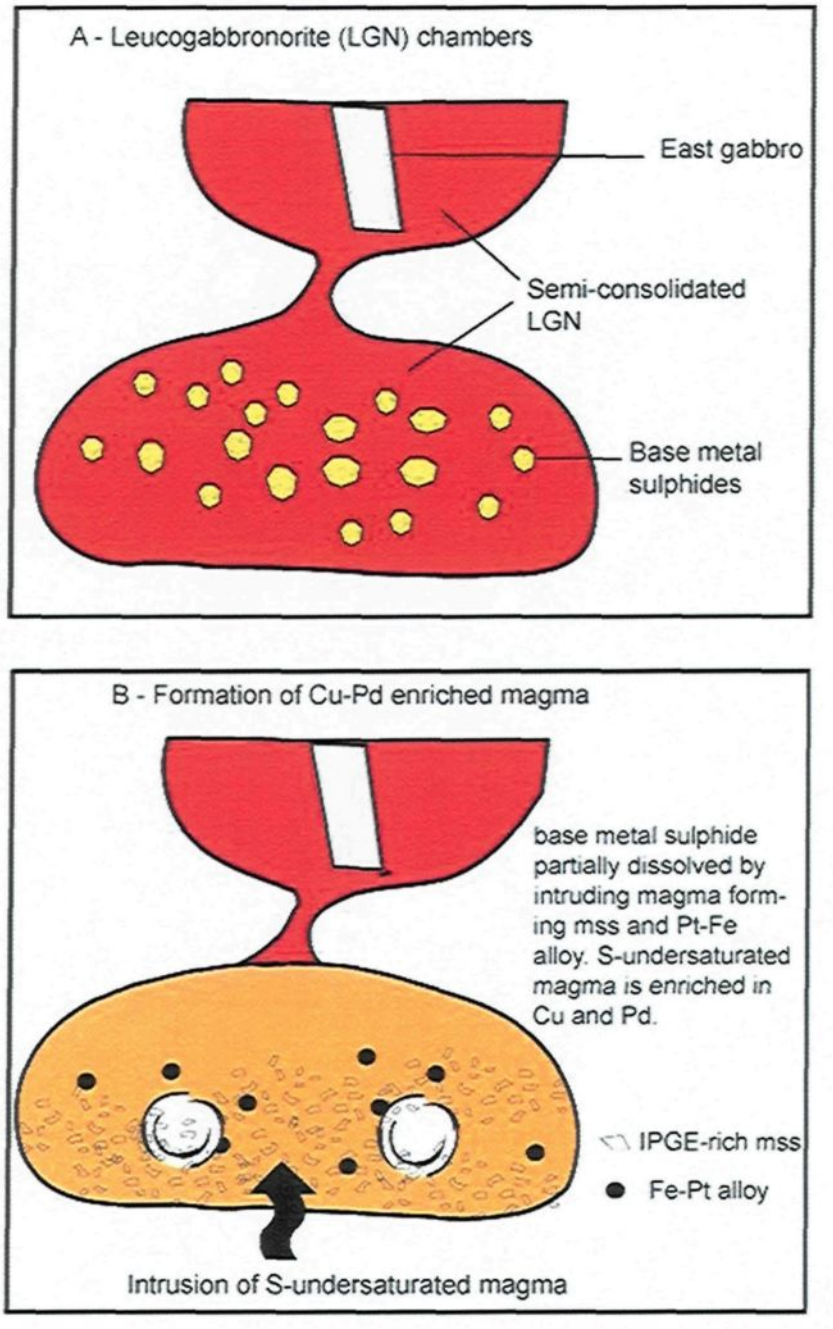

Figure 17a. Proposed model for the formation of the Lac-des-Iles-Complex. See text for the details.

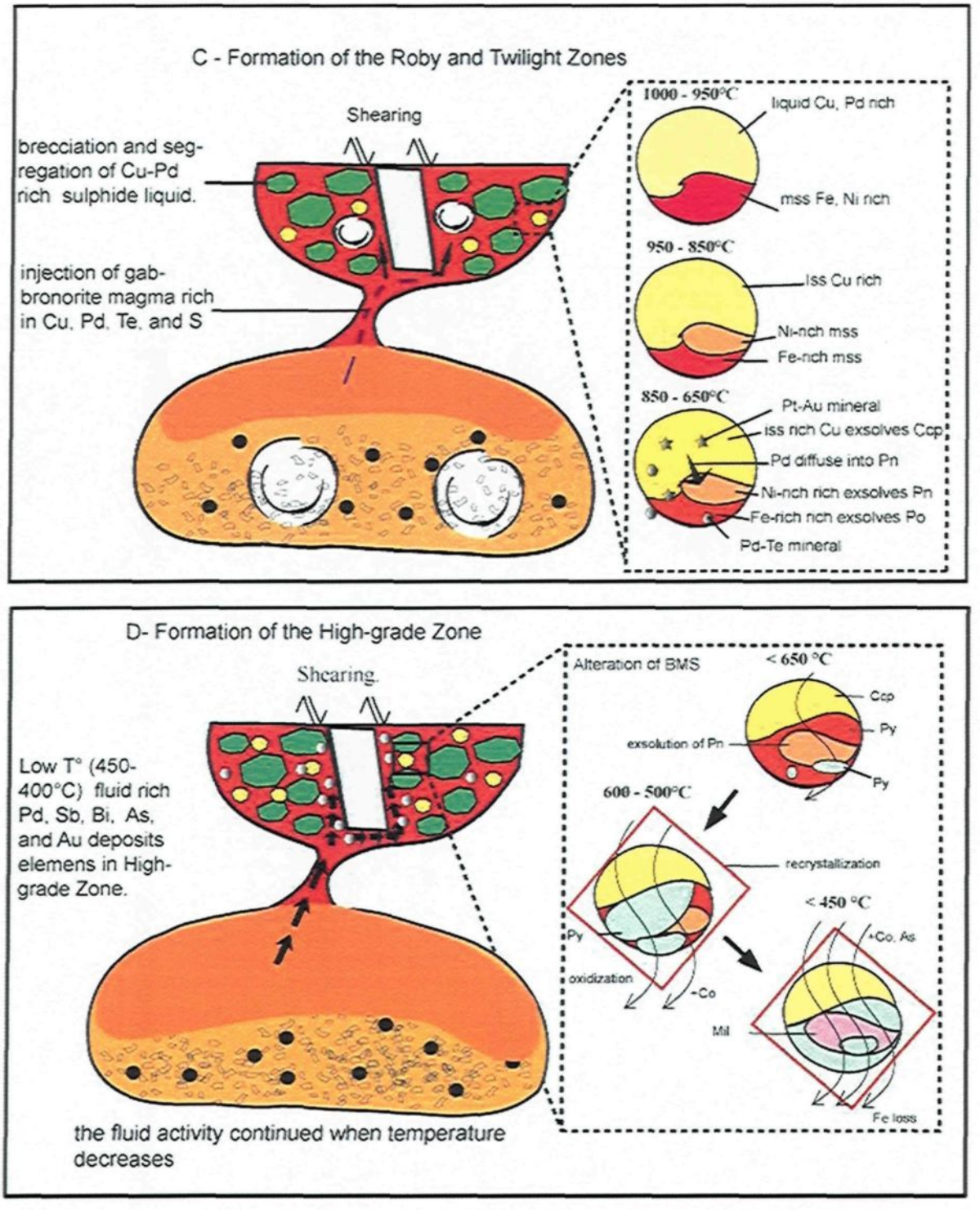

Figure 17b. Proposed model for the formation of the Lac-des-Iles-Complex. (See text for the details).

Conclusions

Detailed geochemical, mineralogical and microtextural analysis of the Lac-des-Iles -Complex indicate that:

1) The mineralogy and textures of BMS assemblages do not evolve directly with the alteration of silicate minerals. Only Po-Pn-Ccp (± Py) assemblages are preserved in gabbronorite and equilibrated between 856 and 622°C. However Py-Ccp-Pn and Py-Ccp ± Mil assemblages are preserved in metagabbronorite and chlorite-actinolite schist that equilibrated between 713 and 456°C and between 615 and 417°C successively.

2) The BMS and the PGM are the only phases which controlled the PGE. Palladium in the magmatic rocks was concentrated by a sulfide liquid that crystallized monosulfide solid solution (MSS) which then exsolved to pentlandite and pyrrhotite. Pentlandite controls 20 to 30% Pd when it is present in gabbronorite and metagabbronorite. The rest of Pd is controlled by the PGM which are associated with sulfide minerals. In the chlorite-actinolite schist, Pd is mainly present as a variety of PGM which are not associated with the sulfides.

3) Kotulskite (PdTe) is a dominant PGM of Lac-des-Iles-Complex. Most of it is associated with BMS suggesting that this PGM exsolved from BMS during the cooling of the sulfide liquid.

4) The presence of IPGE in pyrite, pyrrhotite and pentlandite suggest that pyrite formed from the alteration of pyrrhotite and pentlandite during the hydrothermal activity.

5) The enrichment of Pd occurred during the late stage of hydrothermal activity as deuteric fluid percolated along a zone of enhanced permeability at low temperature (<500 ° C). This fluid is inferred to be rich in Pd, As, Sb and Bi and was concentrated into the permeable shear zone, which now corresponds to the High-Grade Zone, and there precipitated Pd in the form of Pd-Bi-Te, Pd-Sb, Pd-As, Pd-S and Pd-Te.

CHAPITRE III

CONCLUSION GÉNÉRALE

Afin de mieux comprendre l'enrichissement du Pd dans le Complexe mafique du Lac-des-Iles en Ontario, le but principal de cette étude était axé sur l'identification des phases minérales qui contrôlent particulièrement le palladium et les autres éléments chalcophiles dans les zones minéralisées du Complexe mafique.

Les résultats retenus suivis de leur interprétation indiquent qu'il y'a 3 assemblages de sulfures : un assemblage sulfuré magmatique incluant pyrrhotite-pentlandite-chalcopyrite±pyrite, et deux assemblages sulfurés post-magmatiques incluant la pentlandite-chalcopyrite-pyrite et pyrite-chalcopyrite-millerite. Il a été suggéré que le changement des sulfures magmatiques pour les sulfures post-magmatiques pourraient être du à la mobilization du Fe des sulfures pendant l'altération hydrothermale.

Seule la pentlandite quand elle est présente contrôle 20 à 30 % de palladium comme tel est le cas dans la plus part des dépôts magmatiques d'éléments du groupe de platine. Dans les roches moins altérées, considérées comme magmatiques (les gabbronorites et certaines métagabbronorites), le reste de palladium est inclus dans les minéraux du groupe de platine qui sont associés aux sulfures. Cependant dans les roches très altérées où la pentlandite est presque inexistante (particulièrement les chlorite-actinote schistes et quelques métagabbronorites) le palladium est contrôlé par

les minéraux du groupe du platine qui ne sont pas associés aux sulfures mais qu'on retrouve généralement dans les minéraux silicatés secondaires.

La distribution du type et de la proportion des minéraux du groupe du platine en fonction des assemblages de sulfures suggèrent que les éléments comme Bi, Sb, As et Pd se sont concentré par un fluide deuterique tardif qui a précipité ces éléments comme minéral du groupe de platine et qui probablement est responsable de l'enrichissement de Pd dans la Zone High-Grade.

PERSPECTIVE À VENIR

Cette étude serait largement complétée si un accent additionnel pourrait être mis sur :

- L'étude des inclusions fluides afin de connaître la chimie et la composition originelle des fluides mise en évidence.
- Une étude in-situ d'isotopes stable d'oxygène afin de déterminer l'origine des fluides.
- Une méthode de dosage du Bi et Te afin de déterminé la concentration exacte de ses éléments dans la roche totale.

REFERENCES

Andrews DR, Brenan JM (2002) Phase-equilibrium constraints on the magmatic origin of laurite + Ru-Os-Ir alloy. The Canadian Mineralogist 40:1705–1716

Barnes S-J, Naldrett A J (1985) Geochemistry of the J-M (Howland) Reef of the Stillwater Complex, Minneapolis Adit Area. I. Sulphide Chemistry and Sulphide-Olivine Equilibrium. Economic Geology 80:627-645

Barnes S-J, Acterberg E, Makovicky E, Li C (2001a) Proton probe results for partitioning of platinum group elements between monosulphide solid solution and sulphide liquid. South African Journal of Geology 104:337–351

Barnes S-J, Maier WD (2002) Platinum-group elements and microstructures of Normal Merensky Reef from Impala Platinum Mines, Bushveld Complex. Journal of Petrology 43:103-128

Barnes S-J, Prichard HM, Cox RA, Fisher PC, Godel B (2007) Highly siderophile elements in platinum-group element ore deposits. Geochimica Et Cosmochimica Acta 71: A62-A62

Barnes S-J, Cox RA, Prichard HM, Fisher PC, McDonald I et al (2008) Siderophile and chalcophile elements in sulphides from the Morokweng LL meteorite and implications for platinum-group element deposits. Geochimica et Cosmochimica 72:A57-A57

Barnes S-J, Prichard HM, Cox RA, Fisher PC, Godel B (2007) Highly siderophile elements in platinum-group element ore deposits. Geochimica Et Cosmochimica Acta 71:A62-A62

Barnes ST, Wells MA,Verrall MR (2009) Effects of Magmatic Processes, Serpentinization, and Talc-Carbonate Alteration on Sulfide Mineralogy and Ore Textures in the Black Swan Disseminated Nickel Sulfide Deposit, Yilgarn Craton. Economic Geology 104:539-562

Becker H, Horan MF et al (2006) Highly siderophile element composition of the Earth's primitive upper mantle: Constraints from new data on peridotite massifs and xenoliths. Geochimica et Cosmochimica Acta 70:4528–4550

Bedard LP, Barnes S-J (2002) A comparison of the capacity of FA-ICP-MS and FA-INAA to determine platinum-group elements and gold in geological samples. Journal of Radioanalytical and Nuclear Chemistry 254:319-329

Bedard LP, Savard DD, Barnes S-J (2008) Total sulphur concentration in geological reference materials by elemental infrared analyzer. Journal of Geostandards and Geoanalysis 32:203-208

Blundy JD, Holland TJB (1990) Calcic amphibole equilibria and a new amphibole-plagioclase geothermometer. Contributions to Mineralogy and Petrology 104:208–224

Boudreau AE, Meurer WP (1999) Chromatographic separation of the platinum-group elements, gold, base metals and sulfur during degassing of a compacting and solidifying igneous crystal pile. Contributions to Mineralogy and Petrology 134:174-185

Brugmann GE, Naldrett AJ, Macdonald AJ (1989) Magma Mixing and Constitutional Zone-Refining in the Lac-Des-Iles Complex, Ontario - Genesis of Platinum-Group Element Mineralization. Economic Geology 84:1557-1573

Brugmann GE, Reischrnann T, Naldrett AJ, Sutcliffe RH (1997) Roots of an Archean volcanic arc complex; the Lac des îles area in Ontario, Canada. Precambrian Research 81:223-239

Cabri LJ, Laflamme JHG (1979) Mineralogy of Samples from the Lac des Iles Area, Ontario. CANMET Report 79-27:20

Cabri LJ (2002) The Platinum-Group Minerals, In Cabri, L. J.(ed.) Geology, Geochemistry, Mineralogy and Mineral Benefication of Platinum Group Element. Canadian Institute of Mining, Metallurgy and Petroleum 54:13-129

Craig JR (1973) Pyrite-pentlandite and other low temperature assemblages in the Fe-Ni-S system. American Journal of Science 273A: 496-510

Dare SAS, Barnes S-J, Prichard HM (2010) The distribution of platinum group elements (PGE) and other chalcophile elements among sulfides from the Creighton Ni–Cu–PGE sulfide deposit, Sudbury, Canada, and the origin of palladium in pentlandite. Mineralium Deposita 45:1-29

Desborough GA, Finney JJ, Leonard BF (1973) Mertieite, a new palladium mineral from Good news Bay, Alaska. American Mineralogist 58:1-10

Dionne-Foster C (2002) Étude Minéragraphique et Pétrologique de la Zone Twilight, Complexe du Lac des Îles, Ontario. Projet de fin détude, Université du Québec à Chicoutimi

Dunning GR (1979) The Geology and Platinum-group mineralization of the Roby Zone, Lac des îles Complex, Northwestern Ontario. MSc thesis, University of Toronto

Ernst WG, Liu J (1998) Experimental phase-equilibrium study of Al- and Ti-contents of calcic amphibole in MORB; a semiquantitative thermobarometer. American Mineralogist 83:952-969

Godel B, Barnes S-J (2008) Platinum-group elements in sulfide minerals and the whole rocks of the J-M Reef (Stillwater Complex): Implication for the formation of the reef. Chemical Geology 248:272-294

Godel B, Barnes S-J, Maier WD (2007) Platinum-group elements in sulphide minerals, platinum-group minerals, and whole-rocks of the Merensky Reef (Bushveld Complex, South Africa): Implications for the formation of the reef. Journal of Petrology 48:1569-1604

Gomwe ST (2008) The formation of the palladium-rich Roby, Twilight and High-grade Zones of the Lac des Iles Complex. PhD Thesis, Université du Québec à Chicoutimi

Hattori KH, Cameron EM (2004) Using the high mobility of palladium in surface media in exploration for platinum group element deposits: Evidence from the Lac des Iles Region, northwestern Ontario. Economic Geology 99:157-171

Helmy HM, Ballhaus C, Berndt J, Bockrath C, Wohlgemuth-Ueberwasser C (2007) Formation of Pt, Pd and Ni tellurides: Experiments in sulfide-telluride systems. Contributions to Mineralogy and Petrology 153:577–591

Hey MH (1954) A new review of the chlorites. Mineralogical Magazine 30:277-292

Hinchey JG, Hattori KH (2005) Magmatic mineralization and hydrothermal enrichment of the High Grade Zone at the Lac des Iles palladium mine, northern Ontario, Canada. Mineralium Deposita 40:13-23

Hinchey JG, Hattori KH, Langne MJ (2005) Geology, petrology, and controls on PGE mineralization of the southern Roby and Twilight zones, Lac des Iles mine, Canada. Economic Geology 100:43-61

Hoffman E, MacLean WH (1976) Phase relations of michenerite and merenskyite in the Pd-Bi-Te System. Economic Geology 71:1461–1468

Holwell DA, McDonald I (2007) Distribution of platinum-group elements in the Platreef at Overysel, northern Bushveld Complex; a combined PGM and LA-ICP-MS study. Contributions to Mineralogy and Petrology 154:171-190

Huminicki MAE, Sylvester PJ, Cabri LJ, Lesher CM, Tubrett M (2005) Quantitative mass balance of platinum-group elements in the Kelly Lake Ni-Cu-PGE deposit, Copper Cliff Offset, Sudbury. Economic Geology 100:1631 – 1646.

Kaukonen R (2008) Sulfide-poor platinum-group element deposits A mineralogical approach with case studies and examples from the literature. PhD thesis, University of Oulu

Keele R, Nickel EH (1974) The geology of a primary millerite-bearing sulfide assemblage and supergene alteration at the Otter shoot, Kambalda, Western Australia. Economic Geology 69:1102-1117

Kelley KD, Leach DL, Johnson CA, Clark JL et al (2004) Textural, compositional, and sulfur isotope variations of sulfide minerals in the Red Dog Zn-Pb-Ag deposits, Brooks Range, Alaska: Implications for ore formation. Economic Geology 99:1509–1532

Kullerud G, Yung RA, Moh GH (1969) Phase relations in the Cu-Fe-S, Cu-Ni-S, and Fe-Ni-S systems. Economic Geology Monograph 323-343

Lavigne MJ, Michaud MJ (2001) Geology of North American Palladium Ltd.'s Roby Zone Deposit, Lac des Iles. Exploration and Mining Geology 10:1-17

Large RR, Maslennikov V, Robert F, Danyushevsky LV,Chang Z (2007) Multistage sedimentary and metamorphic origin of pyrite and gold in the giant Sukhoi Log deposit, Lena gold province, Russia. Economic Geology 102:232–1267

Li C, Naldrett AJ (1993a) PGM from the Deep Copper zone of the Strathcona deposit, Sudbury, Ontario. The Canadian Mineralogist 31:31-44

Li C, Maier WD, Waal SA (2001) Magmatic Ni-Cu versus PGE deposits: Contrasting genetic controls and exploration implications. South African Journal of Geology 104(4):309 - 318

Makovicky E (2002) Ternary and quaternary phase systems with PGE. Canadian Institute of Mining, Metallurgy and Petroleum 54:121–175

Michaud MJ (1998) The Geology, Petrology, Geochemistry and Platinum-Group Element-Gold-Copper-Nickel Ore Assemblage of the Roby Zone, Lac des îles Mafic-Ultramafic Complex, Northwestern Ontario. MSc thesis, Lakehead University

Mountain BW, Wood SA (1988b) Solubility and transport of platinum-group elements in hydrothermal solutions; Thermodynamic and physical chemical constraints. Geo-Platinum 87, edited by HM Prichard, PJ Potts, JFW Bowles, SJ Cribb, Open University 57-82

Naldrett AD (2004) Magmatic sulfide deposits: geology, geochemistry and exploration. Springer-Verlag, Heidelberg, Berlin

Naldrett A D, Gasparini E C, Barnes S-J, Von Graenewaldt G, Sharpe MR (1986) The Upper Critical Zone of the Bushveld Complex and the origin of the Merensky-type ores. Economic Geology 81:1105-1117

Oberthür T, Cabri LJ, Weiser TW, McMahon G, Muller P (1997) Pt, Pd and other trace elements in sulfides of the main sulfide zone, Great Dyke, Zimbabwe: a reconnaissance study. The Canadian Mineralogist 35:597–609

Peregoedova A, Barnes S-J, Baker DR (2004) The formation of Pt-Ir alloys and Cu-Pd-rich sulfide melts by partial desulfurization of Fe-Ni-Cu sulfides; results of experiments and implications for natural systems. Chemical Geology 208:247-264

Peregoedova A, Barnes S-J, Baker DR (2006) An experimental study of mass transfer of platinum-group elements, gold, nickel and copper in sulfur-dominated vapor at magmatic temperatures: Chemical Geology 235:59-75

Piña R, Romeo I, Ortega L et al (2010) Origin and emplacement of the Aguablanca magmatic Ni-Cu-(PGE) sulfide deposit, SW Iberia: A multidisciplinary approach: Geological Society of America 122: 915-925

Pye EG (1968) Geology of the Lac des îles area, District of Thunderbay. Ontario. Department of Mines Geology Report 64-47

Ripley EM (1981) Sulfur isotopic studies of the Dunka Road Cu-Ni deposit, Duluth Complex, Minnesota. Economic Geology 76:610-620

Savard D, Barnes S-J, Meiseil T (accepted) Comparison between nickel-sulfur fire-assay Te-co-precipitation and isotopic-dilution with high pressure asher techniques for determination of platinum-group elements, rhenium and gold. Geostandarts and Geoanalytical Research

Stone D, Lavigne MJ, Schnieders B, Scott J, Wagner D (2003) Regional Geology of the Lac des Iles Area. Summary of Field Work and Other Activities Open File Report 6120, Ontario Geological Survey

Sutcliffe RH (1989) Magma Mixing in Late Archean Tonalitic and Mafic Rocks of the Lac Des Iles Area, Western Superior Province. Precambrian Research 44:81-101

Talkington RW, Watkinson DH (1984) Trends in the Distribution of the Precious Metals in the Lac-Des-Iles Complex, Northwestern Ontario. The Canadian Mineralogist 22:125-136

Tossell JA, Vaughan DJ, Burdett JK (1981) Pyrite, marcasite, and arsenopyrite-type minerals; crystal chemical and structural principles. Physics and Chemistry of Minerals 7:177–184

Ortega L, Lunar R, Garcia PalomeroF, Moreno T, Martin Estevez JR et al (2004) The Aguablanca Ni–Cu–PGE deposit, Southwestern Iberia: magmatic ore-forming processes and retrograde evolution. The Canadian Mineralogist 42:325-350

Vaughan DJ, Craig JR (1978) Mineral Chemistry of Metal Sulfides: Press, Cambridge University

Viljoen MJ (1999) The nature and origin of the Merensky Reef of the western Bushveld Complex based on geological facies and geophysical data. Geological Society of South Africa 102(3):221–239

Von Gruenewaldt G, Hatton CJ, Merkle RKW, Gain SB (1986) Platinum-group element chromitite associations in the Bushveld Complex. Economic Geology 81:1067-1079

Von Gruenewaldt G, Hulbert LJ, Naldrett AJ (1989) Contrasting platinum-group element concentration patterns in cumulates of the Bushveld Complex. Mineralium deposita, 24-219-229

Wagner PA (1925) Notes on the Platinum Deposits of the Bushveld Igneous Complex. Transactions of the Geological Society of South Africa 28:83-133

Watkinson DH, Dunning GR (1979) Geology and platinum-group mineralization, Lac des îles Complex, northwestern Ontario. Canadian Mineralogist 17-453-462

Watkinson D H, Lavigne MJ, Fox PE (2002) Magmatic-Hydrothermal Cu- and Pd-rich Deposits in Gabbroic Rocks from North America;The Geology,

Geochemistry, Mineralogy and Mineral Beneficiation of Platinum-Group Elements. Canadian Institute of Mining, Metallurgy and Petroleum 299-320

Wilson SA, Ridley WI, Koenig AE (2002) Development of sulfide calibration standards for the laser ablation inductively-coupled plasma mass spectrometry technique: Journal of Analytical Atomic Spectrometry 17:406–409

Wood SA, Mountain BW, Pan P (1992) The aqueous geochemistry of platinum, palladium and gold: Recent experimental constraints and a re-evaluation of theoretical predictions. Canadian Mineralogist 30-955-982

Zientek ML, Cooper RW et al (2002) Platinum-group element mineralization in the Stillwater Complex, Montana In: Cabri LJ (ed) The Geology, Geochemistry, Mineralogy and Mineral Beneficiation of Platinum-Group Elements. Canadian Institute of Mining and Metallurgy 459-481

ANNEXES

Table A1. Electron microprobe analyses of plagioclase from the Lac-des-Iles-Complex.

Sample	Assemblage	SiO2 wt.%	Al2O3 wt.%	CaO wt.%	FeO wt.%	Na2O wt.%	K2O wt.%	Total	Si at.%	Al at.%	Ca at.%	Fe2+ at.%	Na at.%	K at.%
TZ1 1c	Po-Pn-Ccp±Py	50.1	31.3	14.5	0.26	3.31	0.05	99	2.29	1.69	0.71	0.01	0.29	0.003
TZ1 2g	Po-Pn-Ccp±Py	50.5	30.7	14.3	0.33	3.48	0.15	99	2.31	1.66	0.70	0.01	0.31	0.009
TZ1 3f	Po-Pn-Ccp±Py	48.9	32.0	15.5	0.31	2.80	0.15	99	2.24	1.73	0.76	0.01	0.25	0.009
TZ1 3c	Po-Pn-Ccp±Py	50.9	30.9	14.2	0.30	3.48	0.19	100	2.32	1.66	0.69	0.01	0.30	0.01
TZ1 3e	Po-Pn-Ccp±Py	49.1	32.3	15.7	0.34	2.65	0.09	100	2.24	1.74	0.77	0.01	0.23	0.006
TZ7 1g	Po-Pn-Ccp±Py	52.5	30.3	13.2	0.22	4.19	0.08	100	2.37	1.61	0.63	0.009	0.36	0.005
TZ7 1f	Po-Pn-Ccp±Py	52.3	30.9	13.2	0.16	4.18	0.04	100	2.35	1.64	0.63	0.006	0.36	0.003
TZ7 2g	Po-Pn-Ccp±Py	51.0	31.3	14.0	0.20	3.80	0.04	100	2.31	1.67	0.68	0.008	0.33	0.003
TZ7 2h	Po-Pn-Ccp±Py	50.4	32.7	15.6	0.29	2.78	0.06	101	2.26	1.73	0.75	0.01	0.24	0.004
TZ7 2j	Po-Pn-Ccp±Py	52.0	30.4	12.8	1.10	4.37	0.08	100	2.35	1.62	0.62	0.04	0.38	0.005
TZ7 3f	Po-Pn-Ccp±Py	52.7	30.0	12.7	0.14	4.47	0.06	100	2.38	1.60	0.61	0.006	0.39	0.004
TZ7 3d	Po-Pn-Ccp±Py	52.6	29.8	12.6	0.22	4.45	0.09	100	2.38	1.59	0.61	0.008	0.39	0.006
TZ7 3d1	Po-Pn-Ccp±Py	50.0	32.2	15.1	0.21	3.13	0.06	100	2.26	1.72	0.73	0.008	0.27	0.004
TZ7 4g	Po-Pn-Ccp±Py	51.7	30.4	13.2	0.20	4.17	0.03	99	2.35	1.63	0.64	0.008	0.36	0.002
TZ7 4f	Po-Pn-Ccp±Py	52.2	30.2	12.9	0.35	4.34	0.03	100	2.36	1.61	0.63	0.01	0.38	0.002
TZ7 4e	Po-Pn-Ccp±Py	47.1	33.7	17.2	0.24	1.97	0.01	100	2.16	1.81	0.84	0.009	0.17	0.001
TZ7 5d	Po-Pn-Ccp±Py	48.3	32.8	16.1	0.16	2.50	0.01	100	2.21	1.77	0.79	0.006	0.22	0.001
TZ7 6c	Po-Pn-Ccp±Py	51.4	30.8	13.7	0.22	3.91	0.01	100	2.33	1.65	0.67	0.008	0.34	0.001
TZ7 6d	Po-Pn-Ccp±Py	47.1	33.9	17.1	0.25	1.94	0.01	100	2.15	1.83	0.84	0.01	0.17	0.001
TZ7 7c	Po-Pn-Ccp±Py	47.7	33.6	16.7	0.18	2.26	0.01	100	2.18	1.80	0.82	0.007	0.20	0.001
TZ7 7f	Po-Pn-Ccp±Py	52.2	30.6	13.3	0.20	4.20	0.12	100	2.35	1.63	0.64	0.008	0.36	0.007
TZ19 1f	Po-Pn-Ccp±Py	50.0	32.1	14.8	0.25	3.20	0.05	100	2.27	1.72	0.72	0.01	0.28	0.003
TZ19 1g	Po-Pn-Ccp±Py	51.3	31.0	13.6	0.18	3.88	0.04	100	2.33	1.66	0.66	0.007	0.34	0.003
TZ19 1h	Po-Pn-Ccp±Py	49.5	32.4	15.0	0.18	3.14	0.03	100	2.25	1.74	0.73	0.007	0.27	0.002
TZ19 1i	Po-Pn-Ccp±Py	47.7	32.4	15.3	0.22	2.65	0.06	98	2.21	1.77	0.76	0.009	0.23	0.004
TZ19 2f	Po-Pn-Ccp±Py	51.5	31.0	13.5	0.09	4.01	0.02	100	2.33	1.65	0.65	0.004	0.35	0.001
TZ19 2g	Po-Pn-Ccp±Py	49.4	32.2	14.8	0.18	3.11	0.02	99	2.26	1.73	0.72	0.007	0.27	0.002
TZ19 3g	Po-Pn-Ccp±Py	51.6	30.7	13.4	0.23	3.84	0.13	100	2.34	1.64	0.65	0.009	0.33	0.008
TZ19 3h	Po-Pn-Ccp±Py	49.5	32.0	15.0	0.26	3.02	0.06	100	2.26	1.72	0.73	0.01	0.26	0.004
TZ19 3i	Po-Pn-Ccp±Py	50.6	31.6	14.2	0.21	3.50	0.05	100	2.29	1.69	0.69	0.008	0.30	0.003
TZ19 3f	Po-Pn-Ccp±Py	50.7	31.2	14.0	0.27	3.58	0.13	100	2.31	1.67	0.68	0.01	0.31	0.008
TZ19 4h	Po-Pn-Ccp±Py	51.1	30.7	13.9	0.24	3.65	0.14	100	2.33	1.65	0.67	0.009	0.32	0.009
TZ19 4g	Po-Pn-Ccp±Py	51.2	30.9	13.6	0.24	3.79	0.18	100	2.32	1.65	0.66	0.009	0.33	0.01
TZ19 4f	Po-Pn-Ccp±Py	50.7	31.0	14.0	0.22	3.65	0.15	99	2.31	1.67	0.68	0.008	0.32	0.009

Sample	Assemblage	SiO2 wt.%	Al2O3 wt.%	CaO wt.%	FeO wt.%	Na2O wt.%	K2O wt.%	Total	Si at.%	Al at.%	Ca at.%	Fe2+ at.%	Na at.%	K at.%
TZ19 4e	Po-Pn-Ccp±Py	50.1	31.8	14.7	0.32	3.34	0.09	100	2.27	1.70	0.71	0.01	0.29	0.005
TZ19 5f	Po-Pn-Ccp±Py	50.4	31.5	14.1	0.21	3.68	0.05	100	2.29	1.69	0.69	0.008	0.32	0.003
TZ19 5g	Po-Pn-Ccp±Py	51.3	31.1	13.6	0.16	4.00	0.03	100	2.32	1.66	0.66	0.006	0.35	0.002
TZ19 5h	Po-Pn-Ccp±Py	51.1	31.3	13.7	0.2	3.88	0.05	100	2.31	1.67	0.66	0.008	0.34	0.003
TZ19 5i	Po-Pn-Ccp±Py	51.3	30.8	13.5	0.3	3.94	0.05	100	2.33	1.65	0.66	0.01	0.34	0.003
TZ19 5j	Po-Pn-Ccp±Py	51.5	31.0	13.5	0.38	3.98	0.11	100	2.33	1.65	0.65	0.01	0.35	0.006
TZ19 6g	Po-Pn-Ccp±Py	49.8	32.0	14.8	0.20	3.24	0.02	100	2.27	1.72	0.72	0.008	0.28	0.001
RZ30 1g	Po-Pn-Ccp±Py	51.6	29.2	12.6	0.14	4.49	0.06	98	2.38	1.59	0.62	0.006	0.40	0.004
RZ30 1e	Po-Pn-Ccp±Py	50.8	31.4	15.2	0.24	2.99	0.01	100	2.3	1.67	0.74	0.009	0.26	0.001
RZ30 4d	Po-Pn-Ccp±Py	52.1	29.7	13.2	0.19	4.21	0.10	99	2.37	1.59	0.64	0.007	0.37	0.006
RZ30 4e	Po-Pn-Ccp±Py	51.2	30.9	13.8	0.07	3.80	0.05	99	2.33	1.65	0.67	0.003	0.33	0.003
TZ15 1c	Pn-Ccp-Py	47.5	32.4	16.0	0.42	2.54	0.09	99	2.20	1.77	0.79	0.01	0.22	0.006
TZ15 2g	Pn-Ccp-Py	50.3	31.3	14.5	0.29	3.43	0.03	99	2.29	1.68	0.71	0.01	0.30	0.002
TZ15 3b1	Pn-Ccp-Py	48.3	32.6	16.0	0.22	2.50	0.04	99	2.22	1.76	0.79	0.008	0.22	0.003
TZ15 3e	Pn-Ccp-Py	50.1	31.7	14.8	0.43	3.16	0.13	100	2.28	1.70	0.72	0.01	0.27	0.008
TZ15 3e1	Pn-Ccp-Py	48.9	32.4	15.0	0.32	3.06	0.06	100	2.24	1.74	0.74	0.01	0.27	0.004
TZ15 4h	Pn-Ccp-Py	50.1	31.5	14.3	0.25	3.57	0.05	99	2.28	1.69	0.70	0.01	0.31	0.003
TZ15 4g	Pn-Ccp-Py	50.2	31.1	13.9	0.19	3.82	0.03	99	2.30	1.68	0.68	0.008	0.34	0.002
TZ15 5d	Pn-Ccp-Py	48.5	32.4	15.8	0.96	2.59	0.04	100	2.22	1.74	0.77	0.03	0.22	0.003
TZ15 6d	Pn-Ccp-Py	49.6	32.4	15.0	0.40	3.25	0.06	100	2.25	1.73	0.73	0.01	0.28	0.004
TZ15 6f	Pn-Ccp-Py	48.9	32.2	15.5	0.32	3.02	0.05	100	2.23	1.74	0.76	0.01	0.26	0.003
TZ15 7h	Pn-Ccp-Py	48.4	32.6	15.8	0.28	2.64	0.03	99	2.22	1.76	0.77	0.01	0.23	0.002
RZ17 2e	Pn-Ccp-Py	50.9	30.6	13.6	0.25	3.92	0.04	99	2.33	1.65	0.67	0.01	0.34	0.002
RZ17 3f	Pn-Ccp-Py	47.7	33.0	16.1	0.41	2.34	0.03	99	2.19	1.79	0.79	0.01	0.20	0.002
RZ17 4b	Pn-Ccp-Py	50.6	31.3	14.2	0.14	3.62	0.04	100	2.30	1.68	0.69	0.005	0.32	0.002
RZ17 4c	Pn-Ccp-Py	67.0	20.9	1.22	0.01	11.1	0.01	100	2.92	1.07	0.05	0.001	0.94	0.001
RZ3 2d	Py-Ccp-Mil	51.6	30.5	13.4	0.20	3.96	0.03	99	2.35	1.63	0.65	0.008	0.35	0.002
RZ3 2e	Py-Ccp-Mil	52.3	30.3	12.6	0.39	4.49	0.04	100	2.37	1.61	0.61	0.01	0.39	0.003
RZ3 3c	Py-Ccp-Mil	53.0	29.7	11.8	0.13	4.96	0.05	99	2.40	1.59	0.57	0.005	0.43	0.003
RZ3 3d	Py-Ccp-Mil	52.7	30.2	12.2	0.22	4.68	0.03	100	2.38	1.61	0.59	0.009	0.41	0.002

Table A2. **Electron microprobe analyses of Ca-amphibole from the Lac-des-Iles-Complex.**

Sample	Assemblage	SiO2 wt.%	TiO2 wt.%	Al2O3 wt.%	FeO wt.%	MgO wt.%	MnO wt.%	CaO wt.%	Na2O wt.%	K2O wt.%	NiO wt.%	H2O wt.%	F wt.%	Cl wt.%	Total	Si at.%	Ti at.%	Al at.%	Mg at.%	Ca at.%	Mn at.%	Fe2+ at.%	Fe3+ at.%	Ni at.%	Na at.%	K at.%
TZ1 1b	Po-Pn-Ccp±Py	51.1	0.07	4.09	13.8	14.9	0.47	12.1	0.39	0.04	0.08	1.86	0.39	0.05	99	7.48	0.01	0.71	3.26	1.9	0.06	0.93	0.73	0.01	0.11	0.01
TZ1 5f	Po-Pn-Ccp±Py	52.2	0.11	3.11	14.8	14.9	0.4	12.0	0.3	0.03	0.09	2.04	0.04	0.04	100	7.58	0.01	0.53	3.24	1.88	0.05	0.97	0.79	0.01	0.08	0.01
TZ1 7a1	Po-Pn-Ccp±Py	49.9	0.07	3.36	18.2	11.8	0.54	11.8	0.32	0.11	0.16	1.72	0.49	0.15	98	7.53	0.01	0.6	2.67	1.91	0.07	1.57	0.69	0.02	0.09	0.02
TZ19 1a	Po-Pn-Ccp±Py	47.5	1.45	7.69	11.0	15.8	0.12	11.9	0.81	0.67	0.16	1.98	0.13	0.05	99	6.92	0.16	1.32	3.45	1.86	0.01	0.52	0.79	0.02	0.23	0.13
TZ19 1b	Po-Pn-Ccp±Py	50.4	1.04	5.98	10.7	16.9	0.12	12.1	0.75	0.4	0.14	2.1	0.00	0.02	100	7.19	0.11	1	3.59	1.85	0.01	0.51	0.73	0.02	0.21	0.07
TZ19 1c	Po-Pn-Ccp±Py	50.1	0.96	6.93	10.7	16.1	0.17	12.3	0.67	0.14	0.21	2.1	0.00	0.02	100	7.15	0.1	1.16	3.43	1.89	0.02	0.64	0.62	0.02	0.19	0.03
TZ19 2e2	Po-Pn-Ccp±Py	48.4	0.12	7.77	15.4	13.2	0.31	11.5	0.72	0.09	0.08	1.96	0.14	0.09	99	7.1	0.01	1.34	2.89	1.82	0.04	0.83	1.01	0.01	0.2	0.02
TZ19 4c	Po-Pn-Ccp±Py	52.2	0.16	3.7	14.5	15.8	0.5	10.4	0.32	0.05	0.03	2.07	0.00	0.03	99	7.55	0.02	0.63	3.42	1.63	0.06	0.17	1.52	0	0.09	0.01
TZ19 6e	Po-Pn-Ccp±Py	51.4	0.33	3.79	13	15.8	0.22	12.4	0.26	0.04	0.11	0.77	2.72	0.03	100	7.46	0.04	0.65	3.43	1.94	0.03	0.84	0.71	0.01	0.07	0.01
TZ19 6c1	Po-Pn-Ccp±Py	47.8	1.3	7.44	11.2	15.6	0.1	11.8	0.86	0.62	0.1	2.05	0	0.04	99	6.98	0.14	1.28	3.4	1.86	0.01	0.63	0.72	0.01	0.24	0.12
RZ30 1e1	Po-Pn-Ccp±Py	49.2	0.28	5.45	11.1	18.2	0.17	10.2	0.67	0.06	0.06	0.78	2.65	0.06	99	7.21	0.03	0.94	3.99	1.61	0.02	0	1.31	0.01	0.19	0.01
RZ30 2a	Po-Pn-Ccp±Py	47.1	1.34	7	9.41	17.0	0.1	12.0	0.84	0.53	0.15	2.02	0.03	0.02	97	6.94	0.15	1.21	3.75	1.9	0.01	0.27	0.85	0.02	0.24	0.1
TZ1 1g	Po-Pn-Ccp±Py	53.0	0.12	2.53	12.8	16.1	0.38	12.3	0.27	0.03	0.02	2.07	0	0.03	99	7.66	0.01	0.43	3.47	1.91	0.05	0.92	0.60	0	0.08	0.01
TZ1 5g	Po-Pn-Ccp±Py	52.5	0.09	2.74	14.0	15.1	0.41	12	0.25	0.04	0.22	1.7	0.73	0.05	100	7.65	0.01	0.47	3.28	1.87	0.05	0.97	0.71	0.03	0.07	0.01
TZ1 5f1	Po-Pn-Ccp±Py	54.4	0.1	1.8	10.9	17.7	0.16	12.6	0.16	0.02	0.05	2.09	0.01	0.04	100	7.74	0.01	0.3	3.77	1.93	0.02	0.77	0.51	0.01	0.05	0
TZ1 5e	Po-Pn-Ccp±Py	52.9	0.11	2.43	13.9	16.0	0.45	11.5	0.24	0.03	0.1	2.06	0	0.04	99	7.67	0.01	0.42	3.46	1.78	0.06	0.59	1.05	0.01	0.07	0.01
TZ1 7e	Po-Pn-Ccp±Py	49.6	0.57	5.41	9.08	15.8	0.11	12.8	0.48	0.3	0.1	1.99	0.06	0.02	96	7.34	0.06	0.94	3.5	2.03	0.01	1.12	0	0.01	0.14	0.06
TZ1 7c	Po-Pn-Ccp±Py	52.8	0.07	1.55	16.2	14.1	0.53	12.0	0.12	0.03	0.15	2.03	0	0.06	99	7.76	0.01	0.27	3.09	1.89	0.07	1.26	0.70	0.02	0.03	0.01
TZ1 7a	Po-Pn-Ccp±Py	51.1	0.63	5.27	9.24	18.4	0.09	12.1	0.51	0.32	0.16	0.39	3.6	0.04	101	7.28	0.07	0.89	3.91	1.85	0.01	0.12	0.95	0.02	0.14	0.06
TZ7 4a	Po-Pn-Ccp±Py	54.8	0.11	1.62	9.86	19.0	0.14	12.0	0.2	0.02	0.07	2.12	0	0.02	100	7.76	0.01	0.27	4.02	1.83	0.02	0.27	0.86	0.01	0.05	0
TZ7 4e2	Po-Pn-Ccp±Py	56.4	0.11	1.74	7.38	21.7	0.16	11.1	0.35	0.02	0.03	2.17	0.03	0.01	101	7.76	0.01	0.28	4.47	1.65	0.02	0	0.82	0	0.09	0
TZ7 5c	Po-Pn-Ccp±Py	54.2	0.09	1.17	10.2	18.3	0.14	13.1	0.1	0.02	0	2.06	0.07	0	99	7.75	0.01	0.2	3.91	2.02	0.02	0.81	0.40	0	0.03	0
TZ7 6e	Po-Pn-Ccp±Py	50.9	0.04	3.05	19.5	11.0	0.45	10.0	0.31	0.14	0	1.92	0	0.24	97	7.73	0.01	0.55	2.49	1.63	0.06	1.35	1.06	0	0.09	0.03
TZ19 1g1	Po-Pn-Ccp±Py	52.2	0.45	5.88	8.75	19.2	0.14	12.0	0.56	0.08	0.06	2.12	0.05	0.02	101	7.27	0.05	0.97	3.99	1.79	0.02	0	0.99	0.01	0.15	0.02
RZ30 1a	Po-Pn-Ccp±Py	51.4	0.19	3.59	10.6	18.6	0.16	11.0	0.37	0.04	0.11	1.98	0.15	0.06	98	7.46	0.02	0.61	4.02	1.72	0.02	0	1.25	0.01	0.1	0.01

Sample	Assemblage	SiO2 wt.%	TiO2 wt.%	Al2O3 wt.%	FeO wt.%	MgO wt.%	MnO wt.%	CaO wt.%	Na2O wt.%	K2O wt.%	NiO wt.%	H2O wt.%	F wt.%	Cl wt.%	Total	Si at.%	Ti at.%	Al at.%	Mg at.%	Ca at.%	Mn at.%	Fe2+ at.%	Fe3+ at.%	Ni at.%	Na at.%	K at.%
TZ15 1a	Pn-Ccp-Py	52.7	0.09	2.09	12.8	16.7	0.32	11.8	0.19	0.05	0.18	2.06	0.00	0.04	99	7.66	0.01	0.36	3.63	1.84	0.04	0.53	0.99	0.02	0.05	0.01
TZ15 2d	Pn-Ccp-Py	55	0.06	1.77	13.8	17.6	0.41	10.2	0.15	0.03	0.07	2.1	0.03	0.04	101	7.78	0.01	0.3	3.72	1.55	0.05	0.00	1.57	0.01	0.04	0.01
TZ15 2e	Pn-Ccp-Py	54.7	0.32	2.46	10.1	17.9	0.1	13.1	0.16	0.05	0.14	1.7	0.91	0.02	101	7.68	0.03	0.41	3.76	1.97	0.01	0.85	0.32	0.02	0.04	0.01
TZ15 3c	Pn-Ccp-Py	50.7	0.87	6.17	9.6	13.6	0.09	12.2	0.75	0.44	0.12	2.03	0.00	0.03	96	7.46	0.1	1.07	3	1.93	0.01	1.19	0	0.01	0.21	0.08
TZ15 5e	Pn-Ccp-Py	54.1	0.14	3.04	12.6	17.0	0.28	11.8	0.2	0.03	0.14	2.1	0.04	0.02	101	7.64	0.01	0.51	3.58	1.79	0.03	0.47	0.98	0.02	0.05	0.01
TZ15 6c	Pn-Ccp-Py	54.0	0.06	1.47	12.0	17.3	0.41	11.4	0.11	0.05	0.04	2.06	0.04	0.02	99	7.8	0.01	0.25	3.72	1.78	0.05	0.43	0.98	0.01	0.03	0.01
TZ15 7d	Pn-Ccp-Py	52.4	0.05	2.74	12.6	17.0	0.31	11.7	0.21	0.03	0.07	2.01	0.11	0.02	99	7.59	0.01	0.47	3.68	1.82	0.04	0.36	1.12	0.01	0.06	0.01
TZ15 7e	Pn-Ccp-Py	54.4	0.55	1.91	12.2	17.1	0.34	11.8	0.12	0.03	0.13	2.11	0.00	0.01	100	7.73	0.06	0.32	3.62	1.81	0.04	0.60	0.82	0.01	0.03	0.01
TZ15 7e2	Pn-Ccp-Py	53.3	0.2	3.42	13.6	15.7	0.3	11.6	0.29	0.06	0.06	2.09	0.00	0.02	100	7.63	0.02	0.58	3.35	1.78	0.04	0.72	0.86	0.01	0.08	0.01
RZ17 1a1	Pn-Ccp-Py	54.5	0.07	1.82	8.64	19.4	0.21	12.4	0.19	0.02	0.04	2.12	0.00	0.00	99	7.73	0.01	0.3	4.1	1.89	0.03	0.31	0.69	0	0.05	0
RZ17 2b	Pn-Ccp-Py	54.8	0.02	0.48	13.2	16.3	0.26	13.0	0.04	0.01	0	2.09	0.00	0.01	100	7.87	0	0.08	3.5	2.01	0.03	1.32	0.25	0	0.01	0
RZ17 2a	Pn-Ccp-Py	53.7	0.2	2.6	12	15.6	0.2	12.8	0.17	0.06	0.15	2.08	0.00	0.02	99	7.73	0.02	0.44	3.35	1.98	0.02	1.34	0.09	0.02	0.05	0.01
RZ17 3c	Pn-Ccp-Py	54.4	0.06	2.09	11.1	17.9	0.23	12.2	0.36	0.02	0.26	2.12	0.00	0.01	100	7.7	0.01	0.35	3.79	1.85	0.03	0.51	0.77	0.03	0.1	0
RZ17 5c	Pn-Ccp-Py	55.2	0.09	1.49	10.3	16.4	0.16	12.7	0.13	0.03	0.17	2.09	0.00	0.01	98	7.92	0.01	0.25	3.5	1.96	0.02	1.24	0	0.02	0.04	0.01
RZ50 5b	Py-Ccp-Mil	54.7	0.04	1.48	10.8	17.8	0.25	12.5	0.08	0.02	0.12	2.11	0.00	0.01	100	7.79	0	0.25	3.78	1.91	0.03	0.71	0.56	0.01	0.02	0
RZ50 2c	Py-Ccp-Mil	53.5	0.06	2.77	9.79	18.3	0.23	12.3	0.19	0.04	0.06	2.02	0.18	0	99	7.63	0.01	0.47	3.9	1.89	0.03	0.39	0.75	0.01	0.05	0.01
RZ50 1a	Py-Ccp-Mil	52.2	0.43	4.8	9.57	17.8	0.23	11.9	0.4	0.2	0.17	1.33	1.64	0.01	100	7.43	0.05	0.81	3.77	1.81	0.03	0.27	0.84	0.02	0.11	0.04
RZ50 3a	Py-Ccp-Mil	54.8	0.03	1.51	9.75	17.8	0.23	12.6	0.09	0.02	0.03	1.91	0.41	0.00	99	7.84	0	0.25	3.8	1.93	0.03	0.83	0.32	0	0.02	0
RZ50 4c	Py-Ccp-Mil	54.3	0.03	1.29	10.1	18.3	0.21	12.3	0.09	0.02	0.21	2.07	0.06	0.00	99	7.78	0	0.22	3.92	1.9	0.03	0.51	0.68	0.02	0.02	0
RZ3 4c	Py-Ccp-Mil	53.4	0.11	2.42	10.4	18.1	0.3	12.3	0.37	0.03	0.19	1.74	0.75	0.02	100	7.63	0.01	0.41	3.86	1.88	0.04	0.44	0.77	0.02	0.1	0.01
RZ3 4a	Py-Ccp-Mil	52.4	0.07	1.95	9.25	18.6	0.38	12.4	0.28	0.02	0.03	1.19	1.82	0.02	98	7.64	0.01	0.34	4.05	1.94	0.05	0.36	0.74	0	0.08	0

Table A3. Electron microprobe analyses of platinum group mineral from the Lac-des-Iles-Complex.

Sample	Assemblage	Te wt.%	Sb wt.%	Pd wt.%	Pt wt.%	S wt.%	Bi wt.%	As wt.%	Total	Te at.%	Sb at.%	Pd at.%	Pt at.%	S at.%	Bi at.%	As at.%
Tz1-2	Po-Pn-Ccp±Py	48.7	0.30	44.1	0.00	0.03	6.76	0.00	100	45.4	0.30	49.4	0.00	0.11	3.85	0.00
Tz1-3	Po-Pn-Ccp±Py	47.6	0.33	44.1	0.01	0.04	7.33	0.00	99	44.9	0.33	49.9	0.005	0.14	4.22	0.00
Tz1-9	Po-Pn-Ccp±Py	46.5	0.26	42.5	0.00	0.00	9.79	0.00	99	44.6	0.26	48.9	0.00	0.01	5.73	0.00
Tz1-10	Po-Pn-Ccp±Py	48.2	0.31	43.8	0.00	0.03	7.08	0.00	100	45.2	0.30	49.4	0.00	0.11	4.06	0.00
Tz1-15	Po-Pn-Ccp±Py	47.9	0.31	43.1	0.03	0.01	7.97	0.00	100	45.4	0.31	49.1	0.02	0.05	4.61	0.00
Tz1-17	Po-Pn-Ccp±Py	48.4	0.27	43.5	0.00	0.03	7.15	0.00	100	45.6	0.27	49.2	0.00	0.10	4.11	0.00
Tz1-13	Po-Pn-Ccp±Py	44.7	0.28	36.3	0.00	0.02	8.26	0.00	89	47.4	0.31	46.2	0.00	0.06	5.34	0.00
Rz30 A3	Po-Pn-Ccp±Py	48.0	0.61	40.4	0.14	0.65	5.41	0.07	97	44.9	0.60	45.3	0.08	2.42	3.09	0.11
Rz30 d1	Po-Pn-Ccp±Py	47.8	0.37	39.0	0.00	0.03	6.60	0.00	94	47.8	0.39	46.8	0.00	0.11	4.03	0.00
Rz30 d2	Po-Pn-Ccp±Py	56.3	0.31	6.06	31.6	0.03	1.24	0.00	99	63.9	0.37	8.2	23.4	0.14	0.86	0.00
Rz17-58	Pn-Ccp-Py	49.8	0.41	42.2	0.00	0.00	0.48	0.02	93	49.1	0.42	49.8	0.00	0.00	0.28	0.02
Rz17-57a	Pn-Ccp-Py	0.60	0.37	75.2	0.00	0.24	0.01	18.4	95	0.49	0.31	72.9	0.00	0.76	0.006	25.3
Rz17-57b	Pn-Ccp-Py	3.31	0.00	0.74	51.1	0.10	0.01	41.9	98	3.00	0.00	0.80	30.2	0.37	0.008	64.5
Rz17-39	Pn-Ccp-Py	47.0	0.32	39.9	0.00	0.02	1.65	0.00	90	48.3	0.34	49.2	0.00	0.09	1.03	0.00
Rz8-30	Py-Ccp-Mil	27.6	0.19	39.6	0.00	0.02	32.4	0.00	100	28.9	0.21	49.7	0.00	0.10	20.7	0.00
Rz8-35	Py-Ccp-Mil	30.1	0.26	39.9	0.04	0.006	29.5	0.00	100	31.1	0.29	49.4	0.03	0.02	18.6	0.00
Rz8-27	Py-Ccp-Mil	27.9	0.21	39.2	0.00	0.004	32.2	0.00	100	29.2	0.23	49.2	0.00	0.01	20.5	0.00
Rz8-28	Py-Ccp-Mil	28.4	0.20	38.0	0.00	0.04	30.9	0.00	98	30.2	0.22	48.3	0.00	0.17	20.0	0.00
Rz8-31	Py-Ccp-Mil	29.8	0.26	39.8	0.03	0.01	30.4	0.00	102	30.4	0.28	48.7	0.02	0.06	18.9	0.00
Rz54-7	Py-Ccp-Mil	30.9	0.20	36.8	0.00	0.02	22.6	0.00	91	34.0	0.23	48.6	0.00	0.10	15.2	0.00
Rz54-5	Py-Ccp-Mil	53.3	0.35	5.69	29.3	0.005	1.73	0.00	91	64.4	0.44	8.25	23.1	0.02	1.28	0.00
Rz54-1	Py-Ccp-Mil	41.9	0.24	38.9	0.00	0.04	10.2	0.00	92	43.1	0.26	48.0	0.00	0.15	6.41	0.00

Table A4. **Results of the calculation of the length of the inclusions observed during the laser ablation of the base metal sulfides.**

Sample	sulfide	PGM type	Ti ms	Tf ms	Tia ms	ablation rate (2 µm/s) DI	µm/s LI case 1	µm/s LI case 2	Length (min)	Length (max) µm	average µm	Area um2	T.a
Tz-1	Po	Pd-Te	67956	69460	1504	3.01	3.01	1.73	1.73	3.01	2.37	5.62	C
Tz-1	Po	Pd-Te	62078	64014	1936	3.87	3.87	2.23	2.23	3.87	3.05	9.32	C
Tz-1	Po	Pd-Te	65663	66810	1147	2.29	2.29	1.32	1.32	2.29	1.80	3.27	B
Tz-7	Pn	Pd-Te	26021	27168	1147	2.29	2.29	1.32	1.32	2.29	1.80	3.27	B
Tz-7	Pn	Pt-As	70465	72401	1936	3.87	3.87	2.23	2.23	3.87	3.05	9.32	B
Tz-19	Pn	Pt-Te	72974	74121	1147	2.29	2.29	1.32	1.32	2.29	1.80	3.27	C
Tz-19	Py	Pt-Te	49032	50105	1073	2.14	2.14	1.23	1.23	2.14	1.69	2.86	B
Rz-45	Py	Pd-Te	25448	28027	2579	5.15	5.15	2.97	2.97	5.15	4.06	16.5	C
Rz-30	Pn	Pt-Bi	54121	56200	2079	4.15	4.15	2.40	2.40	4.15	3.27	10.7	B
Tz-15	Py	Pd-Sb	66164	68387	2223	4.44	4.44	2.56	2.56	4.44	3.50	12.2	B
Rz-26	Py	Pd-Bi-Te	48960	50107	1147	2.29	2.29	1.32	1.32	2.29	1.80	3.27	C
Rz-26	Mil	Pd-As	49390	50537	1147	2.29	2.29	1.32	1.32	2.29	1.80	3.27	B
Rz-26	Mil	Pd-As	60071	62007	1936	3.87	3.87	2.23	2.23	3.87	3.05	9.32	B
Rz-26	Py	Pd-Te	36844	38206	1362	2.72	2.72	1.57	1.57	2.72	2.14	4.61	C
Rz-26	Py	Pd-Te	51111	53118	2007	4.01	4.01	2.31	2.31	4.01	3.16	10.0	C
Rz-26	Py	Pd-Te	45949	47311	1362	2.72	2.72	1.57	1.57	2.72	2.14	4.61	C
Rz-50	Mil	Pd-Te	56057	60430	4373	8.74	8.74	5.04	5.04	8.74	6.89	47.5	B
Rz-50	Mil	Pd-Te	62365	65376	3011	6.02	6.02	3.47	3.47	6.02	4.74	22.5	n.d.
Rz-54	Py	Pd-Sb	33906	34910	1004	2.01	2.01	1.15	1.15	2.01	1.58	2.50	C
Rz-54	Py	Pd-Sb	60501	63010	2509	5.01	5.01	2.89	2.89	5.01	3.95	15.6	n.d.
Rz-54	Py	Pd-Sb	70824	71899	1075	2.15	2.15	1.24	1.24	2.15	1.69	2.87	n.d.
Rz-54	Py	Pd-Sb	70537	72616	2079	4.15	4.15	2.40	2.40	4.15	3.27	10.7	n.d.

The length of the PGM inclusion is calculated following the equation: the ablation rate * the time of inclusion ablation (TIA) / 1000. The time of the inclusion ablation (TIA) is is given by Tf -Ti where Tf and Ti are the time at the end and at the beginning of the inclusion ablation, respectively. Abbreviations: Po = pyrrhotite, Pn = pentlandite, Py = pyrite, Mil = millerite, T.a = textural association, B = contact sulfide/silicate, C = included in sulfide.